Preprint Cambridge Centre for Computational Chemical Engineering ISSN 1473 – 4273

# Carbonaceous nanoparticle formation in flames

Jacob W. Martin [1,2], Maurin Salamanca [1], Markus Kraft [1,2,3]

released: 12 November 2020

[1] Department of Chemical Engineering
and Biotechnology
University of Cambridge
West Site, Philippa Fawcett Drive
Cambridge, CB3 0AS
United Kingdom
E-mail: mk306@cam.ac.uk

[2] Cambridge Centre for Advanced Research and
Education in Singapore CREATE Tower
1 CREATE Way
Singapore 138602

[3] School of Chemical and
Biomedical Engineering
Nanyang Technological University
62 Nanyang Drive
Singapore 637459

Preprint No. 263

UNIVERSITY OF CAMBRIDGE

*Keywords:* soot, incipient soot, carbon black, carbon nanodots

**Edited by**
Computational Modelling Group
Department of Chemical Engineering and Biotechnology
University of Cambridge
West Site, Philippa Fawcett Drive
Cambridge, CB3 0AS
United Kingdom

**Fax:** + 44 (0)1223 334796
**E-Mail:** c4e@cam.ac.uk
**World Wide Web:** http://como.cheng.cam.ac.uk/

**Abstract**

The route by which gas-phase molecules in hydrocarbon flames form solid carbonaceous nanoparticles is reviewed. These products of incomplete combustion are introduced as particulates and materials revealing both their useful applications and unwanted impacts as pollutants. Significant advances in experimental techniques in the last decade have allowed the gas phase precursors and the transformation from molecules to nanoparticles to be directly observed. These measurements combined with computational techniques allow for various mechanisms known to date to be compared and explored. Questions remain surrounding the various mechanisms that lead to nanoparticle formation. Mechanisms combining physical and chemical routes, so-called physically stabilised soot inception, are highlighted as a possible "middle way" with reactive aromatics activated by hydrogen of particular interest.

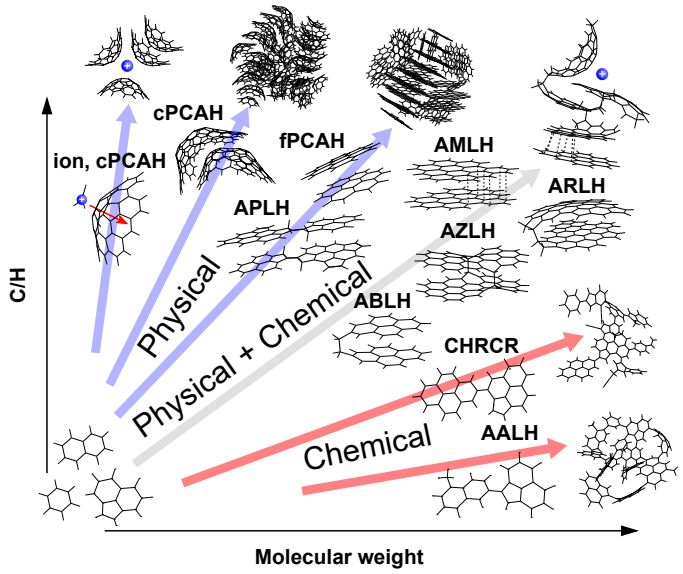


## Highlights:

- The review is motivated by efforts to reduce harmful soot emissions and to control the nanostructure and synthesis of carbon black/nanodots.
- The formation of gas-phase precursor aromatics are reviewed identifying PCAH, aromers and clustering PAH.
- The formation of carbonaneous nanoparticles are reviewed focusing on the known chemical and physical mechanisms.
- Mechanisms combining physical and chemical mechanisms are highlighted with localised $\pi$-radicals of particular interest.

# Contents

# 1 Introduction

The carbonaceous products of incomplete combustion have fascinated and frustrated many. Interest in their illumination, pigments and heating gave way to dissatisfaction as they filled our cities with toxic air. This review attempts to capture this fascination and frustration by examining one of the least well understood aspects of incomplete combustion, the self-assembly of gas-phase molecules into carbonaceous nanoparticles.

This review is written for three main fields: combustion science, aerosol science and chemical engineering. Combustion science is concerned with understanding the physical and chemical processes involved in flames, of interest to many of the great scientists. Michael Faraday wrote, in his famous set of public lectures on the chemical history of a candle [138],

> 'There is not a law under which any part of this universe is governed which does not come into play, and is touched upon in these phenomena. There is no better, there is no more open door by which you can enter the study of natural philosophy, than by considering the physical phenomena of a candle.'

Indeed many doors have been opened by the study of flames, allowing for an unprecedented understanding of chemical kinetics and physical processes. However, the formation mechanism of carbonaceous particles in hydrocarbon flames has remained a perennial unsolved problem in the field, although not for lack of effort (see the many detailed reviews written over the last two decades – Richter and Howard in 2000 [420], Frenklach in 2002 [149], McEnally, Pfefferle, Atakan and Kohse-Höinghaus in 2006 [336], the book edited by Bockhorn, D'Anna, Sarofim and Wang in 2009 [39], D'Anna in 2009 [98], Wang in 2011 [511], Haynes in 2019 [194], Frenklach and Mebel [152] with some recent reviews focusing on experimental aspects by Hansen, Cool, Westmoreland and Kohse-Höinghaus in 2009 [187], Li and Fei Qi in 2010 [295], Desgroux et al. in 2013 [111], Fei Qi in 2013 [407], Niessner in 2014 [384], Kittelson and Kraft in 2014 [256], Michelsen in 2017 [349], Wang and Chung in 2019 [518] and Baldelli, Rogak et al. [18], as well as a recent glossary of soot nomenclature [351]). It has only been in the last decade, however, that experimental and computational techniques in combustion science have been able to peek behind the door to reveal insights into the earliest formation mechanisms of carbonaceous particulates in the flame.

To clarify the problem, carbonaceous particle formation is separated into four main steps and provide a schematic (see Figure 1 based on a schematic by Bockhorn from 1994 [37]):

1. Precursor formation
2. Nanoparticle formation
3. Primary particle formation
4. Aggregate formation

These steps are not strictly distinct but overlap and influence each other (for example, nanoparticles grow into primary particles). However, a distinction is made between nanoparticles and primary particles for the following reasons. Firstly, many of the smallest

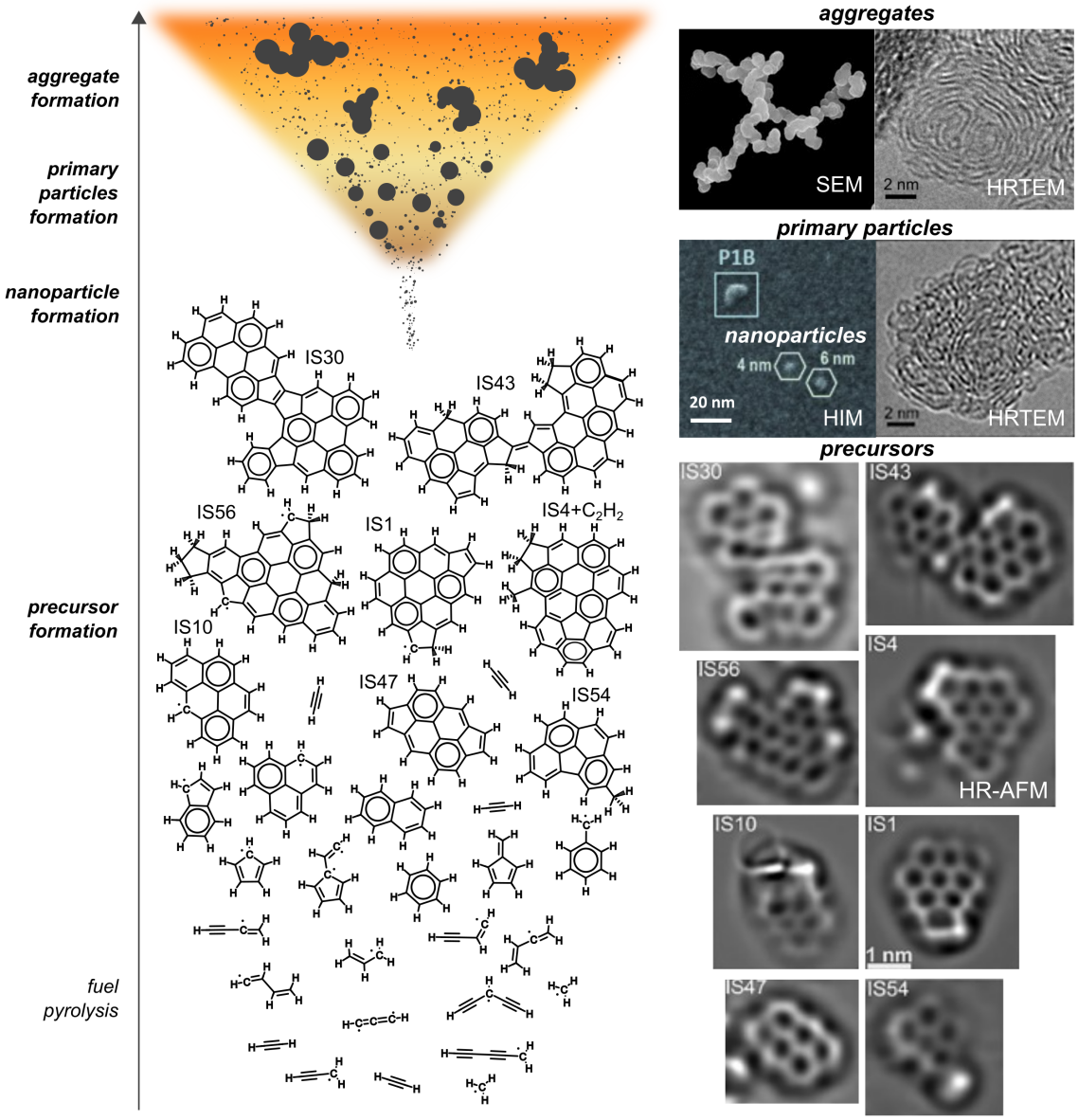


**Figure 1:** *Schematic of carbonaecous particulate (soot or carbon black) formation in flames. Fuel pyrolysis and single ring species from Hansen et al. [187], Johansson et al. [234]. Multiring aromatic structures from Commodo et al. [88]. Nanoparticles imaged with HIM are shown from [437]. Primary particles are also shown in the HIM as well as with HRTEM [323]. Aggregates are shown with SEM for a lamp black particle (Orion carbons) as well as HRTEM of a primary particle [323].*

nanoparticles have very low coagulation efficiencies and are therefore readily emitted alongside larger particles [212, 298, 399]. Secondly, evidence has recently emerged for non-spherical primary particles, indicating coagulation of nanoparticles [437]. Finally, flames can be established which are dominated by nanoparticles [112]. We have also made use of the recent extensive review of soot nomenclature [351]. However, we will

use the term carbonaceous nanoparticles for early soot particles to bridge the combustion, materials and aerosol terminology [98, 133, 141, 238, 242, 363, 374]. This follows efforts to avoid mechanistic language when discussing soot formation and allows for a discussion of variously sized or charged species on the nanoscale. Further details are provided throughout concerning the nomenclature.

For aggregate formation the terminology for carbon blacks is used (quoted from the ASTM D3053 standard with italicised term added by the authors),

> 'Carbon black exhibits aciniform (*grape-like*) morphology composed of spheroidal "primary particles" strongly fused together to form discrete entities called aggregates. The primary particles are conceptual in nature, in that once the aggregate is formed the "primary particle" no longer exists, they are no longer discrete and have no physical boundaries amongst them. The aggregates are loosely held together by weaker forces forming larger entities called agglomerates.'

Soot, unlike carbon black, most commonly contains a significant hydrogen content in the primary particles [483], often also with condensed aromatics on the aggregates (called mixed soot [44]) which has implications for human health [297]. Carbon blacks are thermally treated to near complete carbonisation (loss of heteroatoms leaving a disordered carbon solid) with minimal health impacts [320]. We refer the reader to the recent excellent reviews [18, 250] on the carbonisation of soot as it takes on a shell [52], maturing into a carbon black once hydrogen is fully evolved, but we will not discuss this further.

Aerosol science is concerned with the combustion products as particulates, which are particles suspended in the air. Soot is particularly problematic as an aerosol, posing significant risk for human health and the climate [44]. Chemical engineers are then often tasked with eliminating these emissions. This requires a comprehensive and complete understanding of the process. The problem was most clearly articulated by Palmer and Cullis in 1965 [390],

> 'A major breakthrough in understanding carbon formation will have been achieved when it becomes possible in at least one case to account for the entire course of nucleation and growth of carbon on the basis of a fundamental knowledge of reaction rates and mechanisms.'

Since this was written, scientific advances have allowed for this problem to be partially resolved – models do exist for specific cases. Simple kinetic models, considering acetylene concentrations, allowed the mass of soot emissions to be reproduced [245], but particle numbers were predicted incorrectly. Computational simulations coupled with kinetic experiments in the 1970s and 1980s allowed for models to be developed that considered different nucleation species in detailed chemistry models [228]. It was only in the late 1980s to early 1990s that combining a kinetic mechanism for PAH growth (HACA - Hydrogen Abstraction Carbon Addition) and an irreversible dimerisation of aromatic species allowed particle number to be captured [153, 329–331, 512], with one of the most popular implementations (ABF mechanism) published in 2000 [13] (differing minimally from ref. [512]). This soot model was able to reproduce many experimental observations such as the equivalence ratio threshold ( $\phi > 2$ ) and the low ($\sim$1450 K) and

high temperature thresholds for soot formation (so-called "soot bell curve" or "soot island") [42, 154, 167, 172, 491]. It is important to note that irreversible dimerisation is an empirical model in that by fitting model parameters to particular experimental 'cases' reasonable nucleation rates can be attained. However, for a new combustion system it is rarely predictive.

Attempts to provide such a predictive model for nanoparticle formation have focused on developing more detailed models. Kinetic mechanisms can now be automatically generated for many reaction classes in combustion chemistry (*e.g.* RMG - reaction mechanism generator [158]) and some PAH mechanisms now allow growth of large PAH (up to coronene) [412, 467]. For larger PAH, kinetic Monte Carlo simulations allow the formation of curved aromatics [148, 156, 291, 410, 526–528, 539] as well as crosslinks [100, 286, 505]. Particle dynamics such as coagulation, growth, oxidation and fragmentation can be computed with stochastic approaches, allowing the particle size distribution to be modelled [19, 458, 548]. However, these attempts have not improved our predictive power significantly due to the lack of understanding concerning nanoparticle formation. In fact, experimental and computational work from the last decade has shown that irreversible dimerisation of pyrene at flame temperatures cannot occur [427, 489, 511], with no alternative mechanisms proving any more useful. This leads us to restate our comment from 2014 that [256],

> 'None of the existing soot models have predictive power.'

Until a fundamental understanding of the mechanism (or mechanisms) of soot nanoparticle formation is found, developing a predictive models to control or eliminate carbonaceous combustion products will prove futile.

**The purpose of this paper** is to review the molecule-to-particle transition in detail with a focus on the precursors formed and the nanoparticle mechanisms.

Section 2 explores the detection of nanoparticles as well as the health, climate and material motivation for understanding this mechanism. Much of this extended introduction can be skipped by readers who are already familiar with the field, however the experimental results for nanoparticles will be critically discussed throughout the rest of the document and therefore Section 2.1 is recommend reading. The discussion about mixed soot in Section 2.2 is also important when discussing liquid-like mechanisms for nanoparticle formation.

Section 3 begins the main text with a review of the formation of molecular precursors. The use of sooting propensity scales are briefly discussed, highlighting the important role of aromatic species and 5-membered cycles Formation of pericondensed aromatic hydrocarbons through traditional growth pathways is then explored with recent insights into detection of pentagonal ring-containing PAH. Larger PAH (aromers) formed through crosslinking are then discussed with a focus on the previous difficulties in their detection and their chemical structure, which has recently been exposed. The final precursors discussed are the PAH that cluster to form soot. This section on precursors therefore provides the necessary understanding of the molecular species present in the flame before nanoparticle formation begins.

Section 4 provides a systematic comparison of formation mechanisms for soot nanopar-

ticles. This section has been arranged in a similar manner to Bansal and Donnet's 1993 book 'Carbon Black' [119] but is significantly updated and partially restructured. The reasons for providing this comprehensive overview of mechanisms are recent new insights and the resurfacing of old mechanisms. It does, however, give the impression that the mechanisms are disjointed so we have therefore added a section combining physical and chemical mechanisms, which we argue best describe the partial success of the "irreversible dimerisation" models proposed in the literature.

Finally, Section 5 summarises the mechanisms and experiments, redrawing many important historical plots with the insights from the last decade. An outlook is provided for further scientific and technological directions required to resolve the formation mechanism of carbonaceous nanoparticles in the flame.

# 2 History and motivations

This section introduces the many nanoparticles in combustion systems and provides the motivations for understanding the formation of carbonaceous nanoparticles. The experimental finding concerning carbonaceous nanoparticles in combustion flames will be introduced, drawing on recent reviews [18, 98, 111, 349, 511]. Some motivations for this study from both a human health and climate perspective will be discussed, also drawing on recent reviews [44, 174, 198, 227, 297, 299, 352, 353, 379, 532]. Finally, recent material applications are discussed.

## 2.1 Detection

Particles down to a nanometre in size were initially observed via electron shadow microscopy by Wersborg et al. [524] in 1973. Laser scattering also indicated nanoparticles two years later [94]. Some of the first nanoparticles to be quantitatively detected in the flame were positively charged species with molecular weight of order $10^3 - 10^4$ Da, found in low pressure flames [209]. Small, positively charged molecules are known to form in flames through chemionisation reactions, therefore the presence of charged soot nanoparticles is not surprising [192] (at this stage they were not referred to as nanoparticles but as early soot particles). Their size was limited to below $10^5$ Da [25]. Higher sensitivity nanoparticle detectors have recently found the majority of these sub 1 nm particles to be positively charged [64, 536]. However, in sooting flames the charged nanoparticle modes that are present quickly coagulate with electrons and small charged species to form neutral particles [143, 514].

In 1985, the $C_{60}$ buckminsterfullerene molecule (see Figure 13) was discovered by laser ablation of a graphite target [277] and two years later in low pressure benzene flames [164]. Since this time their combustion synthesis has been developed into a commercial technology (NanoC) generating kilogram scale of magic number fullerenes, for example $C_{60}$ and $C_{70}$, that have found applications in many fields such as organic solar voltaics and medicine [41, 168, 178, 215]. Significant controversy has surrounded the role of fullerenes in soot formation. The formation of fullerenes in flame will not specifically discussed

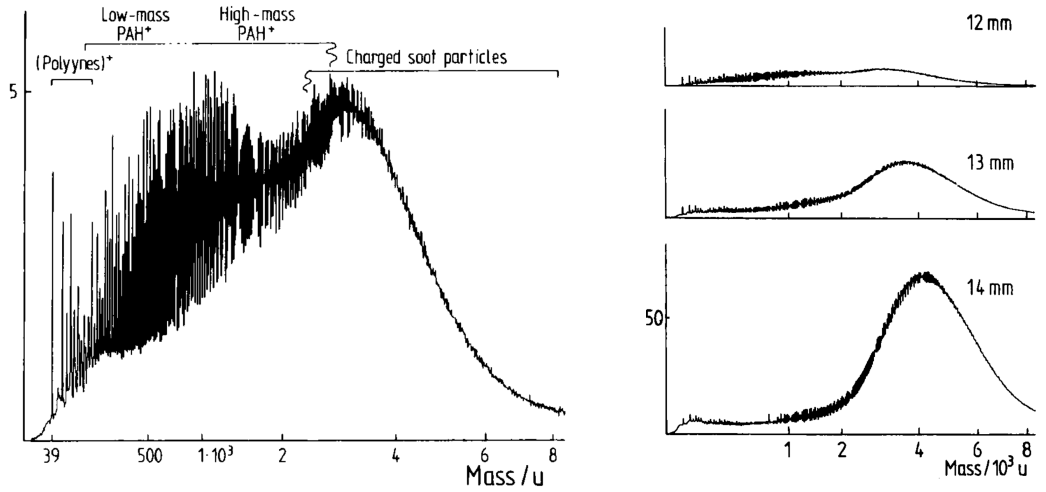


**(a)** *Positive mass spectrum at 12 mm.*

**(b)** *Scaled mass spectrum for 12 mm as seen in (a) as well as mass spectra at 13 and 14 mm.*

**Figure 2:** *Positive ion mass spectrometry of an $C_2H_2/O_2$ low pressure flame $p = 2.7$ kPa at various heights above the burner [25]. Used with permission from John Wiley and Sons ©.*

(see the reviews [208, 366, 422]) but will focus on their role in the formation of larger carbonaceous nanoparticles. Graphene or giant aromatic molecules can also be formed in some particular operating conditions of low pressure acetylene flames [208]. Microwave heating has also been shown to allow graphene synthesis in flames at atmospheric conditions [378, 459]. Flame synthesis of graphene in the gas phase has yet to be developed into a mature technology.

By the 1990s laser scattering and electron microscopy had established that larger (∼2 nm) incipient nanoparticles were present in all sooting flames [95, 117, 125]. Atomic force microscopy allowed for the direct measurements of these nanoparticles [21, 84, 86] (see Figure 5). These nanoparticles were shown to form at an equivalence ratio just below or close to values where soot primary particles or aggregates form [21, 67, 482]. All sooting flames, including aromatic fuels such as benzene flames, were found to possess this mode near 2 nm, which will be referred to as *incipient nanoparticles* in this review [101]. Desgroux and co-workers have studied so-called *nucleation-dominated flames* [31, 36, 112, 221, 373]. Nucleation-dominated flames allow nanoparticles to nucleate but surface growth and coagulation appears marginal, with oxidation dominating, meaning the soot mass increases only by nucleation from the gas phase [112, 373]. These flames can be stabilised at atmospheric and low pressure flames for methane, ethylene and *n*-butane [31, 36, 112, 373] (see Figure 3a).

Evidence for nanoparticle >4 nm was also found. Grotheer and colleagues developed a time of flight reflectron mass spectrometer able to measure millions of mass units [180] and in 2007 they showed that aromatic molecules right through to nanoparticles with millions of mass-to-charge values could be detected using photoionisation [20, 189, 190]. Figure 3b shows similar results from nano differential size mobility analyser (nano-DMA) [83,

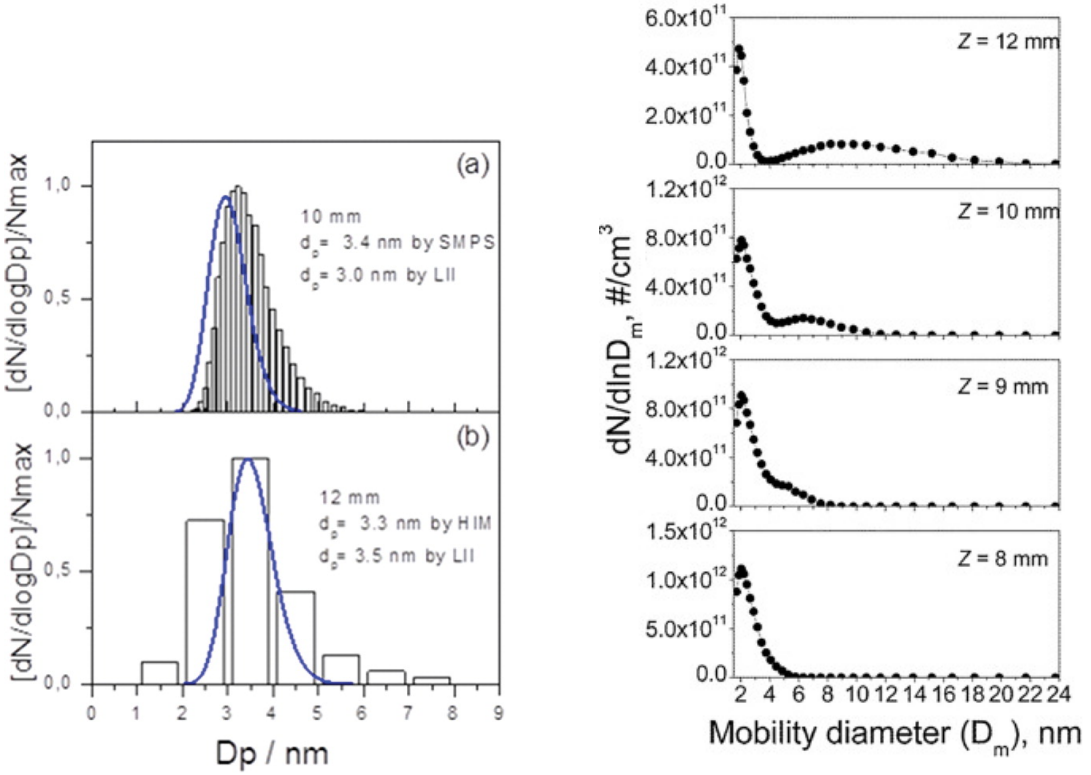


**(a)** *Normalised particle size distributions measured by 1 nm-SMPS (a) bars), HIM (b) bars), and LII (blue line) in an n-butane/$O_2$/$N_2$ $\phi = 1.75$ premixed flame [31].*

**(b)** *Particle size distribution measured on a Vienna style nanoDMA in an $C_2H_4$/air premixed flame [88].*

**Figure 3:** *Used with permissions from Elsevier©.*

448], which also was shown with scanning mobility particle sizing (SMPS) [476]. This figure shows nanoparticles increasing in mass to form primary particles. We will refer to nanoparticles $> 4$ nm mode as *primary nanoparticles*. Helium ion microscopy and electron microscopy have provided evidence for nanoparticles down to 4 nm in size showing their development into primary particles, shown in Figure 5b) [437]. This study also revealed primary particles' non-symmetric structure indicating they form, at least partly, through coagulation of smaller nanoparticles.

Some evidence has emerged for structural or chemical differences between the incipient and primary nanoparticles. Grotheer found that the photoionisation process was a two-photon process for incipient nanoparticles and a single-photon process for primary nanoparticles [181]. The two-photon process indicated that smaller aromatics are the constituents of the incipient nanoparticles [111]. These smaller nanoparticles also lack visible light absorption when measured by laser spectroscopy, suggesting small aromatics with only a few aromatic rings [96] and leading some to label these incipient nanoparticles as "transparent" or nanoorganic carbons (NOC) [126]. The incipient nanoparticles were found to be stable under infrared laser absorption (1064 nm), while the primary nanoparticles fragmented with a laser fluence of 1–3 mJ/mm$^2$. Higher laser fluences (10 mJ/mm$^2$) were found to generate fullerene ions [181]. (It is important to note that fullerenes are

not present in the flame at high concentration but in these experiments are products of the rapid heating of soot, which is well known to lead to significant carbon vapour [170, 422].) IR pulsed laser ablation is known to significantly modify aggregate soot nanostructure, through carbonisation (hydrogen removal), partial graphitisation (thermal transformations towards graphitic structure) [498] and fragmentation [350]. However, recent optical studies indicate only slight differences between the molecular units involved in incipient and primary nanoparticles [109]. Instead the supramolecular organisation was suggested to be the distinguishing feature between these nanoparticles.

Figure 4 shows this fluorescence, which has been observed since the 1980s when rare gas plasma lasers became available [78, 115, 159, 193]. Initially, this was seen as a response from the individual molecules as PAH are known to fluoresce [473]. However, the signal extending well into the visible spectrum suggested an excimer origin. Excimers are long-lived optical states that are formed from the delocalisation of the $\pi$–$\pi^*$ excited state across both stacked aromatic species, and are present in the fluorescence spectra of PAH dissolved in liquids [34, 204].

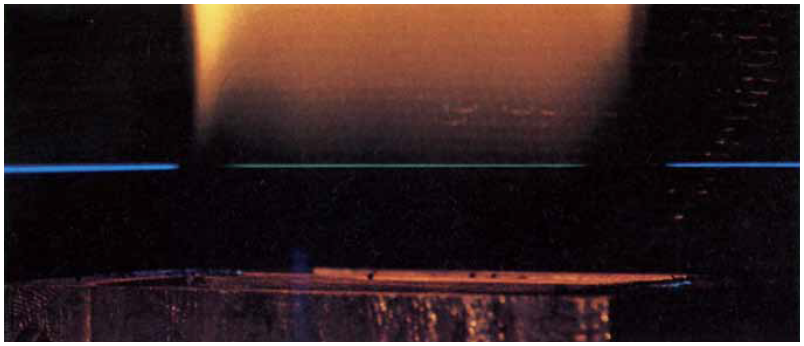

**Figure 4:** *Green fluorescence from UV laser excitation (top) [159]. Used with permission from Springer Nature America ©.*

Time resolved laser induced fluorescence (TR-LIF) experiments have established that this green fluorescence signal belongs to excimers [346, 464]. Excimer states are long-lived (tens of nanoseconds) and TR-LIF confirmed such long-lived states for signals in the range 500–600 nm. Critically, the excimer signal reveals that physically bound, stacked aromatic species are present during soot formation. In Section 3 another change in the flame chemistry is shown with the transition from a nucleation domination flame with larger aromatic species being observed [112].

There is still no consensus on the naming and number of distinct nanoparticles [351] and we do not see a resolution of these issues until the mechanisms involved can be fully understood. Maximally there is evidence for five nanometre-sized species that can exist in various combustion environments;

- *Charged nanoparticles* ($\sim$1 nm)
- *Fullerenes* ($\sim$1 nm, polyhedral carbons)
- *Graphene* ($>$ 1 nm, nanographenes, giant polycyclic aromatic hydrocarbons)

- *Incipient nanoparticles* (<4 nm otherwise called transparent nanoparticles, nanoorganic carbon – NOC, D'Alessio nanoparticles, precursor nanoparticles, soot nuclei, nascent soot, disordered)

- *Primary nanoparticles* (>4 nm otherwise called stacked nanoparticles, growth precursors, soot nuclei, Dobbins nanoparticles, nascent soot)

It is important to mention that many of the naming conventions of nanoparticles are directly associated with the mechanism or model of growth that is thought to occur, thus our reason for choosing the more neutral names of incipient and primary nanoparticles. We will return to the nomenclature of nanoparticles at the beginning of Section 4.

## 2.2 Unwanted particulates

Particulates are an aerosol of particles suspended in the air and are usually undesirable in the context of aerosol/climate science. It is important to outline some semantics when discussing combustion products as particulates. The use of nanoparticles in the aerosol community often refers to all ultrafine particles (<100 nm). We will follow the nomenclature from the combustion community that predominantly refers to these smallest particles (<10 nm) as being called the nanoparticle mode (Nano) or nucleation fraction PM0.01 [98, 297].

To further aid our discussion of the range of combustion products emitted as particulates we have prepared Figure 5. The majority of combustion products fall below 2.5 $\mu$m (PM2.5 or fine fraction) and have significant negative health impacts [15, 169]. Most primary combustion emissions just below this range are soot aggregates (see Fig 5c). As mentioned these are fractal-like arrangements of smaller carbon spheres (called "primary particles" in combustion and "nodules" or "spherules" in materials science). These primary particles are chemically connected to their neighbours, forming a solid aggregate, as opposed to physically connected soot agglomerates (see Figure 5f). Figure 5c) – d) shows the soot emitted from a heavily sooting ethylene flame revealing that with increasing fuel-rich conditions, unburnt hydrocarbons will condense on the soot aggregate. This forms a ''mixed soot" of black carbon (highly carbonised primary combustion product) and brown carbon (collection of unburnt hydrocarbons and small aromatic species) [44, 453]. Even larger brown carbon spheres of condensed unburnt hydrocarbons (often called "tar balls") can form [68, 312]. They are produced from smouldering fires such as agricultural fires. Recent work using high resolution mass spectrometry showed this brown carbon is made up of a large proportion of oxygenated and unsubstituted PAH. These species have the mean molecular mass of benzo[a]pyrene as well as some aliphatic structures with aromatic cores [525]. We will return to the mixed soot with unburnt hydrocarbons when we discuss liquid-like mechanisms in nanoparticle formation.

A further complication arises when comparing the various aerosol modes found in the literature. Often the terminology ''nuclei", "accumulation" and "coarse" modes are borrowed from atmospheric science when discussing engine emissions. Unfortunately, these modes refer to water condensation with the accumulation mode referring to water droplets in the atmosphere. The "nuclei" mode is usually defined as <100 nm or ultrafine PM0.1

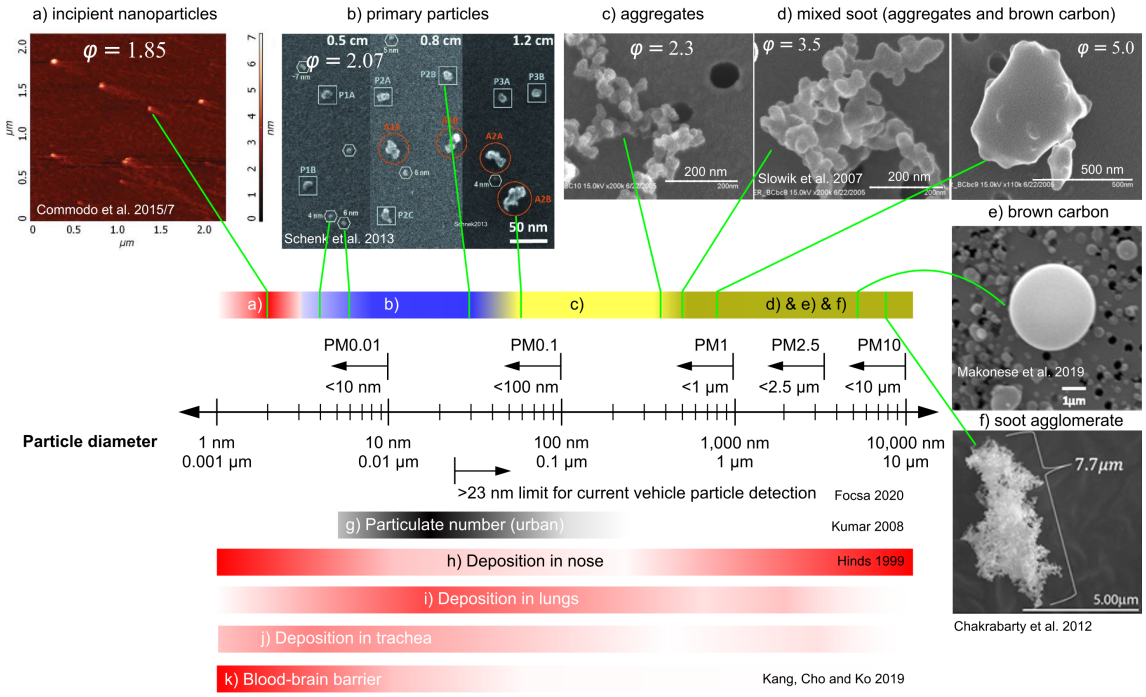


**Figure 5:** *a) – d) Various combustion products sampled from a McKenna burner with an ethylene/air atmospheric pressure flame with varying equivalence ratio. Imaging performed using a) AFM [84], b) HIM [437] and c) SEM [468]. e) – f) Combustion products from solid combustion of coal [312] and biomass [68], respectively, imaged using SEM. g) Particle number distribution in an urban environment [280]. h) – k) Deposition of nanoparticles within mammals from inhalation [200, 239].*

and constitutes most of the soot particulates emitted in the urban environment (see Fig 5g). It could be argued that the condensed aromatics and hydrocarbons lead to a similar accumulation mode in the exhaust of diesel engines, which can be demonstrated by solvent extraction or with a particle thermal denuder [6, 480]. However, as can be shown this condensed brown carbon and mixed soot can span many orders of magnitude and do not necessarily correspond to the range of aerosols found for water droplets in the atmosphere. In short, the “nuclei" mode discussed in aerosol science often refers to water nuclei and not soot nuclei, which are one to two orders of magnitude smaller in diameter.

Many detailed reviews on the health impact of combustion products have been conducted over the past two decades [174, 198, 205, 227, 287, 297, 299, 352, 353, 360, 379, 439, 532] and therefore only a cursory discussion will be provided. We will highlight at the outset, however, that the health impacts of the nanoparticle mode are still not well understood or widely measured [399]. The carcinogenicity of soot and diesel exhaust particulates has been mainly associated with the small aromatic molecules that are present in the brown carbon fraction [17, 47, 417] (such as napthalene, acenaphthylene, acenaphthene, fluorene, phenanthrene, anthracene, pyrene and the particularly active benzo[a]pyrene). Figure 5h) – k) shows the deposition of particles as a function of size [200, 239]. It is clear that the nanoparticles are able to penetrate further into the lungs and translocate

from the lungs into the circulatory system in animals and humans [361, 362] while carrying carcinogenic aromatics [46]. (For engine emissions, other species such as sulfur or transition metals could also adsorb onto the surface of the nanoparticles and may further contribute to their reactivity and oxidative potency.) These nanoparticles have higher surface area to mass ratios compared with larger particles [98, 257]. Due to these large surface areas, nanoparticles are very potent inducers of oxidative stress [46, 367, 535]. Once in the bloodstream they can lead to cardiovascular disease such as heart attacks and strokes due to plaque build-up [114]. There is also evidence that the smallest nanoparticles readily cross the blood-brain barrier in mammals (rodents) [239], causing an inflammatory response and impacting development [8]. *In vitro* toxicological studies have shown that once in the organs, PM0.01 are taken up by cells causing toxicity and mutagenicity [399, 449, 451]. Various studies have also found a significant amount of oxygen on the nanoparticles' surfaces [59, 221, 438] which is correlated to their hydrophilic character [85, 451]. This hydrophilic character leads to partial water solubility, which is cause for concern in human health and suggests an additional impact on the climate through cloud seeding [451]. Black carbon is already implicated in 1.1 W/m$^2$ [44] of climate heating, potentially matching methane's contribution to global heating. Brown carbon has a cooling impact on the atmosphere that offsets the warming caused by black carbon in most agricultural burning [44]. Industrial sources of carbonaceous emissions, on the other hand, are predominantly black carbon and are therefore important to eliminate. These detrimental effects depend on the chemical and structural composition of the nanoparticles, so it is critical that we understand the formation mechanism of these particulates.

Nanoparticles (PM0.01) are emitted by combustion systems, including vehicles, industrial burners and indoor combustion sources like cookstoves/heaters, which are a significant source of airborne nanoparticles [257, 297, 364, 423, 465, 538]. Significantly lower coagulation efficiencies were found for the incipient nanoparticles compared with primary soot particles and have been demonstrated to be emitted from combustion devices [447]. Particularly concerning is that many devices operating with a blue flame, such as natural gas domestic burners or cookstoves, are producing these nanoparticles [364, 399]. The emission of these nanoparticles can be explained by the decreasing physical interactions between nanoparticles below 5 nm leading to low coagulation efficiencies at flame temperatures [212]. The low interaction energy between incipient nanoparticles was confirmed with atomic force microscopy (AFM) studies showing the van der Waals interactions of these particles are decreased compared with primary soot particles [447]. Preliminary work shows that aftertreatment systems are only able to remove 40–50% of particles below 10 nm [463]. Another issue to consider is that fuels which are known to decrease the mass of soot emissions can increase the number of nanoparticles formed, for example biodiesel [313, 465]. Recently, the effective removal of these nanoparticles has been achieved using fibrous and granular activated carbon filters [253]. Challenges still exist for the detection of nanoparticles [144, 258, 259, 509]. Current regulations for the number of particles emitted from vehicles are based on instruments that are only able to measure down to 23 nm reliably [144, 517, 550]. This will be discussed further in Section 5.

## 2.3 Useful materials

Carbon blacks are an old material and yet many new applications are being found for them that rely, critically, on their formation and chemical composition. Examples include conductive carbon black for electronics and battery applications, such as in lithium ion batteries. Some applications that have yet to become widely used include electrodes in dye sensitised solar cells [376], fluorescent carbon nanodots [300] and coherent spin systems for quantum computing [382]. Understanding the earliest stages of carbonaceous particle formation would be beneficial for chemically tuning the properties of carbon blacks. This could provide the means to increase the yield of carbon blacks, thus reducing $CO_2$ emissions. Smaller particles could be produced by understanding particle formation, which can be useful for applications where high surface area is required.

Useful fluorescing carbonaceous quantum dots have also recently been synthesised in flames. As previously mentioned, visible fluorescence is present within sooting flames [159] (see Figure 4). Yet fluorescent nanoparticles were only recently extracted by Liu et al. in 2007 [301]. This was achieved by various acid treatments of candle soot and a size separation using gel electrophoresis to provide nanoparticles with a variety of fluorescent emissions from blue to red (see Figure 6).

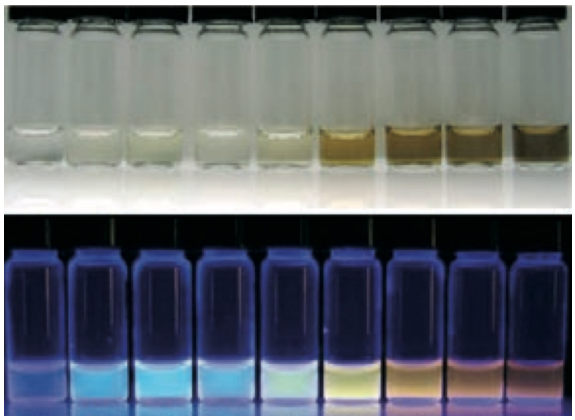

**Figure 6:** *Carbon nanodots illuminated using ordinary light and UV revealing various fluorescence emissions as a function of size [301].*

A simpler solvent-based method was developed using size exclusion chromatography showing similar results [426]. Recently, a one step method was developed by adding various amounts of benzene to a premixed ethylene flame; a single extraction allowed for nanoparticles from blue to yellow to be produced [466]. Raman spectroscopy suggested this tunability was achieved by increasing the size of the aromatic structures within the nanoparticles. Evidence has also mounted for tunability through the nanoparticle diameter [70, 108, 300, 507] (see Figure 7).

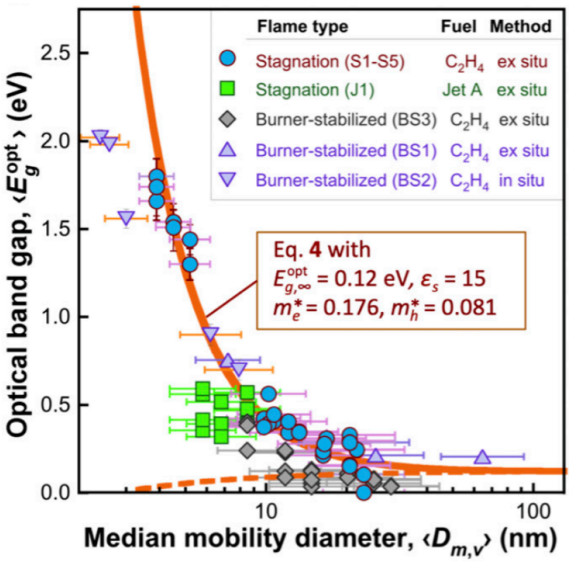


**Figure 7:** *Optical band gap of flame-formed CNPs at room temperature with the expected behaviour of quantum confinement (shown as the solid line) [300].*

# 3 Precursor formation

This section will concentrate on the most important precursors for soot formation, polycyclic aromatic hydrocarbons. Other species that were historically suggested as direct soot precursors to incipient soot nanoparticles including diatomic carbon, carbon monoxide, acetylene, polyynes and chemi-ions will be discussed in Section 4.

## 3.1 Pericondensed aromatic hydrocarbons (PCAH)

In 1825, Faraday demonstrated the significant sooting propensity of aromatic fuels such as benzene, even as he isolated benzene for the first time [137]. The sooting propensity can be illustrated by considering a simple diffusion pool flame (Figure 8), remembering that soot provides the luminosity of the flame (incandescence). For the benzene fuel, soot is rapidly formed at low heights above the burner, but for an aliphatic fuel such as hexane, a "dark zone" is observed that indicates a delay in soot formation [162]. This "dark zone" implies that the aliphatic fuels must be broken down into soot precursor species before becoming soot.

The diffusion flame has been used extensively to assess the sooting propensity of chemicals and fuel blends (see Dryer's 2015 review for a comprehensive discussion [122]). For example, the height reached by a diffusion flame without soot emission occurring (smoke point height) has been a staple of measuring sooting propensities since the beginning of the 20$^{th}$ century [248, 436, 477] (developed into the ASTM D1322 'Standard Test Method for Smoke Point of Kerosene and Aviation Turbine Fuel'). Calcote and Manos in 1983 combined various literature data into a burner agnostic scale – the Threshold Sooting Index (TSI) [60]. Critically, it was found that binary mixtures would follow a linear mixing rule with TSI [165]. (This metric has been extended to oxygenated biofuels

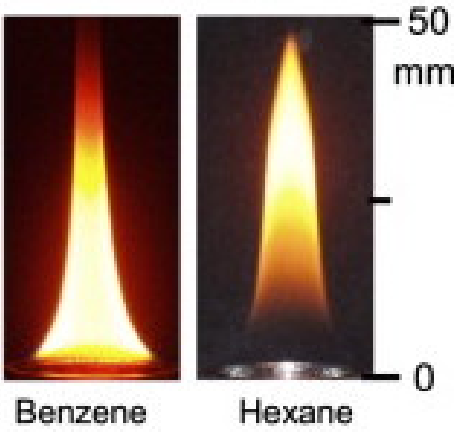


**Figure 8:** *Diffusion pool flame benzene and hexane fuels [263].*

with the Oxygen Extended Sooting Index (OESI) [22], which we will not be discussing in this review.) A theoretical method proposed by Sarofim's group allows prediction of the smoke point of pure hydrocarbon liquids from low-sooting paraffins to highly sooting aromatics; the method was based on structural group contributions [533]. We have recently improved the accuracy of such methods by considering the fuel flow rate as a function of flame height – the so-called fuel uptake rate measurement with threshold imaging (FURTI) method [520]. Independent work confirmed the suitability of this method [309] and further improved the threshold image processing [175]. Another approach is measuring the soot volume fraction using optical approaches such as the yield soot index (YSI) [103, 334]. In the YSI method a methane co-flow diffusion flame is doped with a small amount of the species of interest and the maximum soot volume fraction is measured. This methodology has been found to robustly determine sooting propensities allowing a wide range of species to be analysed, especially larger cyclic and aromatic species that have very low smoke point heights [334, 335, 368]. This model was also expanded to measure and predict the sooting tendency of oxygenated fuels [103]. A methodology was recently developed to improve the Abel transform required to determine the soot volume fraction using a low-cost two-colour pyrometry approach [121]. The micropyrolysis index (MPI) [92, 490] and particle size measurements should also be mentioned for determining sooting propensity [50]. Across the indices the ordering of the sooting propensities follows aromatics>unsaturated aliphatics>saturated aliphatics>oxygenated aliphatics [103, 297, 336]. These results show the critical role fuel structure plays in soot precursor formation. For further discussions we refer the reader to the excellent review by McEnally, Pfefferle, Atakan and Kohse-Höinghaus [336] in which important chemical concepts for fuel decomposition and aromatics formation such as bond energies, resonantly stabilised radicals and unimolecular dissociation of hydrocarbon radicals are explained, as are the decomposition products of several fuels. Several papers summarise new findings related to different kinds of fuels [23, 187, 265, 295, 296, 407] and the development of new techniques for new species to be identified in the fuel decomposition [233, 264, 481, 519]. These results show that aromatic species are critical intermediates of nanoparticle formation. The similarities between many aliphatic fuels also suggest similar thermal fragmentation (pyrolysis) routes to C1–C5 compounds, includ-

ing acetylene ($C_2H_2$), through radical-induced fragmentation to species that subsequently grow into aromatics.

The formation of the first unsaturated ring is of fundamental importance for understanding the formation of polycyclic aromatic hydrocarbons (PAHs) and soot in aliphatic fuels. The formation of benzene and small aromatics has been reviewed previously [35, 149, 264, 336, 420] and three main reaction routes proposed for the formation of the first aromatic PAH, benzene (see Figure 9). The first reaction involves the presence of $C_2H_2$, whereas the others involve resonantly stabilised radicals. In all cases the formation of benzene comes from a sequential addition of small molecules. The acetylene pathway for benzene formation was proposed in the 1980s [35, 155] and has been studied in order to obtain appropriate values of the thermodynamic properties and rate constants of its reactions [340, 472]. This pathway has been found to be dominant at the medium-low temperature regime [151, 354]. Later in 1992, Miller and Melius [354] proposed the self-recombination of propargyl radicals ($C_3H_3$) as the key step in benzene formation. The reaction of two propargyl radicals is favoured over the radical-molecule reaction (C4 radical + acetylene). The reason is that the competing oxidation reactions of $C_3H_3$ are slow due to resonance stabilisation [184]. Therefore, the propargyl pathway is the main mechanism for benzene formation with successive studies recognising this reaction to be predominant at high temperatures [79, 319]. Another proposed mechanism for the first aromatic ring formation is the cyclopentadienyl route, which is a combination of C2 and C3 pathways or the oxidation of aromatics. These radical reactions are in equilibrium; nevertheless, they lead to benzene ring formation that is highly stable due to aromaticity and in this way the reaction is promoted to the products [99, 420]. Recently, the reaction of cyclopentadienyl and acetylene to form tropyl, benzyl and vinylcyclopentadienyl has also been suggested to explain the formation of odd-numbered carbon species [234, 317] and methyl addition [549]. For a more detailed discussion of the early ring formation we recommend the 2020 review by Kohse-Höinghaus [264].

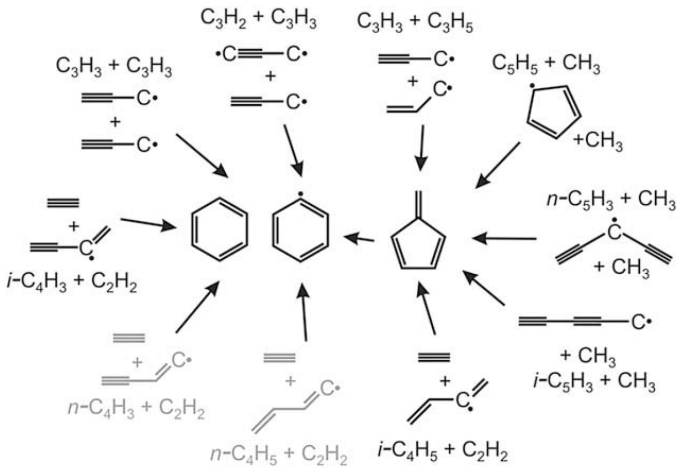


**Figure 9:** *First aromatic ring formation from propangyl ($C_3H_3\cdot$), acetylene ($C_2H_2$), methyl ($CH_3\cdot$), cyclopentadienyl ($C_5H_5\cdot$) with other species possessing a variety of isomeric structures [187].*

Further growth of the aromatics past the first ring proceeds predominantly by a radical

mechanism where a colliding hydrogen radical (or other radical) abstracts an aromatic hydrogen atom, providing a reactive site where acetylene can attach – the so-called hydrogen abstraction carbon (acetylene) addition (HACA) mechanism [149, 155]. Figure 10 shows one pathway that highlights the HACA mechanism, plotting the change in the free energy (at $T = 1800$ K, $P = 1$ atm) and showing a table of species consumed or produced by Wang [511]. The process is seen to be energetically downhill and spontaneous. This is primarily due to the generation of hydrogen gas which entropically drives the aromatic growth [511].

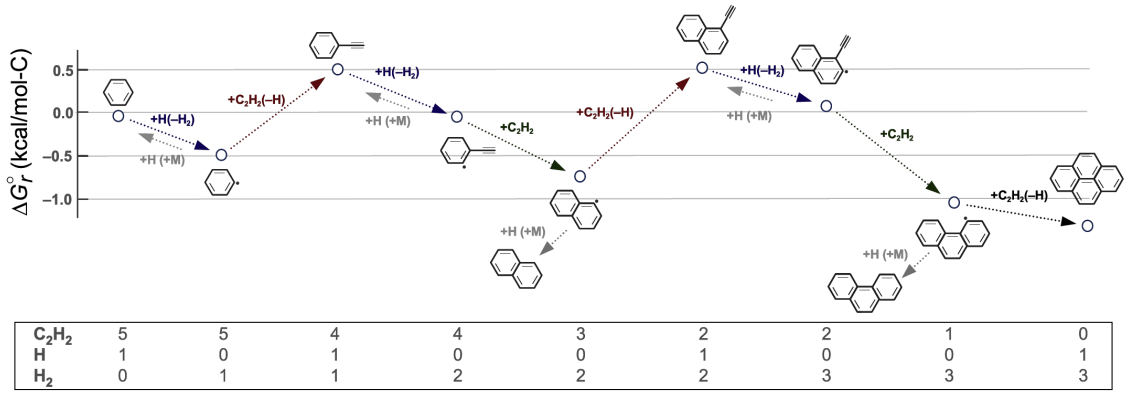


**Figure 10:** *HACA mechanism with energetics of the intermediates and species count highlighting the release of $H_2$ [511]. Used with permission from Elsevier ©.*

As the PAH grows, a variety of topological arrangements of fused aromatic rings are produced. Mass spectrometry allowed the ratio of the carbon to hydrogen ($H/C$ ratio) in the PAH to be measured as $H/C$ =0.3–0.5 [208]. The reason for the presence of these species was explained by considering the thermodynamic stability of pericondensed polyaromatic hydrocarbons (PCAH), revealing an "island of stability" or the "stabilomers" as described by Stein and Fahr, where aromatic rings are fused in a roughly circular fashion [475]. A lower $H/C$ ratio was found than that from PAH with only hexagonal pericondensed rings (maximally pericondensed structures) and explained by the presence of pentagonal rings. Evidence for pentagonal rings has recently been found from tunable photoionisation mass spectrometry, which makes use of synchrotron light sources [231, 234, 347]. For example, many molecular formulas that were historically associated with only 6-membered ring structures were found to be a mixture of isomers with many pentagonal rings. For example, the ion with m/z 202 usually associated with pyrene has been found to be composed of a variety of pentagonal-containing species, such as fluoranthene [231, 234, 347]. Heptagonal rings can also be integrated for specific bay closure reactions next to partially embedded pentagonal rings [292, 343]. This indicates kinetically driven pathways play an important role in PCAH formation and mechanisms that only consider the most thermodynamically stable 6-membered species are incomplete.

Finally, it is interesting to compare the concentration of PCAH with that of soot. It has long been known in mass spectrometry that the concentration of PCAH decreases exponentially with mass [38, 206]. This allows the mole fraction of the species involved in nanoparticle formation to be estimated [511]:

> "If the mole fraction of benzene is $\sim 10^{-3}$, those of pyrene and coronene would be roughly $10^{-5}$ and $10^{-7}$, respectively, which are of the same orders of magnitude as the number densities of soot nuclei ($10^{11}$–$10^{13}$ $cm^{-3}$)"

Therefore, either PCAH the size of pyrene to coronene are involved in soot formation or larger aromatic species of a similar concentration.

## 3.2 Aromers

There has been growing evidence for a larger class of PAH, so-called aromers (=*aro*matic oligo*mers*), from 300–1000 Da [207, 208, 243]. Detection of large aromatic species has been historically challenging [111]. Gas chromatography can detect species up to 8 aromatic rings with liquid chromatography extending this up to 11 rings [28, 206]. The first technique to detect large PAH was positive ion mass spectrometry, allowing species >500 Da to be found in 1965 [45]. However, early laser desorption ionisation mass spectrometry (LDI-MS) in the 1990s was unable to detect these larger aromatics [118]. A breakthrough in LDI came when the laser wavelength was tuned to provide the correct resonance for ionisation of larger PAH species with >11 rings [11, 189, 243] (a more complete explanation of the effect is described in Desgroux et al. [111]). Homann *et al.* demonstrated in low pressure benzene/oxygen rich premixed flames that the concentration of aromatics does not decrease monotonically, as mentioned in the previous section, but increased from 300 Da to 620 Da [208, 243]. Many recent results from LDI and secondary ion-mass spectrometry have reproduced these results [112, 134, 221], while recent advances in mass analysers resolution have shown clear evidence for the presence of large pericondensed aromatics in diffusion [224] and premixed flames [428, 547] with minimal amounts of oxygen present (see Figure 11).

Other evidence for species significantly larger than pyrene came from electron microscopy and spectroscopy. Fringe analysis of high resolution transmission electron micrographs indicate larger species than pyrene are present in early soot [12, 497, 499, 540]. In a recent study comparison with simulated HRTEM images indicated that species closer to circumpyrene in size are present in early soot nanoparticles [3, 49]. Optical spectroscopy also revealed evidence of larger species. Raman spectroscopy suggested aromatic species are approximately 1 nm in size [88]. Optical band gap measurements have been historically employed to suggest the size of the aromatic species [48, 95]. Recent studies show stronger sensitivities to ring topologies [4], functional groups [71], radical character and curvature [341]. On top of this the size of the nanoparticle changes the band gap due to quantum confinement effect [5, 300]. Wang *et al.* demonstrated this size dependence by measuring the optical gap and ionisation energy for nanoparticles >4 nm [108, 300]. This followed quantum confinement, which was shown to be due to stacked aromatic species [5, 70, 507] (see Figure 7). This provided the first possible resolution of a significant question surrounding whether an indirect or direct optical band gap is found in early carbonaceous nanoparticles with the authors concluding that [300] (brackets and italicised text added by the authors of this review):

> "For the CNPs (*carbon nanoparticles*) studied here, however, we find the k exponent is decidedly equal to 2 (*behaves like a material with an indirect*

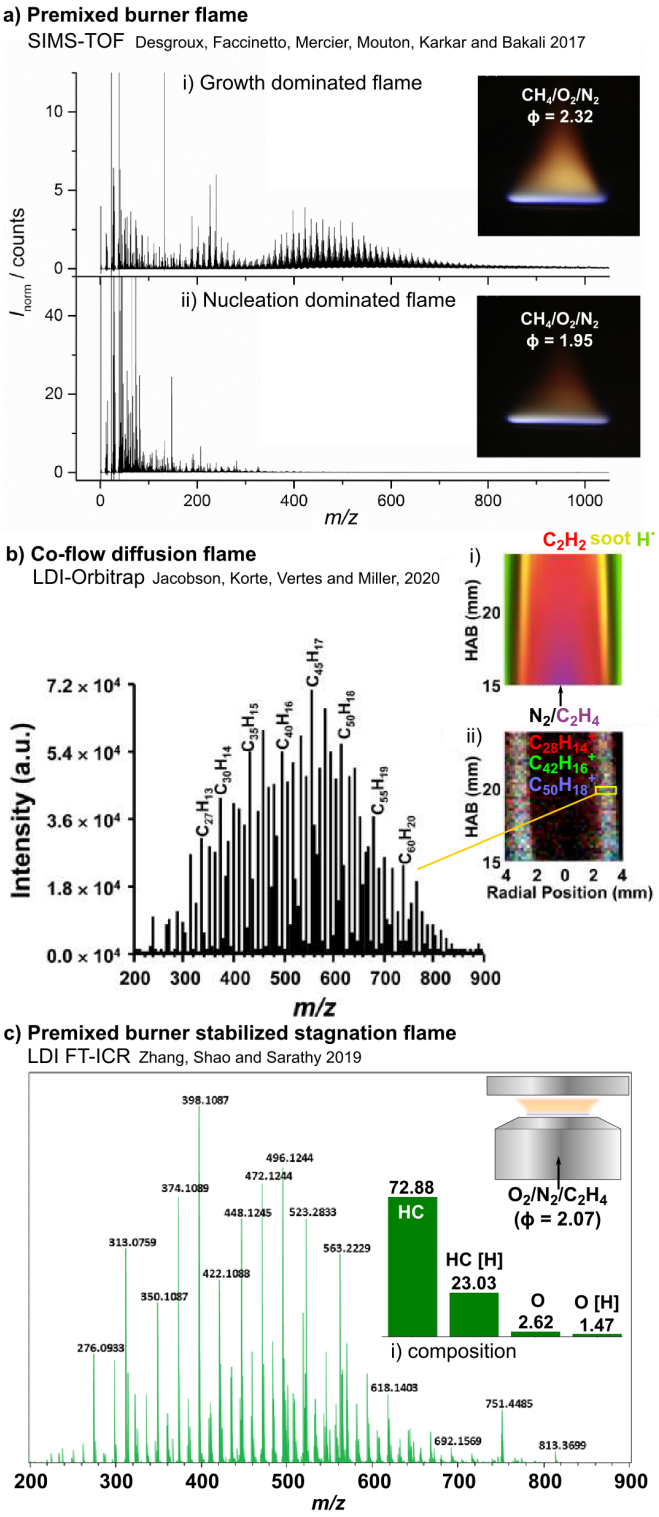


**Figure 11:** *Mass spectrometry results for aromers from Desgroux et al. [112], Jacobson et al. [224], Zhang et al. [547].*

*band gap*) even though the transition is expected to be excitonic ($k = 1/2$). ... Clearly, the band gap exhibits the expected quantum confinement effect."

This size dependency clearly makes the optical band gap less useful for determining the size of aromatic domains.

Further evidence for aromers comes from recent direct imaging of aromatic soot precursors using non-contact or high resolution atomic force microscopy (nc/HR-AFM) from a nearly sooting premixed ethylene flame [88, 444] (see Figure 1). Figure 12 shows the $H/C$ ratio for a collection of these directly imaged molecules with species significantly larger than pyrene seen (up to 650 Da). Additionally, many of these molecules were found to contain a higher concentration of hydrogen than that of maximally pericondensed species (the most condensed a set of hexagonal rings can be in an aromatic), due to methyl groups and the hydrogenation of the edges. This technique was limited to flat aromatics sampled from nearly sooting flames and could not adequately image the 3D aromatic molecules produced in a sooting flame. However, recent advances in HR-AFM have been developed that could allow 3D aromatics to be imaged in the future [327].

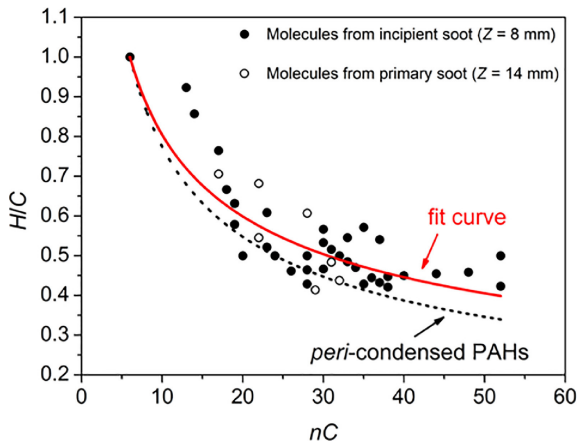


**Figure 12:** *Stoichiometry of aromatics in nearly sooting flames imaged using HR-AFM [88].*

Homann interpreted these larger PAH as containing curved PAH (cPAH) [208]. The evidence for this curvature came from these larger PAH readily forming negative ions. Curved aromatics, as with fullerenes, are known to have a high electron affinity and to easily form negative ions [110]. The type of curvature to which he was referring is due to the complete enclosure of a pentagonal ring within the aromatic network that causes the aromatic molecule to be bent out of plane and curved like a bowl. More direct evidence for curved PAH came from the extraction of corannulene **1a** and completely closed cages of carbon – $C_{60}$ fullerenes – from flames and soot [164, 283] (see Figure 13).

The location of these larger PAH in the flame before the formation of fullerenes, as well as their loss of hydrogen, suggested they were fullerene precursors [16]. Recently, hydrogenated fullerenes have been extracted and crystallised from low pressure flames showing closure can occur before complete loss of hydrogen [484]. However, in most atmospheric flames the conditions for fullerene formation are unfavourable. They are therefore in a low concentration [197] and are unable to contribute to a soot formation mechanism. It appears that curved PAH help to create early soot nanoparticles instead of forming fullerenes. HRTEM has recently demonstrated tortuous fringes suggesting significant curvature [323, 510]. This imaging showed that the earliest soot particles (sampled

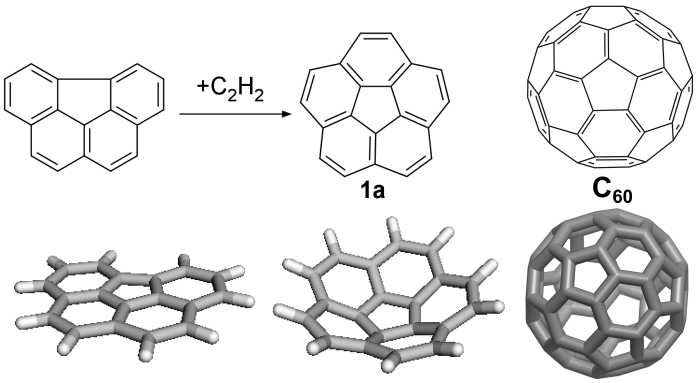


**Figure 13:** *Kekulé and 3D molecular structure of corannulene* ***1a*** *and buckminsterfullerene* $C_{60}$.

from a coflow diffusion flame), in particular, are significantly curved [323] (see Figure 1 HRTEM). The addition of cyclopentadiene [433] and oxygen [216] has also been shown to increase tortuosity of the nanostructure.

It is interesting to consider from where this curvature originates. Figure 14 shows the various mechanisms that have been proposed experimentally or computationally explored for curvature integration due to pentagonal ring embedding. These can be broadly separated into the corannulene pathway and the planar or flat PAH (fPAH) pathways. The corannulene pathway was suggested by Pope and Howard [405]. It involves small PAH and goes through the intermediate corannulene, which is the most well-known curved aromatic. Starting from benzene, a series of HACA reactions generate a variety of fPAH, as well as precursors for the cPAH. Recently, evidence has been found for a HACA pathway starting from cyclopentadiene either with acetylene [234] or methyl addition [531] that generates a variety of fPAH, some with an odd number of $\pi$-electrons giving resonantly stabilised $\pi$-radicals.

The first pentagon integrating reaction is shown in Figure 14i) where an aryl crosslink reaction between benzene and naphthalene is followed by cyclodehydrogenation to form fluoranthene. Aryl crosslinks twist the aromatic species relative to one another so that there is an angle between the two aromatic planes, due to the steric hindrance of the hydrogens neighbouring the crosslink. The $\pi$-bonding is optimal when the two aromatic planes are colinear and therefore at flame temperatures these species rapidly transform into planar structures in a process of cyclodehydrogenation or ring condensation [183]. This reaction is well-known experimentally [388] and is used in many modern mechanisms of soot PAH chemistry [496]. Pope and Howard suggested a mechanism where fluoranthene can also be generated from a thermal edge reconstruction or rearrangement with an edge pentagon becoming embedded and surrounded by three hexagonal rings [405, 445] (Figure 14ii)). HACA growth then can generate the next intermediate, benzo[ghi]fluoranthene, with a partially embedded pentagon enclosed by four hexagonal rings. This intermediate has also been suggested to arise from oxidation of a zig-zag edge [446, 460] or cyclodehydrogenation of the bay edge site of benzo[c]phenanthrene [501] (Figure 14iii) and iv)). Figure 14v) shows the final enclosure of the pentagonal ring through HACA growth onto benzo[ghi]fluoranthene, also referred to as a bay capping reaction. This forms corannu-

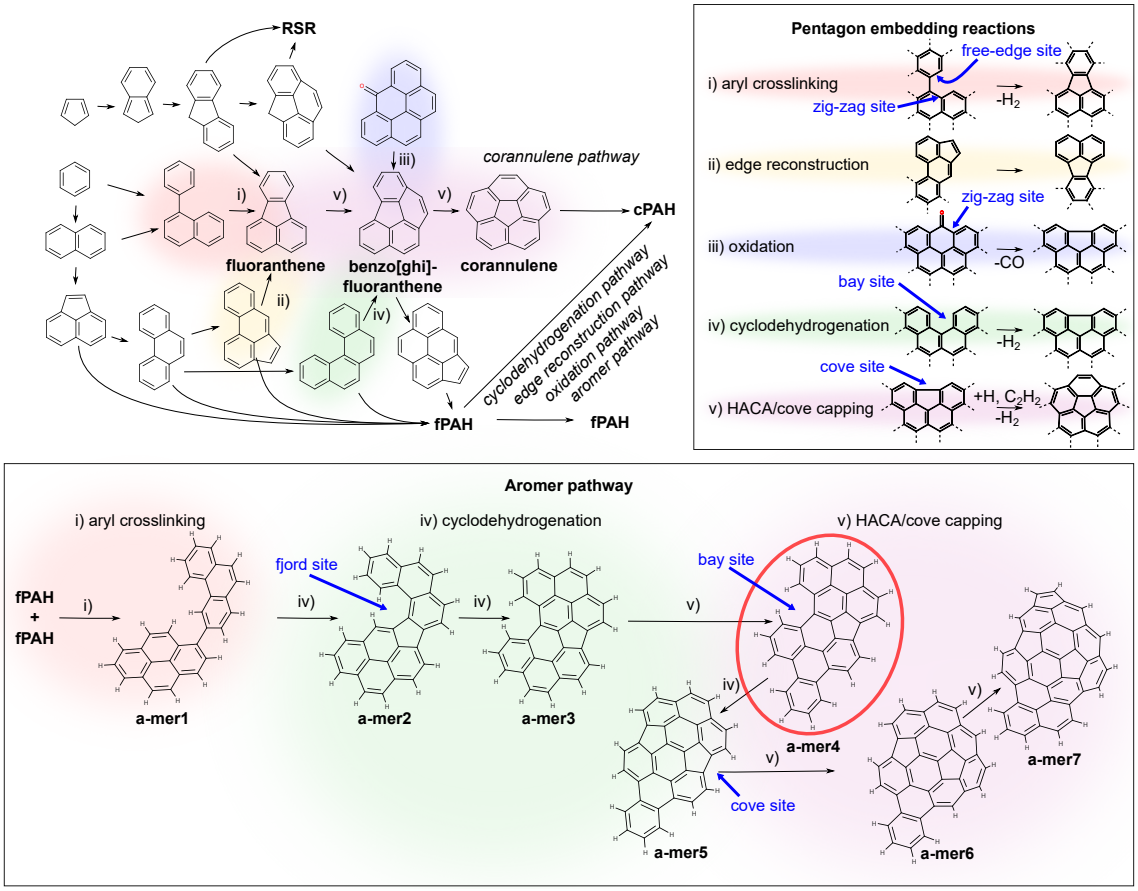


**Figure 14:** *Curvature integration mechanisms. Insets show the pentagon embedding reactions (top right) and an aromer pathway (bottom). The structure circled in red is based on the structure imaged in HR-AFM [88]. Site types are shown with blue arrows to aid the discussion.*

lene, the most well-known curved aromatic with five hexagonal rings enclosing a pentagonal ring [151]. Before this bay capping reaction the aromatic is flat, but afterwards the aromatic is bent into a bowl shape due to the considerable strain created by the enclosed pentagon [324]. This step is critical as the benzo[ghi]fluoranthene is still able to thermally rearrange into a flat aromatic with an edge-based pentagonal ring. However, once the pentagon has become embedded through a HACA reaction the mechanisms for pentagon migration are unlikely to occur. This migration involves $C_2$ rotations (Stone-Thrower-Wales transformations) with significant energetic barriers that kinetically "lock" the less stable pentagonal ring within the hexagonal network, which has been demonstrated experimentally from flash pyrolysis studies [445]. Lafleur et al. [283], however, found corannulene to be in low concentrations in benzene flames [(mass corannulene)/(mass pyrene) from 0.008 to 0.0063]. This pathway therefore appears to not be a primary formation mechanism of cPAH. Given that corannulene is the smallest cPAH known to date [324] this suggests species <300 Da contain rim-based pentagonal rings and partially embedded pentagons present in flat aromatics.

The other curvature integration pathways mirror the reactions seen in the corannulene

pathway yet become more likely as the aromatic grows in size. Cyclodehydrogenation of a bay site followed by HACA growth has been studied using kinetic Monte Carlo simulations of growing aromatics and has been found to enclose pentagonal rings [505, 526, 539]. However, these reactions are slow as they require a particular bay site, which is not readily generated for PAH ∼500 Da in size [152, 292]. This pathway is therefore unlikely to provide the curvatures required to explain the significant curvature integration in flame or fullerene formation [151]. An oxidation pathway is also more likely for larger aromatics [446, 460]. Experimentally it has been found that partially premixed diffusion (Bunsen-type) flames have structures with increasing curvature as a function of oxygen concentration [216] and another recent study using *in situ* HRTEM imaging showed curling of graphene flakes into curved fragments at the surface of a soot particle during oxidation [486]. It is unclear how oxidation contributes to overall curvature integration, however, the low amount of oxygen found in early soot particles [86] and the prevalence of these curved species in diffusion flames [323], with much lower oxygen concentrations, indicates it is also not a primary curvature integration mechanism. Recent Kinetic Monte Carlo simulations of PAH growth from HACA do not support the significant curvature integration observed [152, 292].

Thermal rearrangements have also been found to provide partially embedded pentagonal rings that with further HACA growth produce cPAH. These can be classified into pericondensation and edge rearrangements. Pericondensation involves the rearrangements of orthocondensed (otherwise known as catacondensed) PAH into pericondensed structures with the loss of hydrogen. This has been extensively explored as a synthesis route for buckybowls and graphene. Edges of aromatics are highly mobile above 1300 K and rapidly rearrange into partially and fully embedded pentagonal rings [445]. Some example schemes from buckybowl synthesis are shown in Figure 15.

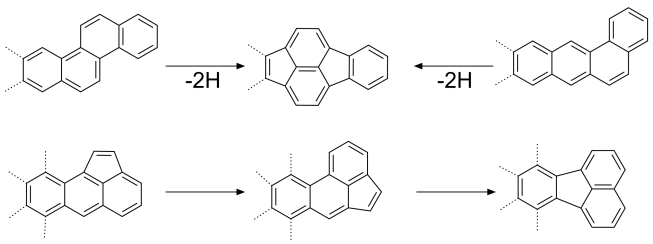


**Figure 15:** *Thermal rearrangements that embed pentagonal rings [445].*

Another recent experimental work on the transformation of ethylene into graphene on an Rh(111) surface using scanning tunnelling microscopy found some interesting thermal transformation of PAH [508]. Long acenes were formed at 470 K, however, heating to 670 K led to the breakup of these long acenes and the formation of pericondensed species, which then grow and fuse into polycrystalline graphene. While in this study the surface likely catalysed the rapid rearrangement reaction, flash pyrolysis experiments demonstrate that past 1300 K aromatics also rapidly rearrange into pericondensed species in the gas phase [445]. However, edge rearrangement competes with the embedding of pentagonal rings by allowing the migration of the ring to an edge (as it does not involve hydrogen loss and is therefore highly reversible). This inhibits the formation of long acenes and was the initial reason curvature integration was not explored in the combustion community for a

long time – the edge rearrangements were thought to provide more thermodynamically stable planar PAH [151].

Homann suggested the aromer pathway, which is a combination of the aryl crosslinking, cyclodehydrogenation and HACA/bay capping reactions, which can be seen in the inset of Figure 14. The experimental evidence for the aryl crosslinking of two fPAH arises from the presence of a separate distribution of larger PAH as mentioned, suggesting a separate mechanism from HACA [243]. Recent tandem mass spectrometry has also been used with collision-induced dissociation to show the fragmentation of this mode at 500 Da [2]. The possible radical sites for aryl crosslinking are shown in Figure 16, which we will consider further in Section 5.

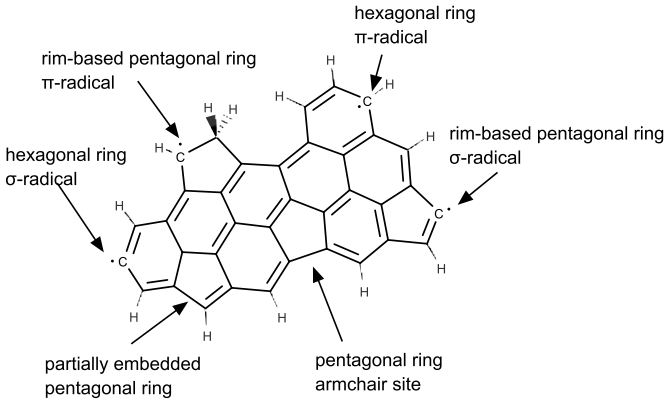


**Figure 16:** *Reactive edges of soot precursors.*

Howard considered $\sigma$-radicals produced from hydrogen abstraction from the edges of hexagonal and pentagonal rings and computed that molecules $\sim$600 Da in size would contain 1–6 of these radical sites each [213]. $\sigma$-radicals are considered to be the most reactive radicals in the flame, reacting readily with acetylene in the HACA mechanism [149]. Homann mentioned the odd number of carbon atoms and suggested a non-bonding $\pi$-radical that is delocalised [243] and has also been imaged in HR-AFM [443]. These resonantly stabilised $\pi$-radicals are important in benzene formation, as mentioned – being less reactive than $\sigma$-radicals, they have longer lifetimes in the flame [187]. Frenklach also suggested a partially saturated rim-based pentagonal ring that forms a $\pi$-radical, showing it impacts surface rearrangements and growth processes, but did not explore the reactivity with other aromatic species [148, 526].

Subsequent cyclisation of these aryl crosslinked species has been experimentally found to favour the partial embedding of a pentagonal ring as opposed to a hexagonal ring [375, 435] (*e.g.* the free edge found to preferentially react with the zig-zag edge in pyrene pyrolysis, forming a pentagonal ring). Evidence for the crosslinking and partial embedding of pentagonal rings has also been found in HR-AFM with species found containing two aromatic segments with predominantly hexagonal rings linked via pentagonal rings [88]. These species are then highly orthocondensed and will thermally rearrange and cyclodehydrogenate to further embed the pentagonal rings, with HACA growth also contributing to pentagon enclosure. **a-mer4** from Figure 14 is highlighted as this aromatic network was experimentally observed in HR-AFM experiments [88] (see Figure 1 IS4). This species

can rapidly cyclodehydrogenate or have HACA growth to form the curved species. Evidence for this suggestion comes from the slightly higher concentration of hydrogen rich species in the 300 to 700 Da range and the fact that dehydrogenation rapidly gives way to species in the region with $H/C$ ratios suggesting pericondensed structures [16]. More recently principal component analysis of SIMS-TOF MS of soot from flames provides strong evidence that the aromers arise from the crosslink of small aromatics with a subsequent dehydrogenation of 4–8 hydrogens [135].

Aryl crosslinks and further thermal rearrangements are known to integrate curvature and close cage structures completely [420]. However, it appears that multiple crosslinks are required for the integration of sufficient curvature to allow for complete formation into fullerenes. This is not possible in most atmospheric sooting flames but is possible in some low pressure flames [208, 505]. It is interesting to note that Homann originally suggested that this process was enhanced by the physical interactions holding PAH dimers together while the edge zipped up [25, 208]. This was based on an early model of fullerene formation called the zipper mechanism [222]. The summarised synthesis work on buckybowls highlights that no such physical interactions are required and that crosslinks, cyclodehydrogenation and thermal rearrangements are sufficient to integrate curvature.

## 3.3 Clustering (reactive) PAH

Reactive PAH were reported in one of the first mass spectrometry studies of aromatic species in flames in 1967 [207]. Of course, the naming "reactive PAH" contains the connotation of a chemical reaction occurring, which is yet to be shown, therefore we refer to these species as clustering PAH through either physical or chemical routes. It was only during the 2000s that mass spectrometric instruments were able to observe the molecule to particle transition, using soft laser desorption ionisation techniques with reflectron time of flight mass analysers that could extend the range to millions of mass/charge (m/z) units [180]. With these instruments Grotheer and colleagues were able to show clustering of aromatics [190]. Figure 17 shows this series of peaks with a periodicity of $\Delta$ =500 Da. This has since been reproduced in an atmospheric ethylene premixed flame by Carbone *et al.* revealing clustering only for the positive ions with $\Delta$ =450 Da and not for the negative ions [65] (see Figure 48). We will return to this work at the end of the review.

From these mass spectrometric studies the collision efficiency to allow such aromatic species to form was computed [410]. This comes from a simple second order kinetic model that has been found to accurately describe the rate of soot formation,

$$R_{C_{a,b}} = C_E \times \beta_{a,b} \times C_a \times C_b, \tag{1}$$

where the reaction rate, $R_{C_{a,b}}$, of molecules $a$ and $b$ is the product of the collision efficiency, $C_E$ (other authors use $\alpha$ [511], $\beta$ [127] or $\gamma$ [250]); the free molecular collision coagulation kernel, $\beta_{a,b}$; the concentration of molecules $a$, $C_a$; and $b$, $C_b$ (in Kraft notation [410]) (the collision efficiency is often further split to separately consider the van der Waals enhancement, $E_F$, which we will not do in this work). It was found that aromatic species would need to cluster with a collision efficiency $C_E > 0.01$ (see Figure 31). In other studies collision efficiencies ranging from $C_E = 0.01 - 1.0$ have been used to produce the

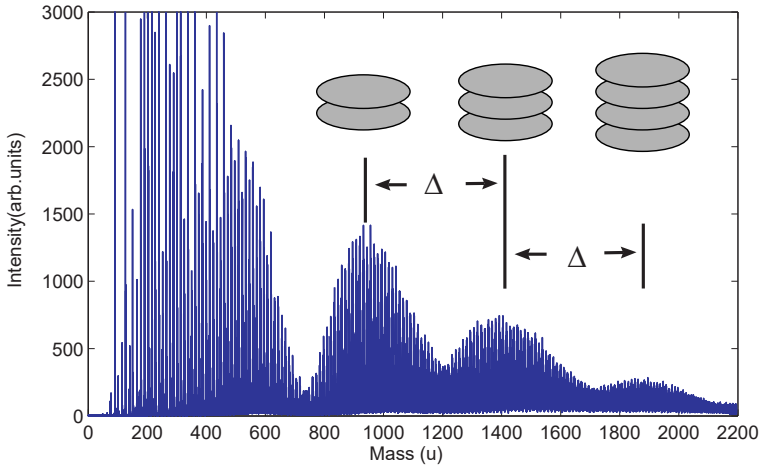


**Figure 17:** *Mass spectrum of high-molecular weight species extracted from a 13 kPa acetylene–oxygen flame ($\phi$ = 3.25) by molecular beam mass spectrometry with 193 nm laser ionisation [190].*

flux of nanoparticles found during soot formation [420]. Therefore the goal of the rest of the review is to explore what is allowing PAH to stably cluster at these high collision efficiencies.

# 4 Nanoparticle formation

Before exploring soot nanoparticle formation some nomenclature must be discussed. There is much controversy around the language used to describe soot nanoparticles [351]. This confusion is unsurprising, given that there is still significant uncertainty surrounding how soot forms. Without understanding the possible mechanisms for soot formation which are operating under different conditions, naming conventions will remain undecided. For the sake of clarity we will make a distinction between chemical and physical soot nanoparticle formation preferring the term *soot inception* unless specifically discussing a physical nucleation mechanism. Mechanisms involving both chemical and physical interactions will be referred to as *physically stabilised soot inception*.

While the transition from molecule to nanoparticle is somewhat arbitrary we will consider any species above 1000 Da to be a nanoparticle. The growth of curved or planar pericondensed PAH is generally not found to extend past 1000 Da. This cutoff is consistent with how the term nanoparticle is used in the combustion literature [98, 351, 511]. There are some exceptions to this definition that are worth mentioning. PAH growth has been seen to extend slightly further than 1000 Da, in low-pressure premixed acetylene flames [208, 243, 521] and inverse diffusion flames [425]. Another exception is the formation of giant fullerenes that can extend to 6000 Da within low-pressure flames [25]. As our focus is on the nanoparticles that lead to primary and aggregate carbonaceous particles these exceptions are not an issue.

Table 1 lists the many mechanisms that have been proposed for the formation of carbonaceous nanoparticles in hydrocarbon flames. The main strengths and weaknesses that have been discussed in the literature are consolidated. We have provided a schematic of the most relevant nanoparticle formation mechanisms in Figure 18.

**Table 1:** *Formation mechanisms for soot nanoparticles*

| Mechanisms | Scheme | Strengths | Weaknesses | Possible |
|---|---|---|---|---|
| ***Disproportionation*** | | | | |
| (a) diatomic carbon | fuel $\rightarrow C_2(g) + H_2 \rightarrow C(s)$ | Presence of $C_2$ [470] | Cyanogen ($C_2H_2$)-oxygen flame sootless [416]. Soot contains hydrogen [483] | N |
| (b) CO | $2CO \rightarrow C(s) + CO_2$ | Boudouard reaction well-known on surfaces low T [26] | Thermodynamics do not support this past 1000 K [203] | N |
| ***Acetylene inception*** | | | | |
| (c) amorphous | $-HC_2\bullet + C_2H_2 \rightarrow -C_2HC\bullet$ | Suggested from photolysis of acetylene [406] | Too slow does not explain aromatic sooting propensity [390] | N |
| (d) $C_2$, acetylene | $C_2 + C_2H_2 \rightarrow 2C_2H + 2C_2H_2 \rightarrow 2C_4H_3 + C_2 \rightarrow 2C_4H_2 + C_2H$ | Presence of $C_2$ [470], reactivity of $C_2H_2$[161]. | Insufficient $C_2$ at flame T [390] | N |
| (e) chemi-ion | $C_3H_3^+ + C_2H_2 \rightarrow PAH^+$ | Ion-neutral reactions are fast. Ions and soot correlated [63] | Reactions are not much faster [513]. Neutral PAH grow at same rate [521]. | N |
| (f) graphene | $PAH(\sigma\bullet) + C_2H_2 \rightarrow PAH$ | Acetylene rapidly forms PAH [149, 155] | Too slow for nanoparticle formation [149] | N |
| (g) icospiral | $PAH(\sigma\bullet) + C_2H_2 \rightarrow$ cPAH $\rightarrow$ icospiral | PAH integrate curvature [179, 284], fullerenes present in flames [164], templated growth is fast [276], spirals and onions observed in HRTEM [218, 494] | Too slow [151] Closure into fullerenes is more likely [208] | N |
| ***Polyyne inception*** | | | | |

| Mechanisms | Scheme | Strengths | Weaknesses | Possible |
|---|---|---|---|---|
| (h) ring condensation | $C_2H_2 \rightarrow C_nH_2 \rightarrow$ PAH $\rightarrow$ C(s) | Many polyynes in the flame [207] thermodynamically stable at high T [273]. | Rigid unlikely to cyclise [304], Radical-induced fragmentation limits growth [163] | N |
| (i) fullerene-like | $C_2H_2 \rightarrow C_nH_2 \rightarrow$ cage (+ PAH) | Fullerenes present in flames [164], High pressure acetylene pyrolysis simulations [544] | Radical-induced fragmentation limits growth [163], fullerenes are formed from aromatic species in flames [208] | N |
| ***Polyaromatic inception*** | | | | |
| (j) PAH, PAH | PAH + PAH $\rightarrow$ PAH–PAH | PAH most stable, resistant to radical-induced fragmentation, so high conc. [149, 475], curved PAH were also suggested [7] | Edges are unreactive in peri-condensed PAH [442] | N |
| (k) aryl, PAH(6) | PAH($\sigma\bullet$) + PAH(6) $\rightarrow$ PAH–PAH | Hydrogen abstraction generates many $\sigma$ radicals [213] | Requires large number of radicals for creating $\sigma$-radicals [511], prone to radical-induced fragmentation [149]. Low collision efficiency [316] | Y |
| (l) aryl, aryl | PAH($\sigma\bullet$) + PAH($\sigma\bullet$) $\rightarrow$ PAH–PAH | Hydrogen abstraction generates many $\sigma$ radicals [213], strong bonds formed [316] | Requires large number of radicals for creating $\sigma$-radicals [511]. Low conc. and collision efficiency [316]. | Y |

| Mechanisms | Scheme | Strengths | Weaknesses | Possible |
|---|---|---|---|---|
| (m) cyclodehydrogenation | PAH–PAH → PAH | Ring condensation rapid at flame temperature [435] reduces impact of radical-induced fragmentation | Slow as relies on the initial crosslinking of aryl radicals (see above) | Y |
| (n) pentaring, pentaring | PAH(5) + PAH(5) → PAH(5)=(5)PAH | Pentaring more reactive than 6-mem ring [434] | Symmetry forbidden [2+2] pericyclic reaction unstable [434] | N |
| (o) aryl, pentaring (AALH) | PAH($\sigma\bullet$) + PAH(5) → PAH–(5)PAH | Pentaring more reactive than 6-mem ring [100] | Requires large number of radicals for creating $\sigma$-radicals [511] Prone to radical-induced fragmentation | Y |
| (p) aryl, RSR (CHRCR) | PAH($\pi\bullet$) + PAH($\sigma\bullet$) → PAH–PAH($\pi\bullet$) | $\pi$ and $\sigma$-radicals are present in flames [213, 243]. Reaction easily lose H to regenerate $\pi$-radical [234]. | Conc. of odd number PAH (likely to be $\pi$-radicals) not reduced [243]. Radical-induced fragmentation likely to compete | Y |
| (q) aryne | PAH($\sigma\bullet$) → PAH($2\sigma\bullet$) + PAH → PAH–PAH | Strong binding energy to PAH [82, 201] | Requires two H-abstraction the second having a significant barrier [211], unlikely due to concentrations of H and PAH($\sigma\bullet$) [213]. | Y |

| Mechanisms | Scheme | Strengths | Weaknesses | Possible |
|---|---|---|---|---|
| (r) furans | PAH($\sigma\bullet$) + O$\bullet$ + PAH $\rightarrow$ Furan | Furan-like PAH found in some flames [232] Oxygen can enhance soot formation [345] | Large oxygen rich PAH not found in most flames [208, 546]. Insignificant oxygen content has been found in early soot particles [86]. Prone to thermal and radical-induced fragmentation [500]. | Y |
| ***Physical nucleation*** | | | | |
| (s) aliphatic polymer | Fuel $\rightarrow$ polymer $\rightarrow$ [polymer]$_n$ | Some vapours are light emitting [147]. Condensible tar is seen in thermophoretic samples from diffusion flames [249, 415], | Aliphatics are found to increase later in the flame [58, 386] Prone to radical-induced fragmentation [414], condensible tar can be removed with fast sampling [51] | N |
| (t) fPAH | fPAH $\rightarrow$ [fPAH]$_n$ | Irreversible dimerisation describes soot particle number [512]. Internal rotors improve stability [442] | Dimerisation not possible <650 Da [427, 489, 511] | N |
| (u) aliphatic chains | PAH + aliphatic $\rightarrow\sim$PAH$\sim\rightarrow$ [$\sim$PAH$\sim$]$_n$ | Evidence from IR spectroscopy [339]. Seen in HR-AFM [444]. Improves clustering [130] | Enhancement is minor $\approx$2.5 kcal/mol [130] | N |
| (v) aromatic polymer | Fuel $\rightarrow$ aromatics $\rightarrow$ polymer $\rightarrow$ [polymer]$_n$ | Large polymers are able to condense [125, 285]. Large polymer can cluster more effectively [217] Extension of polyaromatic routes | Prone to radical-induced fragmentation, aromatically linked PAH have lower dimerisation propensity than fPAH [132, 217] | Y |

| Mechanisms | Scheme | Strengths | Weaknesses | Possible |
|---|---|---|---|---|
| (w) penta-linked (APLH) | (5)PAH($\sigma\bullet$) + (5)PAH $\rightarrow$ PAH(5)=(5)PAH | Imaged HR-AFM [444], provides planar species [396] | Unlikely for (5)PAH($\sigma\bullet$) to react with pentaring, prone to radical-induced fragmentation | Y |
| (x) cPAH | cPAH $\rightarrow$ [cPAH]$_n$ | van der Waals interactions [25]. Dipole-dipole interactions improve clustering [323, 324] | Dimerisation energy similar to fPAH *i.e.* too low [324]. | N |
| (y) ion, fPAH | fPAH + $C_3H_3^+ \rightarrow$ [PAH]$_n^+$ | Long range interactions [266] | Low binding energies [69]. | N |
| (z) ion, cPAH | fPAH $\rightarrow$ cPAH + $C_3H_3^+ \rightarrow$ $[cPAH]_n^+$ | Long range strong interactions [323, 324] | Limited to small clusters [323] | Y |
| ***Physically stabilised soot inception*** | | | | |
| (aa) zipper mechanism | fPAH–fPAH $\rightarrow$ cPAH | Suggested for fullerene formation [7, 25, 208] | aryl-linked aromatics cannot stack | N |
| (bb) internal rotors | [PAH($\sigma\bullet$),PAH(5)]* $\rightarrow$ PAH–PAH | Increase interaction time for polyaromatic reactions [73, 152], bound internal rotors for large PAH [489] | aryl-radical collision did not reveal effect for small PAH [316] | Y |
| (cc) aliphatic, bridge-linked ($CH_2$-ABLH) | PAH($\pi\bullet$) + PAH($\pi\bullet$) $\rightarrow$ PAH–$(CH_2)_m$–PAH | Allows stacking and bonding [125, 130]. Mass spectrometric evidence in some flames [2] | Prone to radical-induced fragmentation [414] high $H/C$ ratio | Y |
| (dd) acetylene bridge-linked ($C_2H_2$-ABLH) | PAH($\pi\bullet$) + PAH($\sigma\bullet$) + $C_2H_2 \rightarrow$ PAH–$C_2H_2$–PAH | Acetylene is abundant and $\pi$-radicals have also been detected [444], stable complex [166] | Prone to radical-induced fragmentation [414], polymerisation mechanism unclear | Y |

| Mechanisms | Scheme | Strengths | Weaknesses | Possible |
|---|---|---|---|---|
| (ee) $O_2$, bridge-linked ($O_2$-ABLH) | PAH($\pi\bullet$) + $O_2$ + PAH $\rightarrow$ PAH–$O_2$–PAH | Oxygen is found to enhance soot formation in some flames [131], binding energies are strong [318] | Insignificant oxygen content has been found in early soot nanoparticles [86]. Prone to radical-induced fragmentation [414], polymerisation mechanism unclear | N |
| (ff) excimer | PAH* + PAH $\rightarrow$ (PAH,PAH)* | Presence of fluorescence in soot forming region [358], excimers formed with stacked PAH [357]. LIF gives long duration fluorescence supporting excimers [346, 464] | Weak interactions over nanoseconds [346], can only stabilise a dimer, trimers weakly bound [102] | N |
| (gg) multicentre-linked (pancake) (AMLH) | PAH(deloc.$\pi\bullet$) + PAH(deloc.$\pi\bullet$)$\rightarrow$ PAH$\equiv$PAH | Many $\pi$-radicals present [444, 506], multicentre bonds allowing stacking [246, 469] | Low interaction energy [93, 246, 324], polymerisation mechanism unclear | Y |
| (hh) zig-zag-linked (AZLH) | 2diradicaloid $\rightarrow$ diradicaloid=diradicaloid | Long acenes have large dimerisation energies [269, 511], large PAH with zig-zag edges can be open-shell singlet multiradicals [401, 545] | Acenes fragment or rearrange into fPAH [508, 511] | Y |
| (ii) rim-linked (ARLH) | PAH(loc.$\pi\bullet$) + PAH($\pi\bullet$)/(5)PAH $\rightarrow$ PAH–PAH | Many $\pi$-radicals present [444, 506]. Strong bonding and less prone to radical-induced fragmentation [324] | Unknown concentrations of PAH(loc.$\pi\bullet$) and collision efficiencies. | Y |

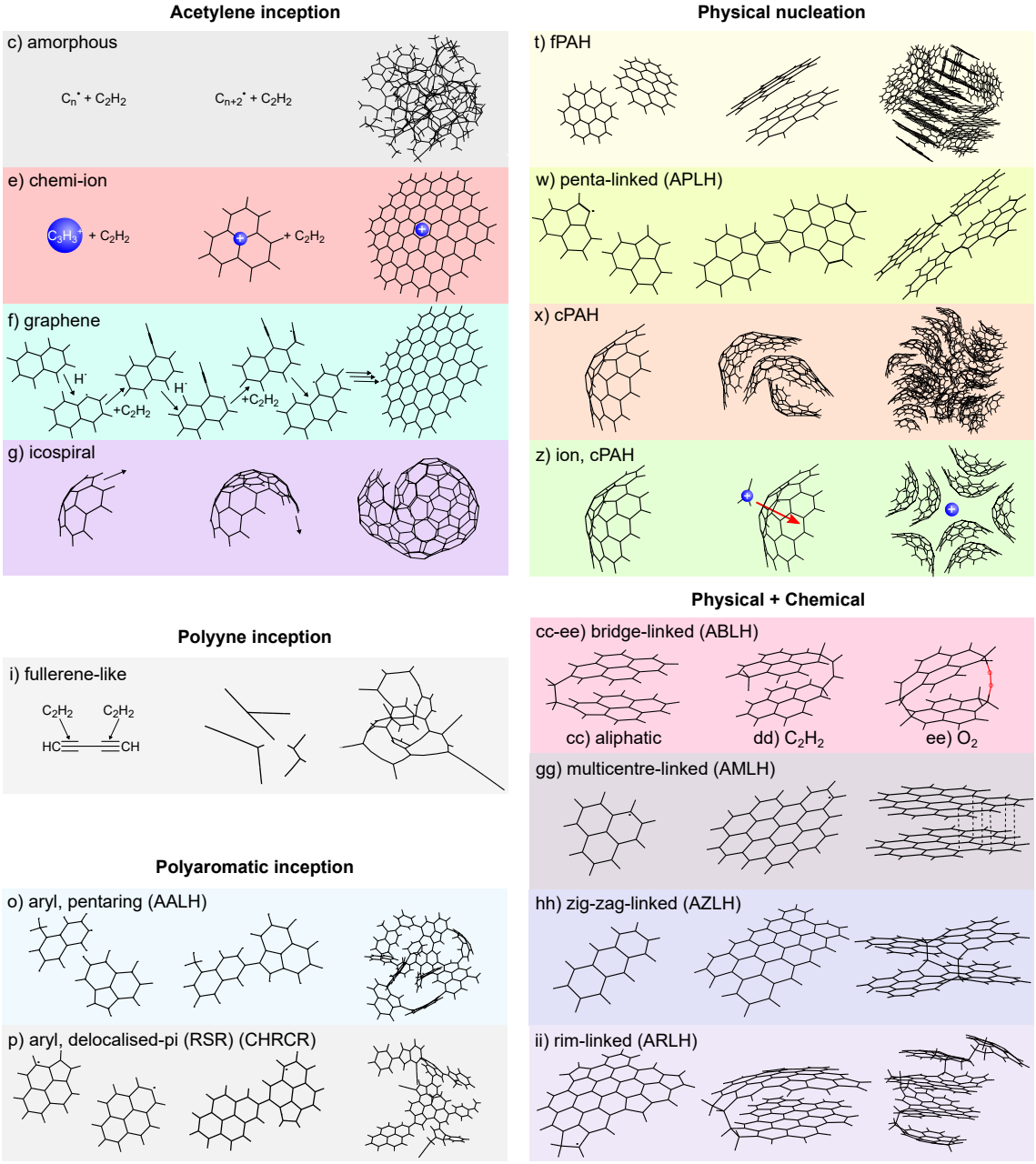


**Figure 18:** *Schematics for a collection of mechanisms from Table 1.*

## 4.1 Disproportionation

### 4.1.1 Diatomic carbon

The earliest view of soot formation was the direct dehydrogenation of hydrocarbon fuel into solid carbon particulates [390]. Flame spectroscopy revealed how the ethylene optical emissions gave way to the $C_2$ Swan bands that cease upon soot formation with increasing fuel/air ratio [470]. This led Smith in 1940 to suggest disproportionation of the fuel

into $C_2$ and $H_2$ with the former reacting to form solid soot [see Table1(a)]. However, the concentration of $C_2$ was found to be too low to support soot formation [162]. Additionally, flames in which $C_2$ was produced in high concentrations, such as cyanogen ($C_2N_2$) [416] and carbon suboxide ($C_3O_2$) [261] were not found to produce significant amounts of soot.

### 4.1.2 Carbon monoxide

Carbon monoxide is produced during fuel pyrolysis and is one of the main products of incomplete combustion [see Table 1 (b)]. The so-called Boudouard reaction was well known in gas works where carbon monoxide decomposes into solid carbon deposits and was also suggested to produce soot in flames [26] [see Table1(b)] according to,

$$2\,CO \rightleftharpoons C + CO_2. \tag{2}$$

An equilibrium analysis revealed that >1000 K carbon formation is not possible from Eq. 2 and therefore carbon monoxide dominates at flame temperatures over disproportionation to solid carbon and $CO_2$ [203].

## 4.2 Acetylene inception

Acetylene was first isolated by Davy in 1836 and he immediately noted the significant luminosity and soot produced by this fuel [107]. It was then found by Berthelot [30] and others that acetylene was formed from the pyrolysis of hydrocarbons in arcs and tube furnaces (the partial combustion of hydrocarbons now being the dominant industrial synthesis route for acetylene). In the 1890s, Lewes then showed that this acetylene formation preceded soot formation in flames. This led him to posit that acetylene was the origin of luminosity and therefore soot in flames [294].

Acetylene was thought to directly decompose into carbon [see Table 1 (c)]. This was supported in the 20$^{th}$ century by Porter's flash pyrolysis experiments which showed acetylene decomposition to a carbonaceous material after photoexcitation with no extractable fractions [406]. Porter suggested a radical chain mechanism where acetylene added to the carbon material and hydrogen was evolved (leading to what we will call an amorphous inception mechanism). Others suggested acetylene reactions catalysed by $C_2$ [390] [see Table 1(d) and Figure 18]. The presence of significant hydrogen in early soot nanoparticles suggested more complex mechanisms were at play and other intermediates such as PAH were important.

### 4.2.1 Chemi-ions

Calcote provided one of the first detailed reviews of various pathways and kinetics involved in acetylene inception [62] [see Table 1(e) and Figure 18]. He showed that none of the chemical mechanisms suggested before the 1980s were rapid enough to explain

nanoparticle formation. Instead he proposed an ionic mechanism based on two observations: the correlation between soot and charged species in the flame and the more rapid reactions between neutral species and charged hydrocarbon ions.

The correlations between soot and charged species are well known and have been thoroughly reviewed by Hayhurst and Jones [192], Lawton and Weinberg [289] and more recently by Fialkov [143]. Briefly, significant concentrations of charged species are found in flames ($10^{15} - 10^{17}$ ions $m^{-3}$) [63]. This significant charge concentration was found to be due to chemi-ionisation reactions and not thermal ionisation [61]. Chemi-ionisation reactions rely on the ejection of an electron in a high energy reaction between an electronically excited molecule and a neutral species. The main reactions are [192],

$$CH^* + O^\bullet \longrightarrow CHO^+ + e^- \quad (3)$$
$$CHO^+ + H_2O \longrightarrow CO + H_3O^+ \quad (4)$$
$$CHO^+ + \text{neutral} \longrightarrow \text{protonated}^+ + CO, \quad (5)$$

where the electronically excited carbyne ($CH^*$) reacts with an oxygen radical ($O^\bullet$) to form the cation radical formyl ($CHO^+$) (Eq. 3). This is a short-lived radical that reacts rapidly with other species including water to form the hydronium ion ($H_3O^+$), which is the predominant ion in combustion exhaust (Eq. 4). Many other small positively charged hydrocarbons are produced through protonation with the formyl cation (Eq. 5).

Under rich flame conditions the primary ion-producing reactions become,

$$CH^* + C_2H_2 \longrightarrow C_3H_3^+ + e^- \quad (6)$$
$$C_3H_3^+ + C_2H_2 \longrightarrow C_5H_5^+ + C_2H_2(=>PAH^+) \quad (7)$$
$$PAH + C_3H_3^+ \longrightarrow PAH^+ + C_3H_2 \quad (8)$$
$$PAH + CHO^+ \longrightarrow PAH^+ + CO \quad (9)$$
$$\text{soot} \rightleftharpoons \text{soot}^+ + e^- \quad (10)$$

where excited carbyne reacts with acetylene ($C_2H_2$) to form propenyl cations ($C_3H_3^+$), which are longer lived as they can cyclise into cyclopropenyl (Eq. 6) [143]. PAH are known to become charged as they grow through reactions with chemi-ions (Eq. 8 and 9) allowing them to be detected in molecular beam mass spectrometry [208]. Soot can also be charged due to thermoionisation (Eq. 10), which is most effective for larger soot particles that are sufficiently carbonised to have a low ionisation potential [143].

Why are these positive species not neutralised by negative charges? The primary negative species are electrons, however, low concentrations of negatively charged species are able to be formed *i.e.* in equilibrium with the electrons.

$$e^- + H_2O \rightleftharpoons H + OH^- \quad (11)$$
$$e^- + C_2H_2 \rightleftharpoons H + C_2H^- \quad (12)$$
$$e^- + \text{cPAH} \rightleftharpoons \text{cPAH}^- \quad (13)$$
$$e^- + \text{soot} \rightleftharpoons \text{soot}^- \quad (14)$$

Formation of negative ions is through electron attachment. However, the electron affinity of most flame species is low, with most electron ion collisions leading to elastic scattering and the majority of negative charge being carried by the electrons [143, 192], explaining the lack of neutralisation. One exception is curved PAH that easily become negatively charged by electron attachment (Eq. 13) as shown by Homann [208]. Soot is also able to become negatively charged through electron attachment. Electron attachment (Eq. 14) and thermoionisation (Eq. 10) provide a charge equilibrium for primary and aggregate soot particles that is in thermal equilibrium and is described by the Saha equation [143]. This list of flame ion reactions is not comprehensive and more complete mechanisms exist for flame ion chemistry [9].

Returning to soot formation, Calcote also drew attention to the location of the ions directly preceding the formation of soot nanoparticles and to the similar soot and ionic concentrations ($10^{14} - 10^{16}$ ions $m^{-3}$), suggesting a causative link [63]. It is well known in atmospheric chemistry that reactions involving charged species and neutral molecules can be significantly faster than neutral-neutral reactions due to the ion-induced dipole forces. Calcote's reaction mechanism was then based on the chemical polymerisation of $C_3H_3^+$with acetylene (Eq. 8) [see Figure 18(e)) [63]. Charged molecules were suggested to polymerise by acetylene addition at a rate sufficient to explain the rapid growth of soot nanoparticles. Preliminary studies supported such a mechanism with positive nanoparticles up to $8\times10^3$ Da being found using mass spectrometry in acetylene flames [25, 163] (see Figure 2). Experiments involving electric fields and easily ionised metals were used to further explore such a mechanism.

Electric fields have long been seen as evidence for an ionic mechanism. Brande in 1814 showed that a diffusion flame can be deflected towards a negative plate within an electric field, suggesting positive ion carriers [57]. The influence on soot inception is complicated by the production of an ionic wind. The accelerated chemi-ions in the flame entrain air in such a way that the flame is aerated, increasing oxidation and thereby reducing soot formation. Weinberg and Place were the first to realise that a counterflow diffusion flame would allow for the ionic wind to have no impact on the aeration of the flame [402]. Counterflow flames provide a flame front nearly perpendicular to the flow field. An electric field applied across the burner provides an ionic wind which merely shifts the stagnation surface. Soot's residence time in the flame was found to be reduced, as was the size of the primary particles. Figure 19 shows the significant impact of the electric field on the formation of soot, recently measured using laser induced incandescence (LII) and the aromatic species and the hydroxyl radical using laser induced fluorescence (LIF) [391].

The application of the electric field shifts the reaction zone, providing some quenching of the production of aromatics, however the impact on soot formation is more pronounced with a complete removal of soot. This effect is most pronounced when the electric field is established in such a way that shifts the chemi-ions formed in the chemiluminescence zone of the flame into the soot-forming region, increasing the charge present during soot formation [143]. Weinberg suggested that this reduces soot formation through the attachment of cations to soot particles;

$$\text{soot} + C_3H_3^+ \longrightarrow \text{soot}^+ + C_2H_2 + H. \tag{15}$$

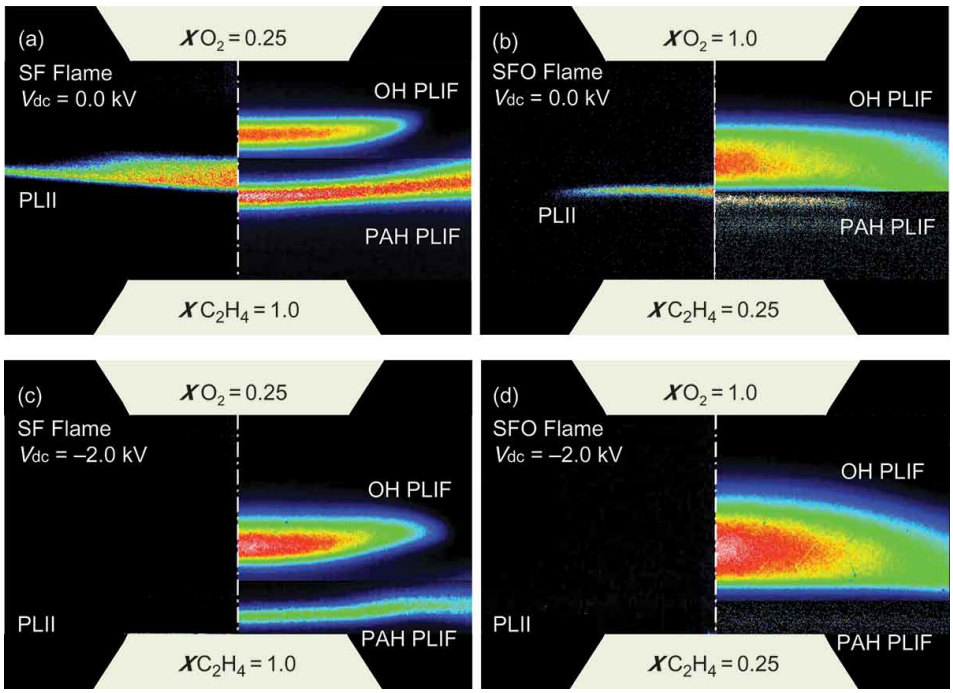


**Figure 19:** *Counterflow $C_2H_4/O_2/N_2$ diffusion flame without (top) and with (bottom) an electric potential difference of 1 kV applied. Luminous carbon particulates measured with LII disappear from the flame upon application of the field (from Park et al. [391]; used with permission from Taylor & Francis ©).*

This charge attachment reduces the coagulation efficiency of soot as an excess of positive charge increases the repulsion between soot primary particles. The reduction in size was then initially attributed to a reduction in the residence time of the charged soot in the flame. By tuning the direct current (DC) electric field strength, these positively charged soot particles were held in the soot forming region allowing them to grow to hundreds of nanometres in size. Weinberg suggested that only soot particles larger than 9 nm are able to become charged due to charge attachment as in Eq. 19 [289]. However, as has been mentioned, smaller charged soot particles were also able to be observed as the resolution of particle mass analysers improved [25]. Furthermore, the electric field uniformly reduces all soot primary particles' diameters, not only the charged soot, indicating that charged and neutral soot formation is linked [143]. Using DC electric fields to explore the impact of ionic soot mechanisms is challenging. The flow fields can be modified through ionic winds and chemi-ions can shift within the flame, which makes distinguishing the impact on soot nanoparticle formation and soot aggregation difficult to decouple. Alternating current electric fields have also shown an impact on soot nanoparticle formation, causing soot emissions to increase or decrease depending on the frequency and voltages used [271]. These results were interpreted as primarily impacting soot nanoparticle formation.

Addition of easily ionised metals to flames provides a further opportunity to explore ionic aspects of soot formation. They have long been studied as anti-smoke additives to diesel engines [311] and in polystyrene combustion have been shown to reduce soot emissions

by 50–90% [76]. These metals increase the ionic concentrations through a variety of processes and reactions:

$$\mathrm{M} \rightleftharpoons \mathrm{M^+ + e^-} \tag{16}$$
$$\mathrm{H_3O^+ + M} \longrightarrow \mathrm{H_2O + M^+ + \mathit{H}} \tag{17}$$
$$\mathrm{C_3H_3^+ + M} \longrightarrow \mathrm{H_2O + M^+ + \mathit{H}} \tag{18}$$
$$\mathrm{soot + M^+} \longrightarrow \mathrm{soot^+ + M} \tag{19}$$
$$\mathrm{M + OH^*} \longrightarrow \mathrm{MOH^+ + e^-} \tag{20}$$

Thermal ionisation (Eq. 16) is the first mechanism considered for alkali metals as they possess a low ionisation potential. Ashton and Hayhurst found the rate of thermoionisation in a hydrogen flame to be determined by the Saha equation to be $k = (9.9 \pm 2.7) \times 10^{-9} T^{1/2} \exp(-E_I/RT)$, where $E_I$ is the ionisation energy [14], with the ionisation energy decreasing down the periodic table. Therefore, larger alkali metals are expected to be more completely ionised in flames. Experimentally, the ionisation effect can be less pronounced as seen in Figure 20 where ionic concentrations are measured in a premixed flame aspirated with water and alkali metal salts [173].

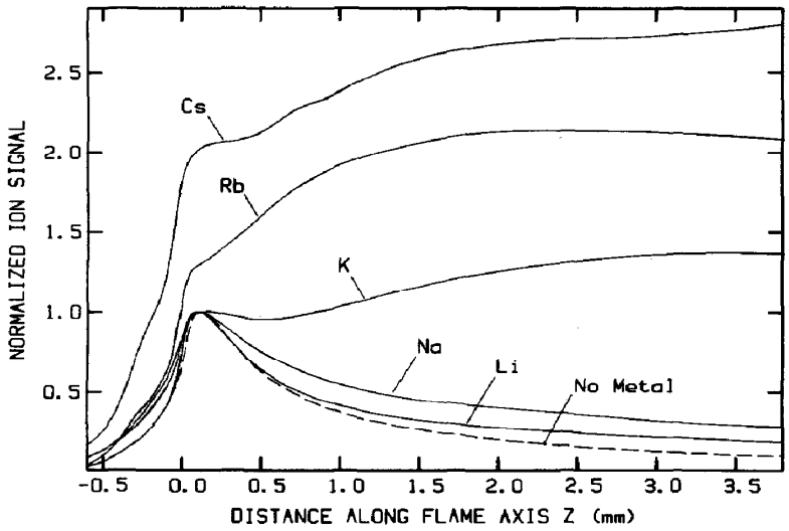


**Figure 20:** *Ionisation signal with different metals addition to a flame [173]. Used with permission from Elsevier ©.*

The delayed increase in the charge concentration for most alkali metals in this flame was explained as being due to the high ionisation potential of these species. The charging later in the flame when the temperature is lower was suggested to be due to charge transfer from hydronium ions (Eq. 17). This late charging is thought to primarily influence coagulation. In this case charge transfer to soot increases the fraction of positively charged soot primary particles (Eq. 19). This reduces the coagulation efficiency due to electrostatic repulsion, producing less aggregated primary particles that are more easily oxidised. A partially premixed coflow ethylene flame ($\phi = 2.27$) probed by small angle X-ray diffraction indicates that the size of primary particles does not change significantly for potassium addition [116]. However, in a different flame (premixed ethylene/air flame on a modified

PerkinElmer burner $\phi = 2.6$) potassium has been found to reduce the size of the primary particles [457]. Another complication in interpreting these results is the catalytic effects of alkali metals. Potassium has been found to reduce the mass of soot as demonstrated by experiments that added the potassium further downstream where coagulation has already occurred, finding a decrease in soot emissions from improved oxidation [421]. Recent x-ray absorption spectroscopy supports a "classic catalytic role of activating $O_2$ into reactive oxygen species, with the mobility of $K_2CO_3$ facilitating the transport of these species to immobilised soot particles" [106]. Similar challenges exist for interpreting the role of alkaline metals such as Ba, Ca, *etc.*, which are known to form cations with excited hydroxyl (Eq. 20) and catalytically produce the aggressive hydroxyl oxidant [143].

Cesium provided the most insight on the impact of ions on soot formation. It has a low ionisation potential and leads to a considerable increase in the ionic concentration in the soot-forming region of most flames [173], as seen in Figure 20. In the mentioned study, a decrease in the chemi-ion corresponding to $C_3H_3^+$ was found, indicating that the metal was able to be charged through charge transfer according to Eq. 18, and was suggested to support a chemical mechanism for soot formation (Eq. 7). The reduction in soot was then explained by Calcote as being due to the reduction in the number of nuclei chemically grown from $C_3H_3^+$ [63]. However, *in situ* small angle X-ray diffraction using synchrotron light sources has recently found that addition of cesium into an ethylene flame doubles the concentration of the smallest carbon nanoparticles [116], which suggests that cesium promotes soot nanoparticle formation. This would indicate a different mechanism for the soot reduction, one which is more in line with that suggested by Howard and Kausch [214] and Bonczyk [43]. In their proposed mechanisms, the ions play a stabilising role for nuclei, producing large numbers of smaller carbon particles with increased surface area allowing for their rapid oxidation and destruction and leading to less soot.

Other significant critiques arose for the chemical ionic mechanism. Firstly, there are a number of soot-producing systems that have insufficient ion concentration such as benzene flames, and shocktube and pyrolysis experiments [420]. Secondly, the molecular beam mass spectrometry of larger PAH found that the growth rates of charged and neutral aromatic molecules were similar [521]. While reaction rates can be enhanced in atmospheric chemistry for ions at room temperature, the high temperatures found in flames provide thermal energies that overwhelm any ion induced-dipole enhancement [513]. The HACA mechanism was able to explain the growth of pericondensed aromatic molecules under flame conditions [149]. We will return to ion-induced nucleation mechanisms in the context of physical nucleation later in this review.

### 4.2.2 Graphene

Graphene inception is the continuous growth of PAH into large graphene molecules that could be considered soot nanoparticles [see Table 1(f) and Figure 18] [143]. This is envisaged to occur through the HACA mechanism reported earlier. It is clear, however, that while this mechanism can explain the formation of small aromatics it cannot explain the rapid formation of soot nanoparticles [149]. There is an exception for low pressure acetylene oxygen flames in which the conditions can be tuned to produce large flat graphene structures [521]. This is of considerable interest for the gas phase synthesis of graphene

for material and electronic applications. Most of the studies have focused on plasma reactors using low sooting fuels, such as alcohols, to produce graphene in the gas phase at atmospheric pressure [104, 105, 380].

### 4.2.3 Icospiral

The discovery of fullerenes by Kroto, Curl and Smalley in 1985 [277] led to a number of new proposed mechanisms for soot formation [275]. The first was that buckminsterfullerene $C_{60}$ could act as the nuclei for soot formation, an idea supported by their detection in many flames [164]. However, the concentration of $C_{60}$ was found to be too low in atmospheric flames to be critical for soot formation [197, 208]. A second suggestion was that an aromatic species was formed that then curved onto itself like a nautilus shell [276] [see Table 1(g) and Figure 18]. This geometry (the icospiral) is achieved by two screw dislocations allowing for the fullerene layers to be wound together (see Figure 21). Evidence came from electron micrographs of soot and carbon black particles, where closed and spiral fringes indicated such an icospiral seed [218, 494]. These early electron micrographs were often formed by strong electron annealing that allowed for the fringes to be clearly imaged. Such annealing is known to convert many zero-dimensional carbon materials such as nanodiamond into fullerene-like carbon onions [495], suggesting these structures were formed during the electron irradiation.

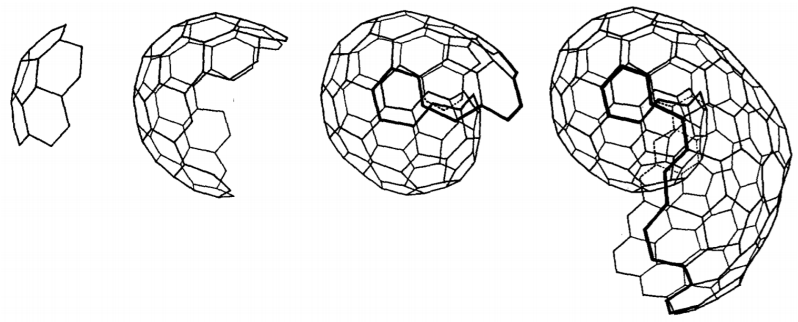

**Figure 21:** *Icospiral growth as envisaged by Kroto [274].*

The icospiral geometry was suggested to allow for a templated growth process, which is known to be rapid and the predominant growth mechanism in crystals [241]. Templated HACA growth of a small aromatic on a larger aromatic structure has recently been studied computationally. Minimal, if any, impact at flame temperatures was found for templated HACA growth due to the weak dispersion forces involved between acetylene and graphene [219]. Some other recent work on curved aromatics has shown that HACA type growth can be enhanced due to curvature integration [409]. While this is of considerable interest, curvature has also been found to modify the rate of oxidation, in most cases increasing it [413, 460]. Therefore, more work is required to determine the impact that curvature has on PAH growth. Nevertheless, the fraction of hydrogen in early soot and the molecular beam mass spectrometry support the view that PAH growth does not extend past 1000 Da in most sooting flames, which would be required for an icospiral [151].

In summary, acetylene is critical for PAH formation and therefore indirectly contributes to soot nanoparticle formation. However, the HACA mechanism is too slow to explain

soot nanoparticle formation through chemi-ions, graphene or icospirals due to weak enhancements to PAH growth from ionic, curvature or templating effects.

## 4.3 Polyyne inception

The first molecular beam mass spectrometry from within flames revealed significant concentrations of polyynes, suggesting they could be potential precursors to soot nanoparticles [207]. The first kinetic mechanism developed focused on the stability of polyynes that are more thermodynamically stable than pericondensed aromatic hydrocarbons at high temperatures ($>$ 2000 K) and suggested a ring condensation where polyynes react to form PAH species [273] [see Table 1(h)]. Recent molecular beam Raman analysis also confirms the significant concentration of polyynes present in soot forming flames [290]. However, mass spectrometry showed that the growth of these species was not found to extend past 150 Da [207, 208]. This is because they are prone to degrade in flame environments [152]. Hydrogen addition to growing polyynes leads to radical-induced fragmentation such as,

$$\mathrm{H{-}C{\equiv}C{-}C{\equiv}C{-}H + H \longrightarrow H{-}{\bullet}C{=}CH{-}C{\equiv}C{-}H \longrightarrow H{-}C{\equiv}C{-}H + {\bullet}C{\equiv}C{-}H,}$$

where the hydrogen addition leads to a radical that fragments through a $\beta$-scission, breaking up the chain [152]. Analysis of polyynes in partial equilibrium with hydrogen radicals and $H_2$ supported a limit to polyyne growth of $C_mH_2$, m$<$ 16 [163, 348]. Long polyynes are unlikely to cyclise into PAH due to their high rigidity [304] and are more likely to degrade to acetylene and C4 species that cyclise into aromatics [187].

Recently a range of reactive molecular dynamics simulations have suggested a fullerene-like polyyne mechanism [185, 302, 544] reminiscent of fullerene cage formation which was explored using similar methods [408] [see Table 1(i) and Figure 18]. In simulations involving highly concentrated mixtures of acetylene and other fuels (0.1 g/cm$^3$), and extreme temperatures (2000–3000 K), large fullerene-like structures were observed [185, 302, 544]. These extreme temperatures led to C$-$H bonds breaking and a large number of radicals. These radicals quickly react in these high density simulations forming long polyyne chains that condense into cage structures. As mentioned, such growth of long polyynes is not observed in hydrocarbon flames. The $H/C$ ratio of early soot particles of 0.3–0.5 is also too high compared with what would be expected from a fullerene-like polyyne mechanism. Careful reactive molecular dynamics of benzene pyrolysis showed the initial formation of aromatic species [429, 430] and only after loss of all hydrogen atoms were fullerene-like cages able to form. This result matches what is observed in the negative mass spectrum during aromatic to fullerene transformations [16, 208, 484].

The discussion of polyynes leads us to recall the comment from Bansal and Donnet from 1993 [119],

> "...the presence of a particular species is not sufficient proof that it is involved in soot formation. A species may be present because it is not reactive."

It also reminds us that a soot mechanism must take into account not only the construction

towards soot nanoparticles (forward reactions) but also the destruction of the growing species (reverse reactions).

## 4.4 Polyaromatic inception

Some of the first to discuss a polyaromatic inception were perhaps Rummel and Veh [424] in 1941 when they suggested that moderately sized PAH molecules react to form soot. These species had by then been extracted from sooting flames. These suggestions were revived in the discussion of meteoric carbon [371] and nanoorganic carbon in flames in the 1990s [96].

We have already mentioned that as PAH grow in the harsh environment within flames they form and fragment producing many stabliomers (highly pericondensed aromatics) [475], which have low reactivity towards each other [see Table 1(j)]. Therefore, most polyaromatic inception mechanisms rely on a radical species recombining with other radicals or crosslinking with reactive PAH.

Experimental evidence for such a mechanism historically came from the significant increase in soot production following the addition of chlorine, which increased the aryl-radical [338] and aromer concentrations [208]. Since then crosslinked species and species strongly suggesting crosslinking have been directly imaged in HR-AFM (see Figure 1) [88]. Indirect evidence has also been provided from the mechanical hardness of primary soot particles measured with *in situ* nanoindentation HRTEM experiments [33]. These experiments combined with reactive molecular dynamics simulations suggested 2–3 crosslinks per aromatic molecule to provide the hardness values measured [395, 397].

### 4.4.1 Aryl-linked (AALH)

Palmer and Cullis suggested that the abstraction of an edge-based hydrogen from a PAH produces an aryl-type $\sigma$-radical able to react with highly pericondensed PAH containing hexagonal rings (PAH(6)) – called aryl, PAH(6) polyaromatic inception [see Table 1(k)]. This follows the well-known pyrolysis reactions of aromatics. Benzene pyrolysis, for example, will yield biphenyl with subsequent phenyl additions giving triphenylene, which involves cyclodehydrogenation [see Table 1(m)] [375]. Unless subsequent cyclodehydrogenation takes place the phenyl addition of an aromatic ring is prone to radical-induced fragmentation [136]; for example, bond energies of only $-20$ to $-23$ kcal/mol are found for the hydrogenated biphenyl/phenyl-benzene complex [392, 456]. Therefore, soot mechanisms involving the reaction between $\sigma$-radicals and highly aromatic PAH were not considered to be thermally stable in the flame under radical-induced fragmentation [149]. However, in pyrolysis systems operating at lower temperatures the aryl, PAH(6) inception appears to be critical for the formation of PAH and possibly carbonaceous nanoparticles [81, 455].

As the aromatic network increases in size, so does the concentration of $\sigma$-radicals. This in turn heightens the chance of the aryl, aryl polyaromatic inception mechanism occurring [see Table 1(l)]. Howard calculated that PAH $\approx$ 600 Da in partial equilibrium with $H^{\bullet}/H_2$ would each possess 1–6 $\sigma$-radicals [213]. However, a reactive molecular dynamics study

of colliding aryl, aryl PAH found collision efficiencies one to two orders of magnitude lower than those required for nanoparticle formation as discussed [316]. Some other reactive molecular dynamics studies have suggested rapid clustering of PAH radicals with close to unity $C_E$ [244, 542]. However, the high densities used, 0.2 g/cm$^3$, significantly enhanced the clustering, overshadowing the importance of fragmentation in flames where PAH densities are closer to $10^{-6}$ g/cm$^3$ [143]. Furthermore, high temperatures (2000–2500 K) have often been used to speed up these simulations, leading to direct hydrogen loss from PAH edges. This does not occur, at any significant rate, at flame temperatures without a radical abstraction, which means that the number of radicals in these simulations is much higher than in the flame itself [244, 542]. Mao *et al.* demonstrated the importance of temperature in reactive molecular dynamics [315]. No clustering was seen at 2000 K for PCAH such as coronene, however increasing the temperature to 2500 K led to hydrogen loss and chemical inception [315]. Chemical inception has been suggested at 2000 K if nickel is added [452]. However, even in combustion systems with large amounts of metals present, such as diesel engines, small amounts of metals are found in the soot suggesting no critical role of metals in soot formation [369]. Finally, aryl-linked hydrocarbons have been suggested to be prone to radical-induced fragmentation [152] and therefore many consider cyclodehydrogenation to be critical for the high temperature stability of these linkages [see Table 1(m)] as was discussed for the aromers.

More reactive edges on PAH molecules than maximally pericondensed were also suggested to contribute to polyaromatic inception, such as rim-based pentagonal rings on acenaphalene or the 9, 10 low aromaticity free edge on phenanthrene [100]. While these edges are not able to crosslink with one another (*e.g.* [2+2] pericyclic reactions are symmetry forbidden [434]) [see Table 1(n) and Figure 18] they have significant reactivity with aryl $\sigma$-radical PAH [see Table 1(o) and Figure 18o)]. Significant bond energies of $-44$ kcal/mol have been calculated between phenyl radicals and acenapthalene crosslinks, suggesting flame stability [503]. However, hydrogen addition to the unsaturated carbon part of the crosslink would lead to its breakdown. This could be overcome if hydrogen abstraction from the saturated carbon formed a closed shell C–C bond, which is highly stable [504] forming aromatic aryl-linked hydrocarbons (AALH) (see Figure 22a). As with the other aryl crosslinks a similar low collision efficiency would be expected as was determined for aryl, aryl crosslinks [316].

Another recent suggestion was a partial dehydrogenation to form a so-called E-bridge structure allowing the formation of 3D structures [152]. Evidence for such an E-bridge can be seen in the fully unsaturated dual pentagon species in Figure 1 IS30 from Commodo et al. [88].

Within an aromatic molecule $\pi$-electrons are able to form aromatically stabilised bonds, providing significant thermal stability within PAH and allowing for radical chain reactions [see Table 1(p) and Figure 18]. An odd number of $\pi$-electrons within hexagonal ring networks gives rise to a resonance stabilised $\pi$-radical (RSR). A mechanism where RSR crosslinks with aryl radicals forms a strong bond (80 kcal/mol) [234]. Critically, this is rapidly further stabilised by a unimolecular loss of hydrogen with a barrier of only 4.5 kcal/mol. This regenerates the RSR and further reactions with aryl radicals can occur. The ability to regenerate the reactive radicals led to the naming of the mechanism as clustering of hydrocarbons by radical-chain reactions (CHRCR) [see Table 1(r)] and

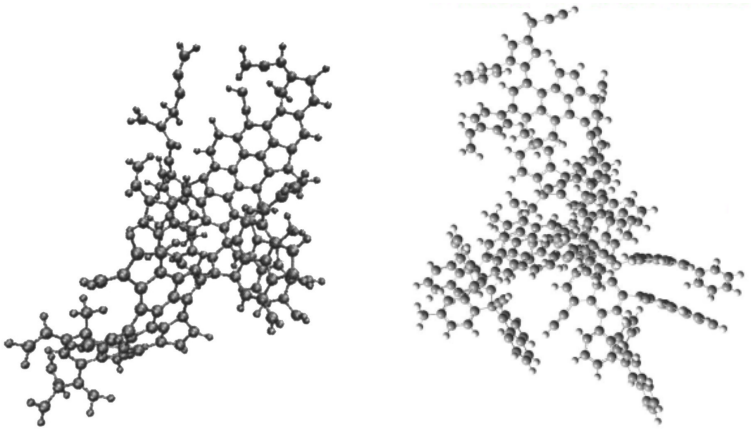

**(a)** *Aliphatically/aromatic linked hydrocarbons nanoparticle [502]. Used with permission from AIP©*

**(b)** *Clustering of hydrocarbons by radical-chain reactions (CHRCR) from RSR and σ-radical [234]. Used with permission from Science AAAS©*

**Figure 22:** *Nanoparticles from chemical inception mechanisms.*

Figure 22b]. Unlike the mechanism between aryl and pentarings [see Table 1(p)] CHRCR does not require a subsequent hydrogen abstraction to produce a stable single bond as hydrogen is instead easily lost, restoring aromaticity to the π-radical.

However, such an increased reactivity for odd numbers of carbon atoms, most likely to be RSR, was not seen experimentally [243]. For this reason Homann suggested that RSR were not very reactive. While it is true that aromatic RSR are less reactive for recombination with themselves, reactions with σ-radicals were calculated to form strong bonds even more so than with pentaring polyaromatic inception [234]. A possible answer to the similar concentration of even and odd carbon fragments in flames could be inferred from the recent HR-AFM analysis of aromatic soot precursors [88]. Many regions of aromatic molecules with an odd number of carbon atoms, where one would anticipate an RSR to form, contained a hydrogen saturated edge carbon (most often on a zig-zag site). Therefore, while aromatic σ-radicals can react with RSR, it is unclear how hydrogen radicals could terminate these chain reactions. Hydrogen addition across the crosslink at the unsaturated carbon atom, or neighbouring site, could also lead to fragmentation [152]. Therefore, experimental evidence for this pathway is required as well as a full reaction mechanism that includes all pathways. A low collision efficiency would also be expected for this mechanism, as with other polyaromatic inception mechanisms (see Section 5.1).

### 4.4.2 Arynes

Arynes can form when two hydrogen abstractions occur from a PAH and have been suggested to allow for PAH crosslinking [82] [see Table 1(q)]. The simplest example is *o*-benzyne (1,2-didehydrobenzene see Figure 23), where benzene loses two neighbouring

hydrogen atoms [82, 201].

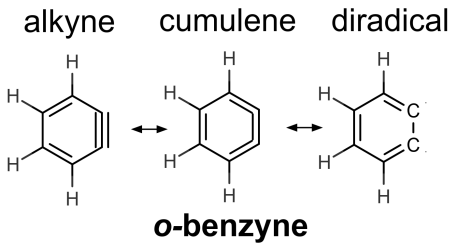


**Figure 23:** *Kekulé structure for o-benzyne.*

There are three main resonances that describe its electronic structure; the alkyne with a triple bond, cumulene with three neighbouring double-bonds and the open-shell diradical. There is little contribution from the diradical resonance structure (given a singlet-triplet splitting of 38 kcal/mol [522]). A more significant diradical character, and reactivity similar to two $\sigma$-radicals, is found for meta and para-benzyne (with singlet-triplet splitting of 21 and 4 kcal/mol respectively [522]). *o*-benzyne is closest to the cumulene structure from NMR studies. Recent HR-AFM suggest larger arynes are also dominated by the cumulene resonance structure, with contributions from the alkyne resonance as we will see. This electronic structure leads to a reduction in reactivity compared with a $\sigma$-radical, however, this may increase their concentration due to their reduced susceptibility to oxidation (as with the C3 pathway for benzene formation) or acetylene addition, making them of interest for polyaromatic inception [80, 82].

*o*-Benzyne rapidly dimerises, like a cumulene, to form biphenylene possessing an anti-aromatic 4-membered ring. Flash vacuum pyrolysis of biphenylene and polyphenylenes show thermal rearrangements to pericondensed aromatics with 5- and 6-membered rings, suggesting this pathway could contribute to PAH growth [398]. It can also react like an alkyne through a concerted Diels-Alder cycloaddition with acenes (see Figure 24). Reaction paths were computed showing a possible role for PAH growth and nanoparticle formation [82]. Fragmentation barriers of 40–47 kcal/mol indicate these crosslinks are thermally stable in flames. Rates for these reactions were not computed making the route difficult to compare with soot formation mechanisms. Other contributions of *o*-benzyne have been suggested in the decomposition of benzyl radicals studied in shocktubes [328] and combinations with ($C_3H_3$) resonantly stabilised radicals leading to a rapid pathway to indene [333], however, more work is needed to determine the role of these species in PAH growth.

The concentration of these species in flames is critical for assessing an aryne mechanism. Phenyl – produced by one hydrogen abstraction – is able to undergo a unimolecular decomposition to *o*-benzyne with a barrier of some 80 kcal/mol. This large barrier makes phenyl concentrations significantly greater than *o*-benzyne in flames [310]. It was also found that above 1500 K, the benzyne ring breaks open and the linear form of $l-C_6H_4$ becomes dominant [310]. For larger PAH, hydrogen abstraction is unlikely to provide two neighbouring sites, given the average 1–6 $\sigma$-radical sites per 600 Da species as mentioned [213]. The other option for aryne creation is the decomposition pathway of the neighbouring hydrogen from larger $\sigma$-radical PAH. This has not been explored in larger

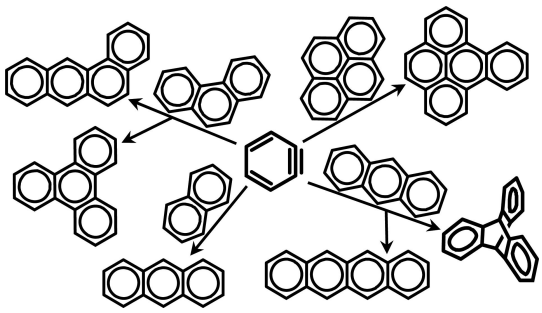

**Figure 24:** *o-benzyne polyaromatic mechanism [82]. Used with permission from Elsevier ©.*

PAH but if similar barriers are seen, as for phenyl, then concentrations of arynes would be expected to be low.

Finally, *o*-benzyne reacting with the rim-based pentagonal ring of acenapthalene has been shown to form a 4/5-membered ring pair that breaks open into the 7-membered ring species pleidene [268]. This species and similar molecules readily dimerise through a cycloaddition reactions due to their diradical character [270]. These species have yet to be explored in the context of soot formation.

Indirect insight into an aryne mechanism in nanoparticle formation can be provided by a recent exploration of the pyrolysis of coronene and dibenzo[a,e]pyrene [387] (see Figure 25).

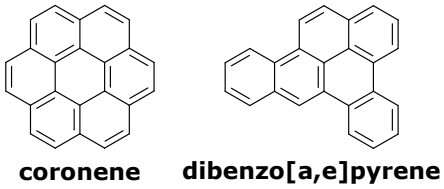


**Figure 25:** *Kekulé structure for dibenzo[a,e]pyrene.*

These two species have the same number of carbon atoms but significantly different edge types: coronene possesses a more condensed structure with six zig-zag and six free edges while dibenzo[a,e]pyrene possesses nine free edges, three armchair edges and two zig-zag edges. If an aryne route was dominant, the species with more free edges would be expected to dimerise more readily, forming more soot. However, dibenzo[a,e]pyrene, with its numerous free edges, inhibits soot formation compared to coronene (with more zig-zag edges than free), suggesting an aryne mechanism is not dominant.

### 4.4.3 Carbenes

Carbenes are neutral species with a valence of two and two unshared electrons. Methylene $:CH_2$ is the most well-known hydrocarbon carbene and is important in combustion for CH radical formation [145]. Carbenes have also been shown to be important intermediates for molecular rearrangements of larger PAH [398]. A variety of electronic spin configurations

are possible for such species (see Figure 26) [54]. For methylene the lowest energy state is the triplet ($^3B_1$) with the singlet ($^1A_1$) lying 9.0 kcal/mol higher in energy [229].

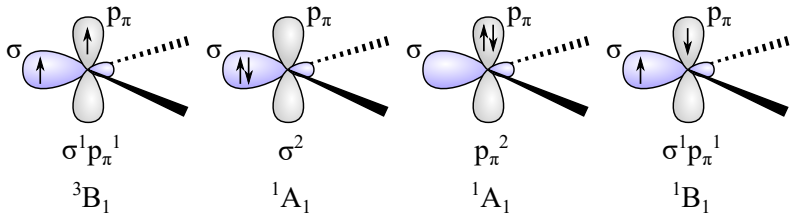


**Figure 26:** *Carbene electronic spin configurations. Redrawn from [54].*

Triplet carbenes possess high reactivity with methylene recombination rates 1–2 orders of magnitude faster than methyl ($\cdot CH_3$ a $\sigma$-radical) at flame temperatures [24]. Carbenes can be stabilised in the less reactive singlet states through heteroatoms [54] or solvation [90], which can lead to reduced reactivity as seen by considerable barriers to dimerisation [54, 171]. However, these effects are unlikely to be present in flames due to the low concentrations of aromatics.

Of interest for polyaromatic inception mechanisms are aryl carbenes (see Figure 27). For example, phenylcarbene could be formed in a combustion environment from hydrogen abstraction from benzyl, benzene with CH radical [196] and perhaps from carbon atom addition to benzene in rare cases [337].

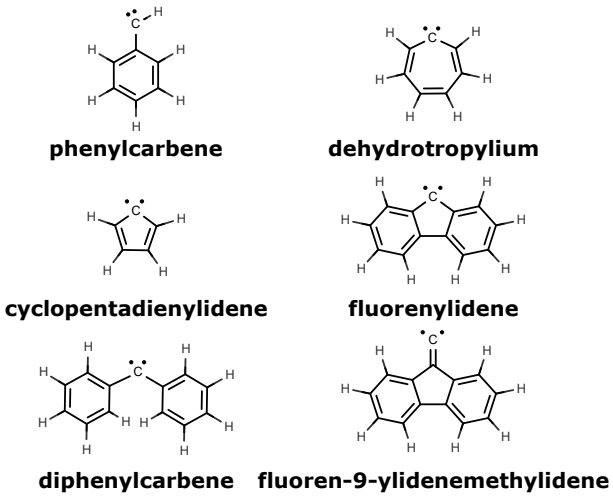


**Figure 27:** *Kekulé structure for aryl carbenes.*

This phenylcarbene could recombine forming the bridge that will be discussed in section 4.6. However, thermal rearrangement of phenylcarbene rapidly forms the more stable dehydrotropylium (or cycloheptatrienylidene) [282]. The electronic structure has yet to be confirmed for this product, however, calculations suggest two triplet states only 1.5 and 3.2 kcal/mol above the singlet ground state [440]. This indicates stabilisation through a cumulene structure as was seen for *o*-benzyne. Nevertheless, this species readily dimerises with rates yet to be determined. Further thermal decomposition of dehydrotropylium gives fulvenallene [282]. Fulvenallene is also known to crosslink [196].

At flame temperatures (1500–2000 K) even further fragmentation of fulvenallene forms cyclopentadienylidene, another carbene [196, 404]. Pentagonal ring containing carbenes such as cyclopentadienylidene and fluorenylidene are found to be reactive with a triplet ground state [40, 440] indicating greater reactivity than dehydrotropylium. Hexagonal ring carbenes with odd $\pi$-electron species such as phenalenyl and zig-zag edges have been suggested to dimerise rapidly [77]. However, reactivities similar to $\sigma$-radicals are predicted due to the delocalisation of the $\pi$-bonding system [389] as indicated by the low barriers for rotation [403]. For all these crosslinked carbene species rapid rearrangement to pericondensed species is found above 1200 K, potentially contributing to PAH formation [523].

A further option includes aromatics crosslinking through a carbene bridge, *e.g.* diphenylcarbene. It is unclear how these would form in the flame, however, some stabilisation and reduced reactivity of the triplet carbene can occur for aromatic extension of phenylcarbene providing decoupled localisable $\pi$-diradicals that polymerise [254, 530]. We will return to these diradicals in Section 4.6.

Finally, unsaturated (or "free") carbenes could allow crosslinks ($(R_2)-C=C:$) *e.g.* fluoren-9-ylidenemethylidene. These could form in flames from hydrogen abstraction *e.g.* 9-methylfluorene. These species are able to dimerise as well as add across a double bond [474], however, these species have not yet been detected or explored in gas phase combustion chemistry.

Insufficient knowledge of the rates and reaction pathways makes it difficult to consider possible contributions of carbene mechanisms to PAH growth and nanoparticle formation. We therefore did not add an entry to Table 1. However, the high concentration of H radicals and $H_2$ in soot forming regions of the flame would suggest a small concentration of carbenes (as has been found from radical scavenging experiments of small aryl carbenes [182]).

### 4.4.4 Furans

Oxygen has been suggested to allow aromatic species to crosslink through 5-membered oxygen heterocycles [131] [see Table 1(r)]. Pyrolysis experiments have demonstrated that aromatic phenols allow for crosslinking followed by ring condensation [537] and there is some recent evidence from biofuel experiments that oxygen content can increase PAH or soot growth under certain conditions [345]. Furan-like PAH are found in some flames [232] and are a significant component of brown carbon [525]. However, large oxygen-rich PAH have not been found in most flames [208, 546], with a recent jet stirred reactor study concluding for oxygenated PAH (OPAH) [305]:

> " ... OPAH chemistry can be ignored in the soot nucleation process, since OPAH have significantly lower concentrations than PAH in soot formation"

Insignificant oxygen content has also been found in early soot particles [86]. A recent comparison of molecules predicted from these oxygen crosslinking reactions with those structures found in HR-AFM [88] indicate an overprediction of furan species [515]

(with none found in HR-AFM), suggesting significant fragmentation pathways are not included [305].

In summary, many polyaromatic inception mechanisms have been suggested. Some have been integrated into kinetic Monte Carlo simulations and have shown the ability to grow nanoparticles $\approx 2$ nm in size [502] (see Figure 22a). We will return to comparing them in the final section.

## 4.5 Physical nucleation

Frankland was perhaps the first to consider a physical nucleation or condensation mechanism for soot formation. Upon lighting a candle at the summit of Mont Blanc he noticed a significant reduction in flame luminosity [146]. Back at the Royal Society he made use of air pumps to reproduce this effect as well as operate a candle above atmospheric pressure finding an increased flame luminosity, which indicated that soot formation was being inhibited or enhanced respectively. Frankland's initial suggestion that the emission of light from flames was not from solid particles but from a dense vapour was quickly disproved [293]. However, the strong pressure dependence of soot formation has long been seen as evidence for physical nucleation of hydrocarbons in flames.

Recent experiments on sooting flames within high pressure chambers further highlights the influence of pressure on soot formation [10, 89, 240]. Figure 28 reveals the increase in primary particle size of soot aggregates, sampled from within the pressure vessel, as the pressure was increased. Such a strong dependence is not seen for kinetically controlled chemical pathways in soot formation [87, 314], for example HACA growth, as they are characterised by reaction rates, which are first order in monomer concentration [511]. However, the significant increase in particle size and non-linear increase in soot volume with pressure [240, 332] suggest condensation, which is second order in monomer concentration [149, 511].

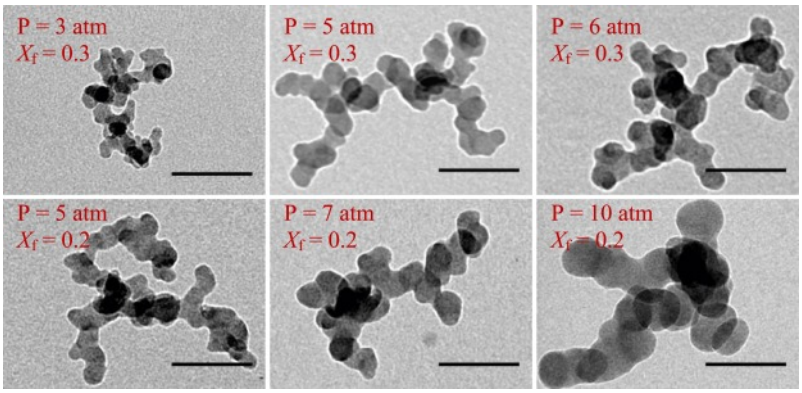


**Figure 28:** *Soot sampled from counterflow diffusion flames over a variety of pressures [10]. Used with permission from Elsevier ©.*

### 4.5.1 Aliphatic polymer

Polymerisation of fuel into an aliphatic polymer that condenses [see Table 1(s)] can be quickly dismissed given the rapid radical-induced fragmentation of aliphatic fuels in flames and that no large liquid particles are detected with laser scattering [195]. However, aromatic polymerisation [see Table 1(t)] has been considered in detail as mentioned in the previous section. After the influential paper of Rummel and Veh [424] suggesting that larger polycyclic molecules precipitate soot particles, Parker and Wolfhard suggested such a mechanism [393]. In their 1950 review they state,

> "Higher hydrocarbons are formed by pyrolysis. The molecular weight and concentration of these increase until the saturation vapour pressure is exceeded, whereupon condensation occurs and fine droplets are formed."

The higher hydrocarbons they discussed are crosslinked PAH that form an aromatic polymer which then condenses into a liquid droplet. The evaporation or thermal breakdown was proposed to be counteracted by carbonisation reactions. This mechanism represents a combination of many mechanisms already discussed, where PAH grow through the HACA mechanism, polymerise according to a polyaromatic inception mechanism and then physically nucleate. Such a proposal relies therefore on the mechanisms preceding condensation and is subject to their limitations.

Liquid halos around soot particles have been suggested to indicate a liquid-like mechanism that subsequently carbonises and forms soot [415]. Recently evidence was found that this halo is most likely a sampling artifact [51, 53]. Invasive sampling often involves injection of a cold probe onto which soot particles are thermophoretically deposited. Figure 29 shows the impact of the probe's residence time in the flame which we obtained using a high speed camera. For long residence times a liquid halo is observed, however, upon decreasing residence time the liquid halo is removed [51, 53]. It was also interesting to observe the evaporation of these halos if the sample was left in the electron microscope's vacuum for 24 hours, indicating it is not persistent at flame temperatures (other insights into the electron beam intensities required to not cause nanostructural changes are also reported [53]). As mentioned, other non-invasive techniques (X-ray or optical scattering) confirm that there is no evidence for these large liquid-like droplets [195].

A simple explanation for this observation in the TEM and AFM is that during the rapid cooling from thermophoretic sampling the soot particles present in the flame act as nucleation sites for the condensation of aromatic soot precursor molecules present in the gas phase. This is supported by the fact that the effect is only seen in diffusion flames or very rich premixed flames, where aromatic concentrations would be high enough to enable condensation [468] (see Figure 5d). As mentioned in Section 2, these species have been previously called brown carbons or tar and have been considered more important in turbulent flames such as forest fires, where aromatic species can escape the flame front and condense on soot.

It is clear, however, that as the primary particles traverse the diffusion flame the brown carbon becomes harder to remove as our sampling is limited in its speed [51]. In particular, just prior to coagulation of the primary particles into aggregates it was found to be

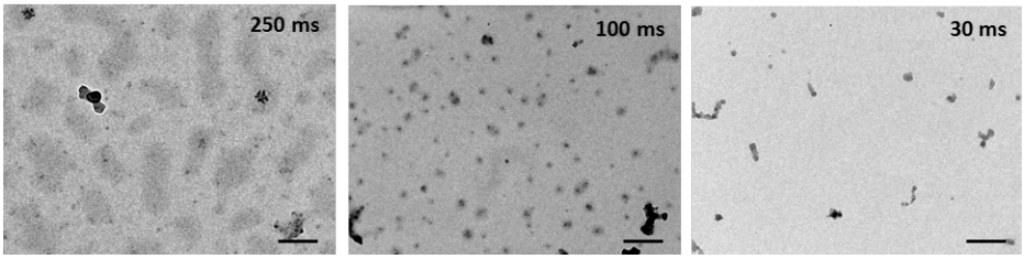


**Figure 29:** *TEM images of soot sampled at 25 mm HAB and different exposure times. The calibration bar in the images corresponds to 200 nm.*

increasingly difficult to sample rapidly enough to remove the halo, suggesting the aromatics are increasing their boiling point as they grow. Wang *et al.* also showed with infrared spectroscopy that the early soot particles are low in aliphatics but that these increase as they mature, which is assumed to be due to hydrogenation of the surface [59]. This suggests an increase in reactivity of the surface. However, these discussions do not principally concern nanoparticle formation.

### 4.5.2 fPAH

Direct physical nucleation of flat PAH species (fPAH) [see Table 1(t) and Figure 18] has been, arguably, the most widely explored mechanism in soot nanoparticle formation. This suggestion was considered unlikely by Haynes and Wagner in their 1981 review given the low boiling/sublimation temperatures for PAH molecules [195]. While condensation was seen as unlikely, the evidence for stacked aromatic species grew following the discovery of a green fluorescence signal in flames in the 1980s (see Figure 4), as mentioned in Section 2.

Miller turned to the formation of molecular clusters and used, as a proxy to cluster stability, the dimerisation of PAH in flames employing intermolecular potentials, suggesting it could be possible for larger species to condense [356, 359]. These results were extended by performing highly accurate calculations of intermolecular energies between PAH and provided a new description of the intermolecular interactions, making use of the SAPT(DFT) method to develop the isotropic PAH anisotropic potential (isoPAHAP) [488]. Experiments confirmed the accuracy of the forcefield in describing both the virial coefficient for benzene and the exfoliation energy of graphene [488]. More recently, scanning tunnelling microscopy of coronene clusters revealed similar morphologies to isoPAHAP clusters compared with other potentials [516] (see Figure 30).

Wang developed a full statistical description of PAH homodimerisation using statistical mechanics [511]. This was combined with the isoPAHAP forcefield allowed for the determination of the intermolecular vibrations, $\nu_i$, and intermolecular interactions, $E_{int}$, for fPAH [488]. The equilibrium constant for dimerisation could then be computed as;

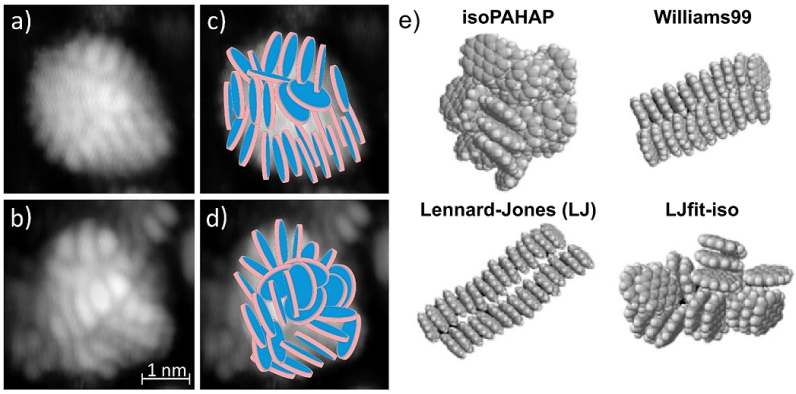


**Figure 30:** *a-b) Scanning tunneling microscopy imaged clusters of coronene molecules. c-d) Shows potential orientations of the coronene molecules in these clusters [516]. e) Shows the computational results from clusters formed during a molecular dynamics simulation of coronene with different forcefields used [394]. Used with permission from Elsevier©.*

$$\Delta H = \sum_{i=1}^{6} \left( \frac{1}{2} + \frac{1}{\exp(h\nu_i/k_BT) - 1} \right) h\nu_i - 4k_BT - E_{int}, \tag{21}$$

$$\frac{\Delta S}{k_B} = \ln \left[ \frac{h^6 p}{\pi^4 (8M)^{3/2} (ek_BT)^4} \frac{\sigma_m^2}{\sigma_d} \frac{(I_{A,d} I_{B,d} I_{C,d})^{1/2}}{I_{A,m} I_{B,m} I_{C,m}} \right] + \sum_{i=1}^{6} \left[ \frac{h\nu_i/k_BT}{\exp(h\nu_i/k_BT) - 1} - \ln(1 - \exp(-h\nu_i/k_BT)) \right], \tag{22}$$

$$K = \exp\left( -\frac{\Delta H - T\Delta S}{k_BT} \right), \tag{23}$$

where $\nu_k$ is the $k$th intermolecular vibrational frequency, $E_{int}$ is the dimer interaction energy, $h$ is Planck's constant, $k_B$ is the Boltzmann constant, $T$ is the temperature, $I_{k,m}$ and $I_{k,d}$ are the moments of inertia for monomer and dimer respectively, for the $k$th principal axis of each, $M$ is the monomer mass and $\sigma_m$ and $\sigma_d$ are the symmetry numbers for the monomer and dimer, respectively. Figure 31 shows the equilibrium constant of dimerisation for various sized fPAH, where $K > 1$ dimerisation is favoured. The curves reveal that species larger than circumcoronene ($C_{54}H_{18}$, 667 Da) would be required to form stable dimers at temperatures in the flame where soot begins to form (1500 K).

Figure 31 also shows collision efficiencies of fPAH, determined from molecular dynamics simulations [489], providing a more straightforward comparison with polyaromatic inception mechanisms. A comparison is drawn with collision efficiency to be required to explain experimental PAH mass spectra [411]. It is clear that insufficient collision efficiencies are found for physical nucleation of the size of species found to cluster in the flame at 1500 K. This analysis is consistent with a recent estimate of the boiling point of fPAH [306]. It was found that a fPAH with 60–65 carbon atoms would be required to form liquid particles at temperatures within the flame where soot forms (1450–1700 K) considering the low partial pressures of aromatics found in flames.

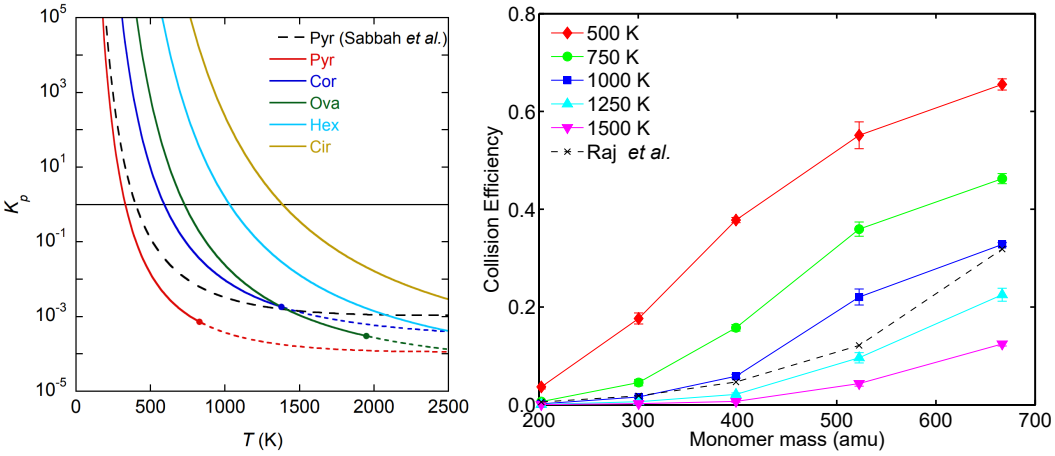


**Figure 31:** *(left) K as a function of temperature for **pyr**ene, **cor**onene, **ova**lene, **hex**abenzocoronene and **cir**cumcoronenene with 4, 7, 10, 13 and 19 rings respectively [489]. (right) Collision efficiency of fPAH derived from molecular dynamics simulations. Experimentally determined values by Raj et al. also shown [411].*

Other suggestions were made for the stabilisation of moderately sized PAH clustering through activation of non-equilbrium internal rotations. In molecular dynamics simulations of colliding PAH species, Miller observed orbiting of the PAH [356]. Schultz and Frenklach explored this effect using a quantum molecular dynamics approach and found evidence for internal rotors [442]. The establishment of internal rotors were suggested to remove thermal energy from intermolecular vibrations between the clustering PAH reducing fragmentation. From vibrational analysis only one bound internal rotor can be identified ($\sim$10 cm$^{-1}$ twisting mode) [489]. In a non-equilibrium scenario it was estimated that at least four internal rotors would be required to provide a significant nucleation flux [152, 511]. Experiments on supersonic jets of pyrene also confirm the lack of stability past its boiling point [427]. These results suggest that non-equilibrium effects are unlikely to enable a physical nucleation of PAH.

### 4.5.3 Aliphatic chains

The presence of aliphatic chains was suggested to improve the clustering of fPAH due to the entropic advantages of more internal degrees of freedom [75, 130] [see Table 1(u)]. These chains have been observed in HR-AFM of PAH [444] (see Figure 32).

Metadynamics simulations were employed that allowed the free energy to be directly and economically computed from molecular dynamics simulations with guided dynamics [75, 130]. Again, similar results were found for pericondensed PAH but soft modes could be included from aliphatic chains. They were found to improve the clustering rate but the collision efficiencies were similar to the pericondensed sub-structure, indicating it is the dispersion interactions between the pericondensed structure that still govern the ability to form complexes at high temperature. However, for 500 Da mass species the chains are still unable to provide the increased intermolecular forces required to allow for clustering

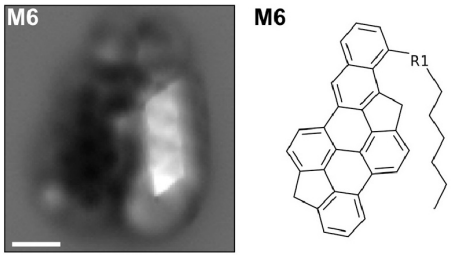


**Figure 32:** *HR-AFM image of an aliphatic chain attached to an aromatic [444].*

at temperatures exceeding 1500 K.

### 4.5.4 Aromatic polymer

Evidence for heterogeneous nucleation, where aromatic polymers are nuclei, has also been seen within some early primary soot particles [see Table 1(v)]. High resolution transmission electron microscopy, which is sensitive to stacked aromatic structures, has found disordered cores without such stacking [223] (see our own image Figure 33). Automated methods to detect these regions have been developed in fringe analysis software [485]. This feature has been interpreted as indicating an aromatic polymer nuclei [181]. It should be mentioned that other fuels provide early primary soot particles with significant internal fringes *i.e.* do not contain disordered nuclei [52].

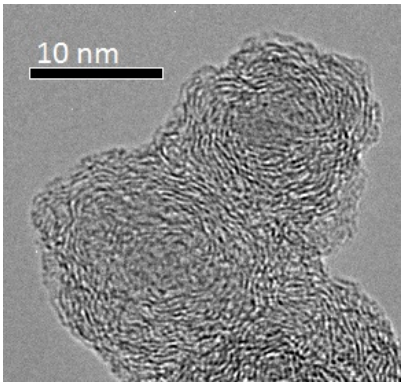


**Figure 33:** *Soot primary particle from a 10% cyclohexane doped hexane co-flow diffusion flame imaged with HRTEM showing disordered cores.*

The possibility of aromatic polymers acting as nuclei for heterogeneous nucleation was explored by Chung and Violi in 2011 [75]. Fullerenes ($C_{60}$ and $C_{180}$) were used as proxies for these nanoparticles. Little impact on the rate of clustering was found for heterogeneous nucleation of fPAH in these simulations. Classical nucleation theory would dictate that the vapour needs to be supersaturated before condensation is possible heterogenenously [241]. Therefore, while the nuclei can reduce the barrier for nucleation and therefore increase the nucleation rate, they cannot allow condensation of species that lack sufficient intermolecular interactions to condense.

The condensation of polyaromatic clusters formed via aryl-linked PAH have also been

suggested. Using molecular dynamics simulations, aryl-linked PAH were found to cluster with greater propensity than their monomeric components, however, the two aromatic planes were not coplanar, which significantly reduced physical interactions compared with similar sized pericondensed PAH [217]. Therefore, for the same reason pericondensed fPAH are unable to cluster, aryl-linked PAH are unlikely to be able to condense until they grow to larger than 5 nm [212] (see Section 5.1 for full comparison).

### 4.5.5 Penta-linked (APLH)

Pentagonal ring linked aromatic species can form planar species with similar cluster behaviour as planar pericondensed PAH [see Table 1(w) and Figure 18]. Recent HR-AFM results demonstrated planar aromatics crosslinked through pentagonal rings (see Figure 1 IS43). It was found that these species could form through a $\sigma$-radical on a rim-based pentagonal ring attacking a rim-based pentagonal ring (aryl-pentaring mechanism) [396] (see Figure 34).

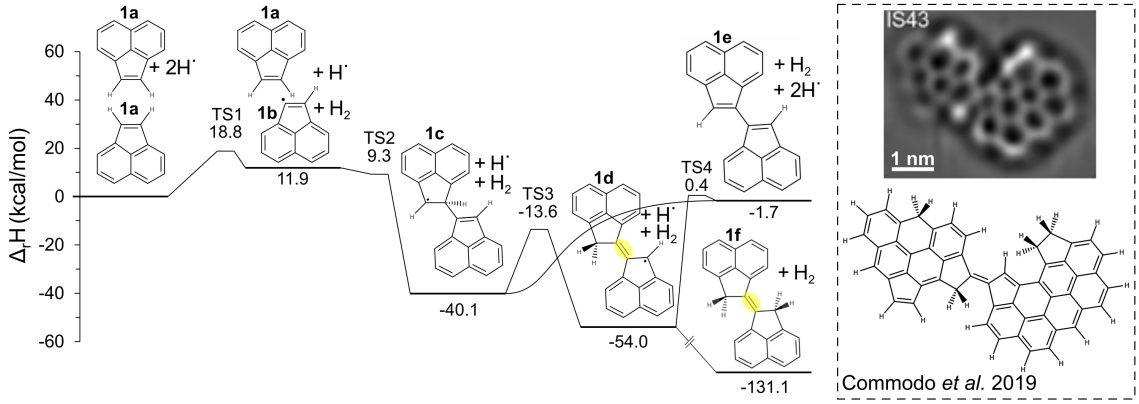


**Figure 34:** *Potential energy surface of the planar crosslinked aromatic molecule with a double bond (highlighted in yellow) (at 0 K with M06-2X/cc-pVTZ+ZPE level of theory). Inset shows similar species from HR-AFM [88] used with permission CC BY-NC-ND 4.0.*

If the pentagonal ring is partially saturated a double bond forms between the two pentagonal rings leading to a flat geometry. Metadynamics studies showed this crosslinked molecule to have a similar free energy profile to a similar sized pericondensed species. Molecular dynamics confirmed that the planar penta-linked species clusters at a similar rate to the pericondensed molecule. Species **1d** in Figure 34 will be discussed later as it is a localised $\pi$-radical able to bond and stack.

Another planar penta-linked aromatic crosslink could be formed by a $\sigma$-radical on a 6-membered ring attacking a rim-based pentagonal ring. Frenklach and Mebel recently showed this species can dehydrogenate to form an E-bridge structure, as mentioned [152]. Further dehydrogenation could lead to a planar structure (see Figure 1 IS43). However, as with fPAH these penta-linked species are unlikely to possess the interaction energies to condense at temperatures within the flame where nanoparticles form.

### 4.5.6 cPAH

Homann was one of the first to consider that curved polycyclic aromatic hydrocarbons (cPAH) could cluster and lead to soot formation [25] [see Table 1(x) and Figure 18]. The discovery of fullerenes in flames helped support such a suggestion [164, 208] as well as the extraction and detection of corannulene in flame products [283]. Evidence was also provided from species found in the negative ion mass spectrometry that led to fullerene formation [208], cPAH being more likely to form negative species due to their high electron affinity [110]. More recently, high resolution transmission electron microscopy suggested a significant fraction of early soot nanoparticles contain cPAH [323, 510].

Figure 35 shows the electrostatic potential surrounding water, corannulene (a cPAH) and coronene (an fPAH). Corannulene possesses a similar dipole moment to water, however, it still has a similar local quadrupolar charge distribution to coronene. This polarity is due to the flexoelectric effect [322], where pyramidalisation of $sp^2$ carbon networks rehybridises the $\pi$-bonding network [123, 237, 281]. Small PAH were unable to curve until at least six rings are present with an internal 5-membered ring being critical [323]. For the size of species found in early soot nanoparticles this dipole is considerable (between 4–6.5 debye) [322]. These larger cPAH ($>$11 rings, $\approx$ 450 Da) were found to be persistently polar at flame temperatures and did not invert at temperatures within the flame where soot forms [326].

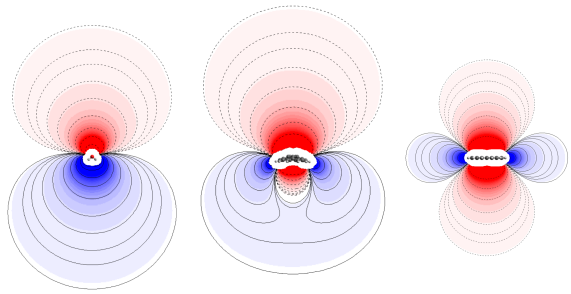

**Figure 35:** *Cross section of the electric potential, (+) blue, (-) red for water, corannulene and coronene [324].*

How does this electric dipole moment possibly improve the clustering of cPAH compared with fPAH [323]. Comparing the dimerisation energy between cPAH and fPAH we found little difference for 1–2 pentagonal rings with a significant decrease in binding energy for cPAH with $\geq$3 internal pentagonal rings [323]. High accuracy calculations (SAPT(DFT)) revealed that while the dipole moment does enhance the binding energy, the steric issues of stacking cPAH led to reduced dispersion interactions [323]. A new forcefield, curPAHIP, was developed to see whether this result translated into an enhanced clustering rate [55]. While collision efficiencies were greater for corannulene compared with coronene, the similar binding energy meant little difference was found in clustering behaviours, thus suggesting cPAH nucleation is as unlikely as fPAH nucleation. Finally, for heterogeneous clusters of cPAH some enhanced interactions were found where the smaller cPAH fits into the concave side of larger cPAH, however, this enhancement was not found to be significant [56].

### 4.5.7 ion, fPAH

Frenklach and Wang in 1991 were among the first to suggest the possibility of an ion-induced physical nucleation mechanism in soot formation [153] [see Table 1(y)]. Experimental work on cationic benzene dimers had found an enhanced binding energy increasing from $-0.5$–3 to $-17$ kcal/mol for the neutral to the cationic dimer, respectively [307, 454]. More recently, computational work on larger PAH cationic dimers found binding energies in the range $-15$–20 kcal/mol for PAH with 4–5 rings [MP2/6-31G(d)] [419]. Larger clusters were recently explored using basin hopping and density functional tight binding methods [120]. More compact clusters were formed with a positively charged dimer or trimer in the centre, indicating that the enhanced binding energy is only reserved the a few molecules in the cluster adjacent to the ion. Cation-$\pi$ interactions are more significant with small cations such as metals or flame ions. Binding energies to benzene of $-108$ and $-151$ kcal/mol were found for $Mg^{2+}$ and $Fe^{2+}$, respectively [266], while the $1+$ cation $Na^{1+}$ was found to be weakly bound with $-21$ kcal/mol. Binding energies of larger PAH (1–4 rings) with more flame relevant chemi-ions were recently computed [69]. Binding energies of $-30$–60, $-18$–27 and $-26$–32 kcal/mol were found between $CHO^+$, c$-C_3H_3^+$ and $H_3O^+$, respectively. Chen and Wang noted;

> "...the cation-enhanced binding remains to be too weak to impact the gas-phase PAH chemistry or the clustering of PAHs leading to soot nucleation."

### 4.5.8 ion, cPAH

Curved PAH, unlike planar PAH, have considerable interactions with ions due to their polarity. This could lead to an ion-induced nucleation mechanism [see Table 1(z) and Figure 18]. cPAH–ion interactions are well known [124] and have been used in lithium ion storage [543]. We have previously mentioned the large number of ions present in flames from chemi-ionisation reactions. In 2018, a binding energy between $c$-$C_3H_3^+$ and a 15 ring cPAH with two pentagonal rings were computed to be $-40.6$ kcal/mol [323], suggesting important interactions for soot formation. Quantum *ab initio* molecular dynamics revealed this complex to be stably bound at 1500 K over 2 ps [326]. Molecular dynamics simulations of corannulene clustering revealed a near doubling of the clustering rate with ions present, while no difference was found for coronene clustering in the presence of ions [55] (see Figure 36). However, only a couple of cPAH can be bound to an ion with further growth requiring supersaturation of the vapour of cPAH from classical nucleation theory [241], which we have previously demonstrated as being unlikely.

Such a mechanism could perhaps explain the positively charged experimentally nanoparticle mode, mentioned in Section 2.1, as correlations have been found with large aromer species in low pressure acetylene flames and this mode [210]. Larger nanoparticles are found to take on a charge distribution given by thermal equilibrium [450, 514], however, the speed with which they acquire their charge indicates it is not from thermal ionisation but from coagulation of charged nanoparticles suggesting a link between larger soot particles and this mode [143]. Finally, recent work showed a high charge fraction (up to 95%) of sub-3 nm nanoparticles in the flame front where the chemi-ion concentration is greatest [536]. This could provide evidence for the charged nanoparticle mode in atmospheric

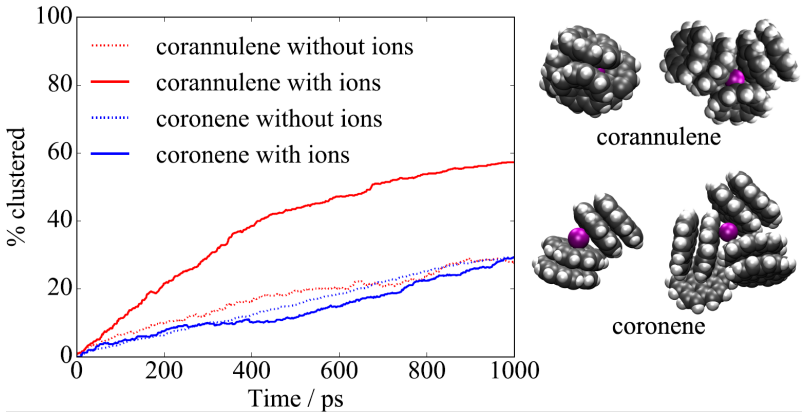


**Figure 36:** *Clustering of cPAH corannulene and fPAH coronene at 500 K with and without ions ($K^+$) present [55].*

flames. However, it is clear that these nanoparticles do not contribute significantly to primary particle formation with a recent study measuring the charge fraction of sub-10 nm nanoparticles concluding that [514]:

> "Ion-induced soot nucleation was not the main contributor to nucleation since the charge fraction was less than 10% when $T_{max} < 2000$ K."

In summary, physical nucleation provides a rapid soot formation pathway, given that sufficiently strong intermolecular interactions allow for a supersaturated vapour to form. However, the clustering PAH in flames of mass 500 Da are found instead to have interactions too weak to explain soot formation.

## 4.6 Physical + Chemical

The crux of the soot formation problem is that the physical and electrical condensation of precursor molecules is rapid but too weak to hold soot together, while most chemical bonds are strong but the mechanisms proposed to date are too slow to account for rapid growth of soot as observed in experiments. A mechanism that combines both aspects, condensation and chemical bonds, is required – so-called physically stabilised soot inception.

One of the first clear articulations of such a proposal was from Harris and Weiner in 1989 [191]:

> "Once coagulated they will quickly become chemically knit together since a significant fraction of the aromatic species are radicals."

Miller followed with a similar suggestion in 1991 that [356]:

> "...if individual PAH or their dimers undergo rapid, irreversible reactions, the net rate of production of the soot nuclei may be sufficiently high so that the

concentration of the nuclei far exceeds the concentrations of the reacting, intermediate species."

Frenklach and Wang developed this suggestion into a kinetic model for soot formation, where PAH dimerisation was assumed to be irreversible, facilitated by some sort of chemical or non-equilibrium process [153]:

> "...one cannot judge the PAH coagulation flux using the equilibrium assumption – these fluxes must be computed kinetically. The equilibrium among individual PAHs and clusters may never be attained, and the mass flux is likely to be driven by an irreversible process following the dimer formation...It is also possible that a PAH dimer is stabilized by a reaction with an aliphatic, forming a covalently bonded link between the PAH layers... the van der Waals enhancement should be larger than the factor or 2.2 assumed in the present study."

This irreversible nucleation of PCAH was the first successful kinetic model of soot formation that captured the particle number as well as the volume fraction [153, 329–331, 512]. Similar suggestions have been proposed recently such as the reactive dimerisation models [251, 252]. These models have arguably been the most successful in describing nanoparticle formation in flames. This section details some possible detailed mechanisms to explain such a "middle way".

### 4.6.1 Zipper mechanism

Homann suggested that an aryl-linked PAH dimer could fold upon itself then react at the rim, releasing hydrogen and becoming a curved PAH or a fullerene – the zipper mechanism [7, 25, 208] [see Table 1(aa)]. Aryl-linked hydrocarbons are unable to bond without disrupting the stacked configuration (for the size of PAH found in flames) due to the direction of the $\sigma$-radical bonding that is optimal when the bond is colinear with the aromatic planes. For fullerene formation it has been found instead that near-complete loss of hydrogen is required before the carbon will curl and close into a fullerene [429].

### 4.6.2 Internal rotors

Frenklach and Mebel recently suggested an enhancement of polyaromatic inception due to colliding PAH activating internal rotations [152] [see Table 1(bb)]. These rotors were argued to provide multiple opportunities for an aryl-radical to attach to a reactive edge of a PAH such as a rim-based pentagonal ring. For an internal rotor to be persistent between non-bonded monomers they must be strongly bound. Interactions in the T-configuration (C–H with $\pi$-network) are too weak to provide a persistent internal rotor [487]. Therefore, the only bound internal rotor that could form, from analysis of the intermolecular vibrations, is the twisting mode of a stacked dispersion stabilised PAH dimer [489], thus the reason for its consideration in this section.

This internal rotor could indeed increase the chance of a radical reacting with a reactive edge. Insights into such a scenario can be gained from recent quantum molecular dynamics simulations of pyrene radical attacking the 9,10-free edge at very low temperatures [73] (see Figure 37). Preliminary results of aryl-radical recombination in reactive

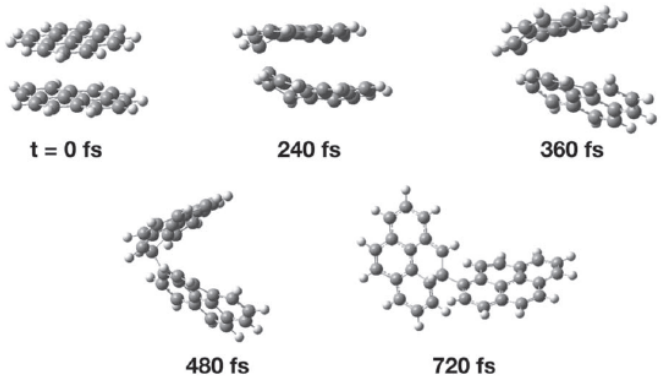


**Figure 37:** *Quantum molecular dynamics simulations at low temperature [$T = 4$ K ADMP B3LYP-D3/3-21G*] of stacked pyrene with the lower species possessing a $\sigma$-radical [73].*

molecular dynamics at flame temperatures did not reveal such an enhancement [316], however, significantly larger PAH would be requires to see the bound internal rotor at temperatures within the flame where soot forms. More work is clearly required to examine the impact of internal rotors in enhancing polyaromatic inception.

### 4.6.3 Bridge-linked (ABLH)

Aliphatic bridges between stacked PAH have also been discussed in detail since the 1990s [see Table 1(cc) and Figure 18]. In relation to the formation of interstellar dust, a mechanism was proposed by which a "cross-linked structure of aliphatic and aromatic hydrocarbons" formed and was suggested to explain soot formation under certain flame conditions [149, 371]. Aliphatic bridges were also included in the early models of stacked species from Homann et al. [25], which showed the first stacked complex that was stabilised by an aliphatic chain. This mechanism was suggested as part of the formation of some of the smallest nanoparticles in flames with D'Alessio commenting during the 1994 Heidelberg soot workshop [125]:

> "We think of two-ring structures connected together with some non-aromatic, some aliphatic bridges. You may also think about oxygen bridges..."

We will come back to the oxygen bridges. This description would later become known as aromatic aliphatic-linked hydrocarbons (AALH) [148] with aryl-linked pentagon containing species being introduced later [100].

Molecular dynamics revealed that aliphatic bridged ($[CH_2]_n$, $n = 2$) aromatics of mass $\sim$250 Da were found to stack below the boiling point of the aromatic species [75, 529].

However, at flame temperatures (above the boiling point) these physical interactions were overcome and clustering of these species was at a significantly lower rate compared with pericondensed PAH. Considering also the hydrogen content required for aliphatically-linked chemical mechanisms at least one $[CH_2]_n$, $n = 1$ linkage would be required per PAH. This would lead to an $H/C$ ratio greater than one, when most early soot nanoparticles have $H/C = 0.5$. However, the rapid carbonisation processes that occur in flames could rapidly decrease the $H/C$ ratio, so this is less conclusive.

Detailed kinetic mechanisms of how these aliphatic crosslinks form and fragment have also not been explored in significant detail. Some kinetic Monte Carlo codes do include such aliphatic crosslinks allowing comparison with other chemical pathways [502, 504, 505]. However, the aryl, aryl bonds continue to be more dominate than these aliphatic links (high collision efficiencies between radicals were assumed). More recently, for a $[CH_2]_n$, $n = 2$ aliphatic crosslink, one conceivable option is the reaction between two benzylic methylene $\pi$-radicals. Simulations and experiments have recently been performed using free electron laser IR radiation and mass spectrometry to probe the pyrolysis products of benzyl and indenyl [202, 461, 462]. The crosslinked species bibenzyl was found and shown to rapidly cyclodehydrogenate into pericondensed structures in a similar manner to the aryl-linked species discussed previously. These methyl radical sites could form from hydrogen abstraction of a methyl group. Methyl radical sites $-C^{\bullet}H_2$ have not been directly imaged using HR-AFM, however, the precursor $-CH_3$ group has been imaged in soot precursor molecules using HR-AFM [88]. Another possible mechanism by Chen and Wang [69] involves $C_3H_3^+$ reacting with the edge of a PAH to provide a methyl radical group. It is also conceivable that for larger PAH the rearrangement reactions could be less important. Aliphatic bridges have yet to be imaged using HR-AFM (while they have been imaged in pitch [72]) although some preliminary evidence for them in the low temperature regions of an inverse diffusion flame has been found [2].

Acetylene groups attached to the edge of PAH have also been suggested to crosslink the PAH, reacting either with an RSR [166] or PAH $\sigma$-radical [542] [see Table 1(dd) and Figure 18]. All aliphatic and acetylene bridges detailed to date are prone to significant radical-induced fragmentation as mentioned in polyaromatic inception Section 4.4 [152, 414].

Finally, an oxygen-containing double crosslink was suggested between PAH where one is a RSR [318] [see Table 1(ee) and Figure 18]. The impact of oxygen crosslinks can be considered minimal in most cases due to the lack of significant oxygen in soot nanoparticles [86] and the ability of pyrolysis reactors to produce soot without oxygen being present [420].

### 4.6.4 Excimers

Excimers have been discussed as evidence for stacking of aromatic species in the previous section but they also provide a bound state that has been suggested to stabilise soot nanoparticles [357]. Figure 38 shows the potential energy surface for the ground and excited states of a stacked aromatic dimer [346, 357, 431]. After laser excitation of a $\pi$-$\pi^*$ transition on one of the aromatic planes, the excited state delocalises over the dimer lead-

ing to an energy reduction. The binding energy $D_e$ is usually defined as the energy for the excimer to dissociate (see Figure 38). A wide range of small fPAH species have been calculated with binding energies up to $-20$ kcal/mol found [278, 346], too low to provide significant stabilisation at flame temperatures. The stabilisation is also only appreciable between pairs of species; the trimer is found to be weakly bound indicating the excimer is only able to delocalise effectively across two species [102].

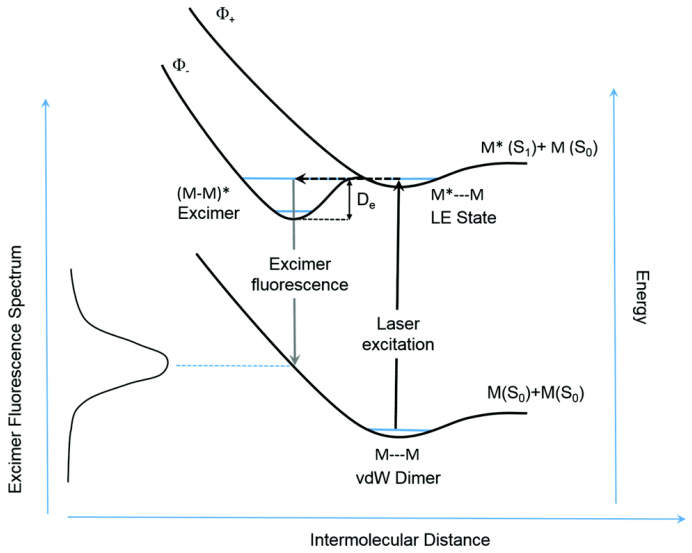


**Figure 38:** *Potential energy surface for the optical states of an aromatic dimer. The binding energy of the excimer is indicated by $D_e$ [346].*

Time resolved studies have found lifetimes of tens of nanoseconds for the excimer state [346], which are too short to provide stability over the hundreds of nanoseconds to milliseconds required for soot nanoparticle formation. Finally, insufficient UV light is produced in the flame to maintain a sufficient concentration of these species. This is evidenced by no spontaneous emission of the excimer signal. These excimers therefore require external, often laser, illumination to maintain and produce the fluorescence response.

An interesting aside is that aliphatically bridged species still produce the excimer signal [278], indicating that stacked, non-conducting bridges also possess the excimer signal (see Figure 39). They were also able to show that the effect is significantly different in excimers containing pentagonal rings forming more tightly bound structures (for cyclopentadiene increasing to $-32$ kcal/mol), leading to a decreased fluorescence emission [279].

### 4.6.5 Multicentre-linked (pancake) (AMLH)

The term "Pancake bond" was coined by Mulliken and Person in the 1960s [377] to describe a multicentre two-electron bond [see Table 1(gg) and Figure 18]. These form when AB stacking of aromatic species, both with an odd number of $\pi$-electrons in an aromatic network, allows for the two singly occupied molecular orbitals (SOMO) $\chi_a$, $\chi_b$ to form a multicentre bonding molecular orbital, $\phi_+ = N_+(\chi_a + \chi_b)$, where $N_+$ is the normalisation constant [246] (see Figure 40). These bonds form between $\pi$-radicals that are delocalised

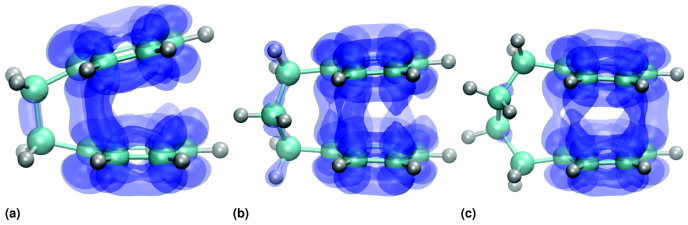


**Figure 39:** *Isosurfaces ($\pm 0.05$) of the orbitals involved in the $S_0 \longrightarrow S_1$ optical transition for aliphatically bridged benzene dimers [278]. Used with permission from the Royal Society of Chemistry ©.*

on the edge of a 6-membered network. For larger non-symmetric aromatic species it was found that the multicentre bond only forms across a few edge carbon atoms [325], which can be seen in Figure 40.

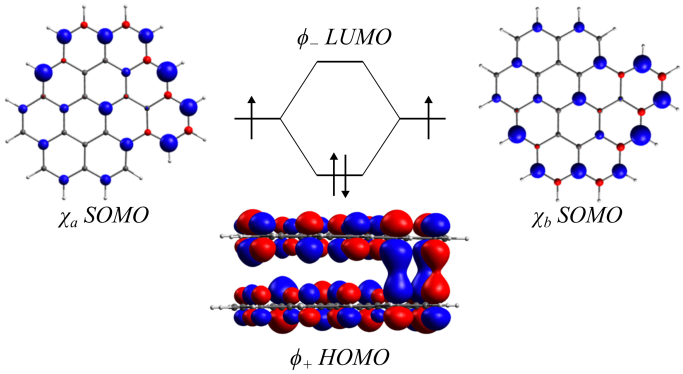


**Figure 40:** *Molecular orbital representation of pancake bonding where two singly occupied molecular orbitals (SOMO) $\chi_a$ and $\chi_b$ form a multicentre two electron bonding highest occupied molecular orbital (HOMO) $\phi_+$. Based on Kertesz [246].*

In flames, odd $\pi$-electron aromatics have been directly imaged in soot precursors using HR-AFM [88] and have been suggested to stabilise soot nanoparticles [469, 506]. However, the pancake bonding is weak due to the strong Pauli replusion from the molecular orbitals not involved in the pancake bond. Therefore, poor overlap between orbitals is found in these multicentre bonds with $<$ 10 kcal/mol of additional interaction above that of the dispersion interactions [246, 325]. They are also highly angle dependent, breaking after rotating by 30°, requiring strict AB stacking [93]. In fact, for small species such as phenanenyl, a non-stacked crosslinked species is lower in energy than the stacked configuration (a so-called $\sigma$-dimerisation [372]). This $\sigma$-dimer has been shown to dehydrogenate forming a 7-membered ring fPAH [493].

### 4.6.6 Zig-zag-linked (AZLH)

Wang was the first to consider localisation of $\pi$-radicals due to diradical character (diradicaloid) in the context of soot formation in 2010 [511] and since then considerable work

has been undertaken to explore their impact on soot formation [see Table 1(hh) and Figure 18]. Localised states have been experimentally observed and computationally studied at the zig-zag edge of graphene [260, 262, 383, 479]. Some aromatic molecules with dual zig-zag edges and an even number of $\pi$-electrons can possess a diradical character. In Section 4.4.3, we introduced carbyne and carbene diradicals formed with $\sigma$-radicals. A 2019 review from Hofmann et al. [478] provided a comprehensive discussion of diradical reactivity of $\pi$-radicals. Firstly, they distinguish between localisable and nonlocalisable diradicals. For the former, an orbital transformation is able to "localize their singly occupied orbitals on different sites so that they do not share a considerable region of space." [478]. Carbynes and carbenes are examples of unlocalisable diradicals for which a complex interplay between exchange and coulomb interactions determines whether the species is closed-shell singlet or triplet and determines the reactivity. This orbital localisation can be performed for most $\pi$-networks, making them localisable diradicals. While many metrics have been proposed, the recommended indicator for diradical character in these localisable diradicals (for which the exchange interactions are weaker) is the singlet–triplet energy splitting $\Delta E_{ST}$. Figure 41 shows the transition from a closed-shell species where the singlet is lower in energy.

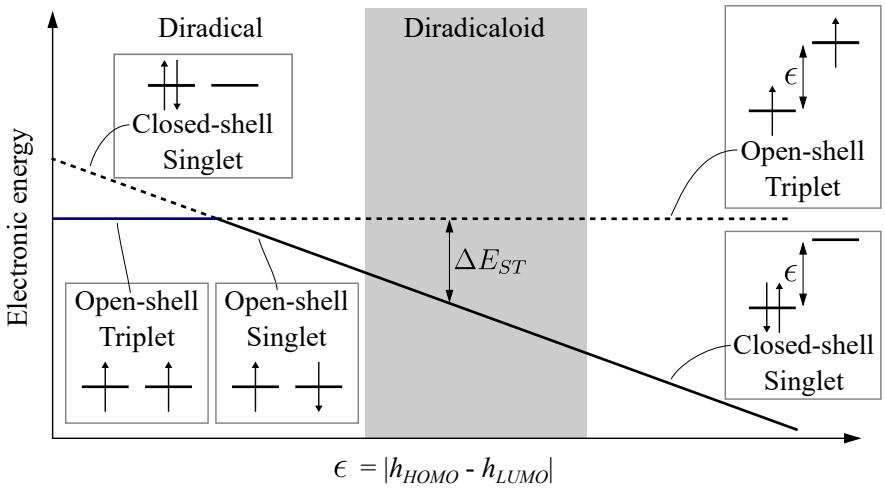


**Figure 41:** *Schematic showing the energies of the triplet and singlet as the degeneracy between the frontier orbitals, $\varepsilon$, is lifted. Redrawn from Stuyver et al. [478]. Note that $h_{HOMO}$ and $h_{LUMO}$ are the one-electron energies associated with the HOMO and LUMO and not the full orbital energies. The triplet is shown as constant to allow for comparison.*

As the difference in the one-electron energy of the frontier orbitals, $\varepsilon$, decreases it gains diradical character, $\Delta E_{ST} \to 0$, which is named a diradicaloid (usually considered to be thermally accessible). A diradical forms when the localisable orbitals become degenerate, $\varepsilon = 0$, giving either an open-shell singlet or triplet, depending on magnitude of the Coulomb and exchange interactions as well as potential spin polarisation effects [478]. A clear indication of diradical character is if the triplet is lower in energy than the closed shell singlet, $\Delta E_{ST} > 0$. A good example of diradicaloids is the polyacene series (anthracene, tetracene, pentacene, *etc.* see Figure 42).

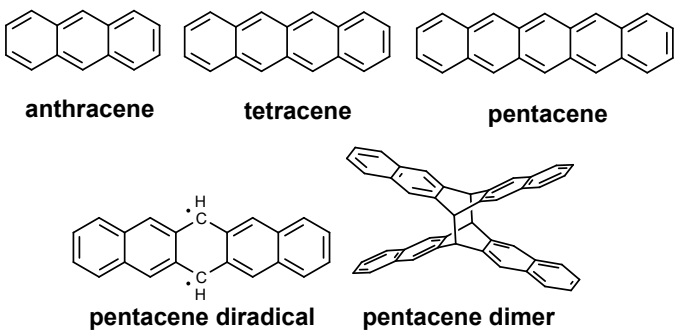


**Figure 42:** *Kekulé structure for acenes.*

As the number of linearly fused rings increases $\Delta E_{ST}$ approaches zero but does not become negative and therefore becomes a open-shell singlet ground state for infinite polyacene [478]. This leads to significant reactivity with >5 rings spontaneously dimerising in solvent at room temperature [27]. This dimerisation is a [4+4] cycloaddition reaction, which is symmetry forbidden but can be achieved through photoexcitation at room temperature or thermal excitation in a flame.

Polyacenes require considerable length of some five rings to attain significant binding energies up to 39 kcal/mol [269, 545], which is nearing a value of significance for soot formation. Given the growth mechanisms found for PAH it is highly unlikely that a concentration of linear acenes with >5 rings will be present as evidenced by the species observed in the HR-AFM [88]. However, a hydrogenated pentacene was directly observed in HR-AFM imaging [88] (PS8 see Figure 43). This is interesting for two reasons. Firstly, it shows that protonation can change the character of a reactive PAH with further protonation potentially leading to a non-reactive closed shell species. Secondly, this protonated diradicaloid takes on a doublet radical electronic state with considerable reactivity. Recent experiments have shown that hydrogenated pentacene can form dimers in the solid state [199] (we calculate a bond energy of −50.1 kcal/mol at the M06-2X/cc-pVTZ//B3LYP/6-311G(d,p) level of theory). These dimers were also found to dehydrogenate to large 14 ring peripentacene species [199].

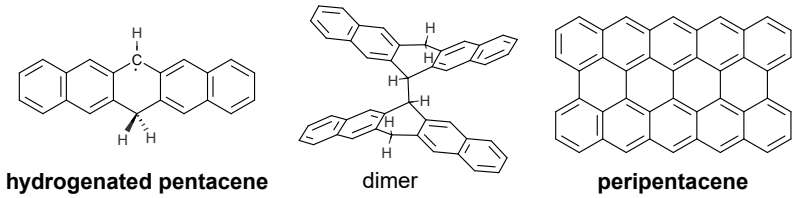


**Figure 43:** *Kekulé structure for acenes.*

Non-acene species have also been considered. Koley et al. [269] considered adding circular pericondensed PAHs to the end of the acene to combine stacked dispersion interactions and acene cycloaddition. However, this type of structure is highly unlikely to form in the flame from a HACA type mechanism and has not been observed in HR-AFM studies [88]. Finally, larger non-acene PAH in roughly rectangular geometry, such as peripentacene, were computed to dimerise along their opposite zig-zag edges [545] [see Figure 18(hh)].

But as with the polyacenes, zig-zag edges of at least 5 rings were required to attain binding energies of 41 kcal/mol. If we consider that in HR-AFM such symmetric species are not widely found and rarely are more than three adjacent zig-zag edges found (with a maximum of four zig-zag edges in a row observed) [88], it is unlikely that this mechanism can explain the clustering of species of mass near 500 Da. However, diradicals are attractive as soot precursors as they can theoretically polymerise and we will return to them.

### 4.6.7 Rim-linked (ARLH)

Rim-bonds arise from localised $\pi$-radicals that allow bonded and stacked configurations with considerable binding energy [see Table 1(ii) Figure 18]. Localised electronic states were discussed in the previous section with regard to diradicaloids in even-numbered aromatic systems.

In odd-numbered $\pi$-electron aromatic systems localisation can also occur through the presence of non-hexagonal rings, *e.g.* fluorenyl and indenyl, or methylene groups. Figure 44 shows the $\pi$-radicals based on localised edge types as compared with phenalenyl-type edges that are delocalised as the network enlarges. Spin density has been found to linearly correlate with the reactivity of a site, both for dimerisation and ability to abstract [478]. It is important to reiterate that by localised we do not mean that the $\pi$-radical is solely localised to a single carbon site, as with the $\sigma$-radical formed from hydrogen abstraction from a PAH, but that the $\pi$-radical is pinned to the edge. For example, while the indenyl-type radical is strictly a resonantly stabilised radical, with the spin density being shared between two equivalent positions, it is still a localised electronic state. This is shown in Figure 44 as the aromatic network is enlarged, minimal changes to the spin density of the most spin rich carbon atoms are seen. The first three localised $\pi$-radicals can be classed as arising from hydrogen abstractions from fluorene, indene and a methyl group and are well known reactive species in the flame.

Partial saturation of aromatic edges from hydrogen addition is the second class of localised $\pi$-radicals. The earliest discussion of this in the soot literature that we could find was by Abrahamson in 1977 [1], in which saturated platelets were suggested to form soot. These partially saturated edges and aromatic interiors were suggested to form reactive localised $\pi$-radicals. The issue with these suggestions and the reason saturation was not generally considered is that at high temperatures, hydrogen is readily lost from partially saturated PCAH (part sat. PCAH-type) with strong aromatic stabilisation [213]. Aromatic stabliomers are predicted to be fully unsaturated from thermodynamic calculations [475].

The recent experimental work from Commodo et al. [88], challenged the lack of saturation by showing that particular ring topologies allow partially and fully saturated aromatic edges. In the previous section, we mentioned partially protonated pentacene had been found in the flame [88] and allowed for strong dimerisation energies. Figure 44 shows minimal delocalisation of the spin density for this partially saturated diradicaloid-type localised $\pi$-radical (Part. sat. diradicaloid-type). The other edge type imaged was a partially saturated rim-based pentagonal ring (part. sat. rim. pent.-type) (see Figure 1 species IS1). This $\pi$-radical is similar in topology to the benzyl-type $\pi$-radical, but is perhaps more likely to form as many more rim-based pentagonal rings were found compared with methyl groups [88]. The importance of these radicals in the HACA mechanism [157]

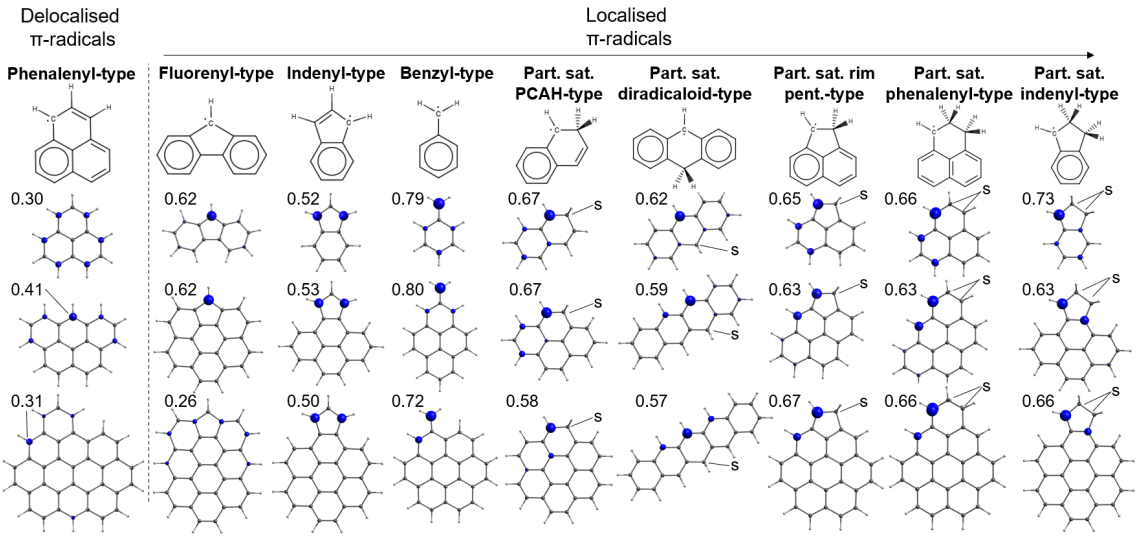


**Figure 44:** *Different classes of π-radicals with spin density isosurfaces=0.025 computed with the B3LYP/6-311G(d,p) level of theory as a function of size. The Mulliken spin density value is shown for the most spin rich carbon site. Carbon atoms marked with s are saturated.*

and shuttling rim-based pentagons along zig-zag edges was first appreciated in calculations performed by Frenklach and coworkers [156, 528]. Wang and coworkers found that this site reacted with the σ-radical phenyl to form a stable species unable to break open across the pentagonal ring (this is opposed to hexaphenylethane, which readily breaks to form free radicals [97]). Further to this, Frenklach and Mebel recently confirmed that this site is also unlikely to fragment at flame temperatures showing remarkable stability against radical-induced fragmentation [152].

Of most interest for soot formation are polyaromatic mechanisms that involve these reactive sites. A recent computational study systematically computed the energetics of polyaromatic crosslinks with localised π-electrons (see Figure 49) [325]. Significant bond energies were found with σ-radicals, but interestingly strong bonds were also formed between localised π-radicals [325]. These results are unsurprising considering that smaller localised π-radicals are known to recombine and form large aromatics in flames *e.g.* benzyl forms phenanthrene [461], indenyl forms chrysene [230], while benzyl and indenyl can form pyrene [462], as mentioned. Further experimental evidence comes from the molecules that readily soot and could be seen as precursors for these localised π-radicals through hydrogen addition or abstraction, such as toluene, fluorene, indene, cyclopentadiene and acenapthalene [103]. Another example is the significantly enhanced sooting of 1,2,4-trimethylbenzene compared with the structural isomer n-propylbenzene [74] (see Figure **??**).

While these small species appear to crosslink and cyclodehydrogenate, larger localised π-radicals could form dispersion-stabilised stacks. One of the first suggestions of dispersion-stabilised stacked and bonded localised π-radicals was perhaps from Tonachini *et al.* in 2015 [318], where a partially saturated rim-based pentagonal ring crosslinks with a PAH through a reaction with oxygen (see Figure 18(ee)). It was found that significant bonding


**Figure 45:** *Kekulé structure for 1,2,4-trimethylbenzene*

could occur in stacked aromatics between localised $\pi$-radicals without any oxygen (see Figure 46). A full thermodynamic equilibrium analysis of the dimer further confirmed the stability of such structures in flames (1500–2000 K) and a significant physical enhancement for larger species [344]. We decided to name these structures rim-bonded to

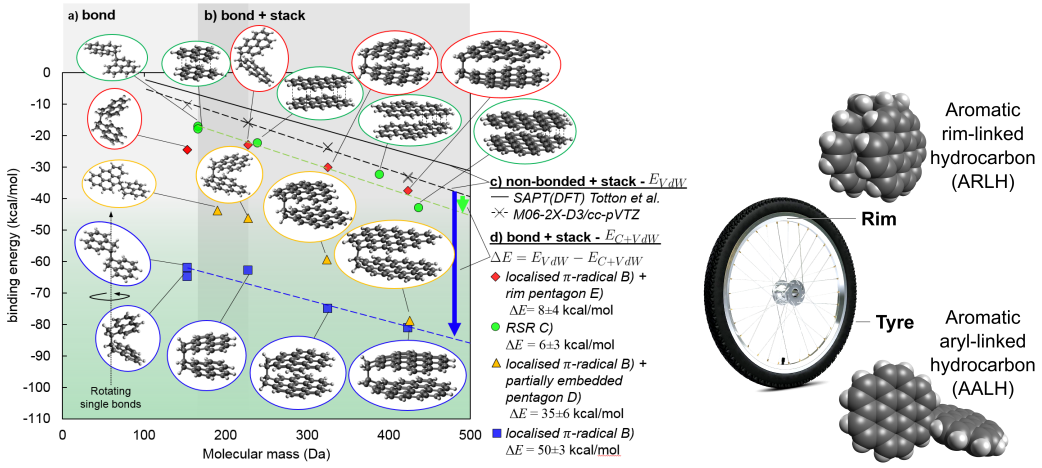


**Figure 46:** *Bonded and stacked binding energies [325]. The blue arrow shows the enhancement due to localised $\pi$-radical bonds compared with only dispersion interactions.*

distinguish them from aryl-bonded. Figure 46 shows the tyre analogy where rim-linked hydrocarbons could be thought to link via the rim of a bicycle wheel, which is only accessible on the face of the molecule. The aryl-linked structure can be thought of linking via the tyre so that the bond is colinear with the aromatic planes. This naming was chosen to also distinguish them from delocalised $\pi$-radicals that can form $\sigma$-dimers when not stacked but form weak multicentre pancake bonds when stacked.

It is still unclear how prevalent such sites are within the flame. In early soot formed from pyrolysis, significant spin concentrations were found ($\approx 10^{21}$ spins/gram) using electron paramagnetic resonance (EPR) [534]. Wang put this number into context in his review stating that [511]:

> "Assuming the residue is made of carbon only, the number of spins is roughly 1/50 atoms, or one free radical for each pair of PAHs of the size of coronene."

. This has recently been explored in EPR experiments on soot collection at different locations in the flame [506]. A change in radical character occurring at soot inception suggested the involvement of $\pi$-radicals. An initial attempt was made to answer

this question using a computational approach by considering localised $\pi$-radicals forming from hydrogen addition and abstraction from a rim-based pentagonal ring on acenapthalene (*i.e.* in partial equilibrium with H/$H_2$ in the flame). This was a similar approach to that employed by Howard in 1991 to consider the formation of $\sigma$-radicals from hydrogen abstraction [213]. It was found that, for temperatures in the flame where soot begins to form (1400–1500 K), 0.1 to 0.01 fraction of rim-based pentagonal rings were localised $\pi$-radicals. This is consistent with the ratio of unsaturated, fully saturated and partially saturated rim-based pentagonal rings found in HR-AFM of 27:12:4 [88]. This is a considerable fraction and under certain circumstances is greater than the mole fraction of $\sigma$-radicals on rim-based pentagonal rings. At higher temperatures (1800–2000 K) the unsaturated rim-based pentagonal ring is favoured. Perhaps most interestingly for a soot mechanism it was shown that multiple localised $\pi$-radicals can exist on a single aromatic molecule. Taking the example of 1,3-diacecoronenyl (see Figure **??**), we calculated the triplet to be considerably more stable than the singlet making it a true diradical as discussed in Figure 41 (B3LYP/6-311G(d,p) $\Delta E_{ST} = 17.7$ kcal/mol). As noted by Abrahamson [1] in 1977, such multiradicals could allow for a chemical polymerisation of aromatics.

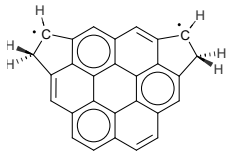


**Figure 47:** *Kekulé structure for 1,3-diacecoronenyl.*

There is also some preliminary evidence from mass spectrometry that protonated aromatics, which are more likely to be localised $\pi$-radicals, cluster. The clustering species from Grotheer et al. have a H/C of 0.4, while the species at 500 Da have a H/C of 0.3 [190]. There was also a preference for an even number of hydrogen atoms in the clustered species that could indicate reaction between species with an odd number of hydrogen, which are more likely to be localised $\pi$-radicals. Recently, Carbone presented a positive mass spectrum, which is more likely to be protonated species [65] (while cPAH are found in the negative mass spectrum as mentioned [208]). Figure 48 shows how the positive species cluster, while the negative mass species did not. As with the earlier work a H/C ratio close to 0.5 indicates reactive species with an excess of hydrogen. However, no definitive experimental evidence has been found to date and significant work is required to justify such an interpretation of these results. This mechanism could also be driven by unsaturated species such as indenyl-type edges that have low H/C ratio, so a high H/C ratio is only a secondary indicator. This preliminary exploration reveals that understanding how hydrogen is gained and lost by the edge as well as ring topology will be critical for understanding the importance of this pathway.

In summary, mechanisms involving both physical and chemical processes were reviewed. These processes present a means to increase the collision efficiency of polyaromatic inception routes. The zipper mechanism, where crosslinked pericondensed PAH stack and dehydrogenate, is not considered to be possible. Internal rotors that enhance polyaromatic inception present an interesting suggestion that requires further calculations. Bridges

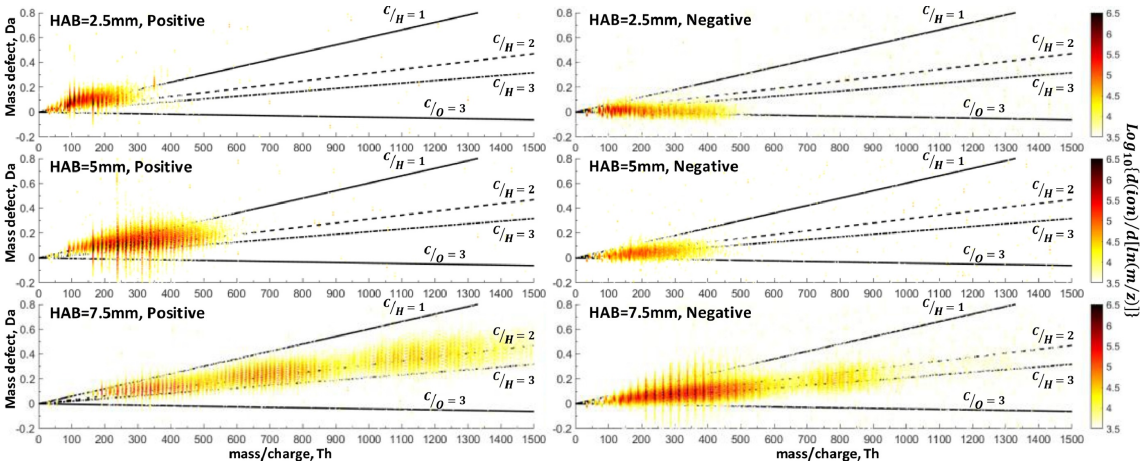


**Figure 48:** *Mass defect vs mass to charge ratio of flame ions (positive left, negative right) sampled in an ethylene/air flame from a McKenna burner [65]. Used with permission from Elsevier ©.*

formed between aromatic units have long been explored – their downsides include them being prone to radical-induced fragmentation and requiring a higher H/C ratio than what is seen. There is an interesting overlap here with rim-bonding, where two benzyl type radicals will form a $–CH_2CH_2–$ bridge. Excimers were shown to be in low concentration and unimportant for driving nanoparticle formation, however, excimers were still shown for bridge species. Multicentre-bonds were described between delocalised $\pi$-radicals due to phenanenyl-type hexagonal networks. Low binding energies were found suggesting minimal enhancement. Localisation of $\pi$-radicals was found to occur for zig-zag edges with diradicaloid character leading to [4+4] cycloaddition. Localisation was also found for odd-numbered carbon networks with strong rim-bonding for these species with the topology of the aromatic network and the saturation of the edge to be critical for understanding this pathways to nanoparticle formation. These localised electronic states allow for true diradicals to form, suggesting a polymerisation reaction may be possible with multiradical reactive PAH. Finally, preliminary evidence for protonation being important for soot formation was also shown.

# 5 Summary and outlook

## 5.1 Mechanism comparison

Physical nucleation of PAH is only possible for large PAH (667 Da) with significantly higher molecular mass than the species seen to cluster in mass spectrometry studies [65, 190]. Previous work [489] reveals that physical nucleation of pericondensed aromatics, such as pyrene, is unable to explain the formation of soot. We therefore conclude that the model of irreversible dimerisation of pyrene can describe aspects of soot formation, yet not because pyrene is actually dimerising – it points to another mechanism with similar concentrations of the critical species and similarly high collision efficiencies. Therefore,

we see this model as acting as a surrogate for the real soot formation model.

We can now systemically consider chemical mechanisms. Figure 49 shows the bond energies between the various reactive edge types that have been detailed in this review (full details can be found in [325] and [344]). The bond energies are used to consider the thermal stability of the first crosslink critical for each chemical mechanism. It has already been established that bond energies above −40 kcal/mol are found to be readily broken in flames (such as $\beta$-scission [414] and PAH dimerisation [511]). Thermal fragmentation is described by the energy barrier between the bound and the transition states. However, we found the Bell-Evans-Polanyi relationship is still observed (the barrier was linearly proportional to the bond energy, for the weakly bound species) and that for many structures the reaction was barrierless or small [344]. Therefore, the bond energy threshold of −40 kcal/mol is considered an appropriate proxy for stability of bonds within a flame.

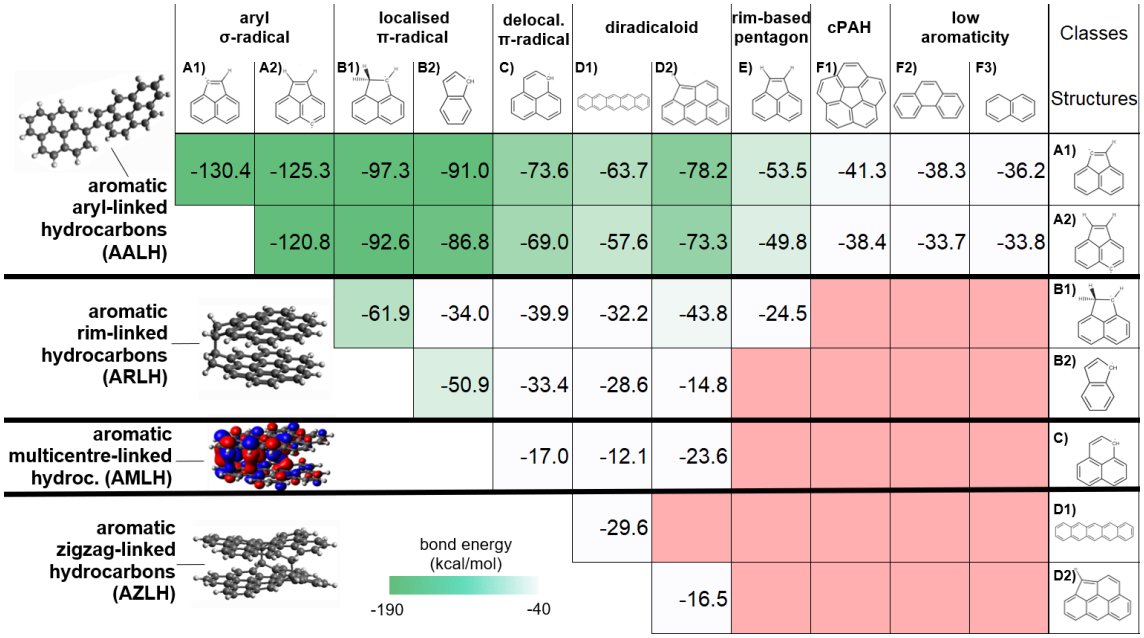


**Figure 49:** *Bond energy between various small aromatic molecules [325].*

The grid suggests a naming strategy based on the reactive species; A) $\sigma$-radicals, B) localised $\pi$-radicals, C) delocalised $\pi$-radicals and D) diradicaloids:

- Aromatic aryl-linked hydrocarbons (AALH), involving aryl-type $\sigma$-radicals A), of which the clustering of hydrocarbons radical chain reactions (CHRCR) mechanism [234] is a subset with aryl-radicals A) attacking delocalised $\pi$-radicals C). What are usually called aliphatic/aromatic linked hydrocarbons [100] are also represented by A)+E) and A)+F2) reactions. Strong, thermally stable bonds are formed.
- Aromatic rim-linked hydrocarbons (ARLH), involving localised $\pi$-radicals B). Strong bonds are only formed with other localised $\pi$-radicals, however, as the aromatic network enlarges dispersion interactions could allow for a physical+chemical mechanism. Multiradicals could also form that would allow for a chain reaction to proceed.

- Aromatic multicentre-linked hydrocarbon (AMLH), involving delocalised $\pi$-radicals PAH C). These react with themselves through pancake bonds but are also able to form non-stacked $\sigma$-dimers, which are shown in this table.
- Aromatic zig-zag-linked hydrocarbons (AZLH), involving diradicaloids D). These react through cyclisations but can also polymerise weakly.

The forward rate constant was also computed for the small aromatics [344]. The maximum rate was $10^{12}$ $cm^3mol^{-1}s^{-1}$ for aryl-radical recombination. Previous work from Frenklach and Mebel showed that even with a forward rate of this order there is still insufficient nucleation flux for nanoparticle formation [152]. This leaves us with the uncomfortable conclusion that no chemical mechanism involving these small aromatics can explain soot nucleation.

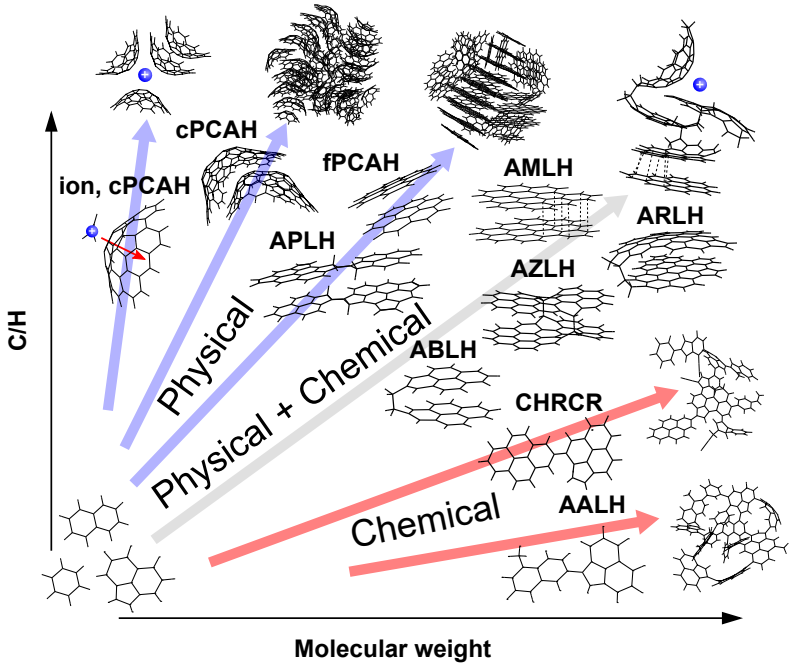


**Figure 50:** *Schematic of various soot nanoparticles arranged as a function of their C/H ratio and molecular weight.*

In Section 4.6 a "middle way" was presented between physical and chemical mechanisms. This can be schematically shown based on the C/H versus molecular weight diagram introduced by Violi in 2007 [39] (see Figure 50). It is important to consider that these mechanisms might not be independent. To illustrate this, a structure with multiple types of bonding is shown in the top right of the figure, with a curved species and ion included to indicate that electrical condensation could also enhance the inception of reactive species.

## 5.2 Outlook

These final comments will concentrate on fundamental gaps in experimental and modelling approaches as well as more practical steps that can be taken to reduce the emission

of these species from combustion.

### 5.2.1 Experimental outlook

To guide the discussion around fundamental gaps in current knowledge we have plotted some representative data for experimentally observed species in a $H/C$ *vs* molecular mass graph that was initially plotted by Wagner, Jander and Homann in 1990 [226] (see Figure 51).

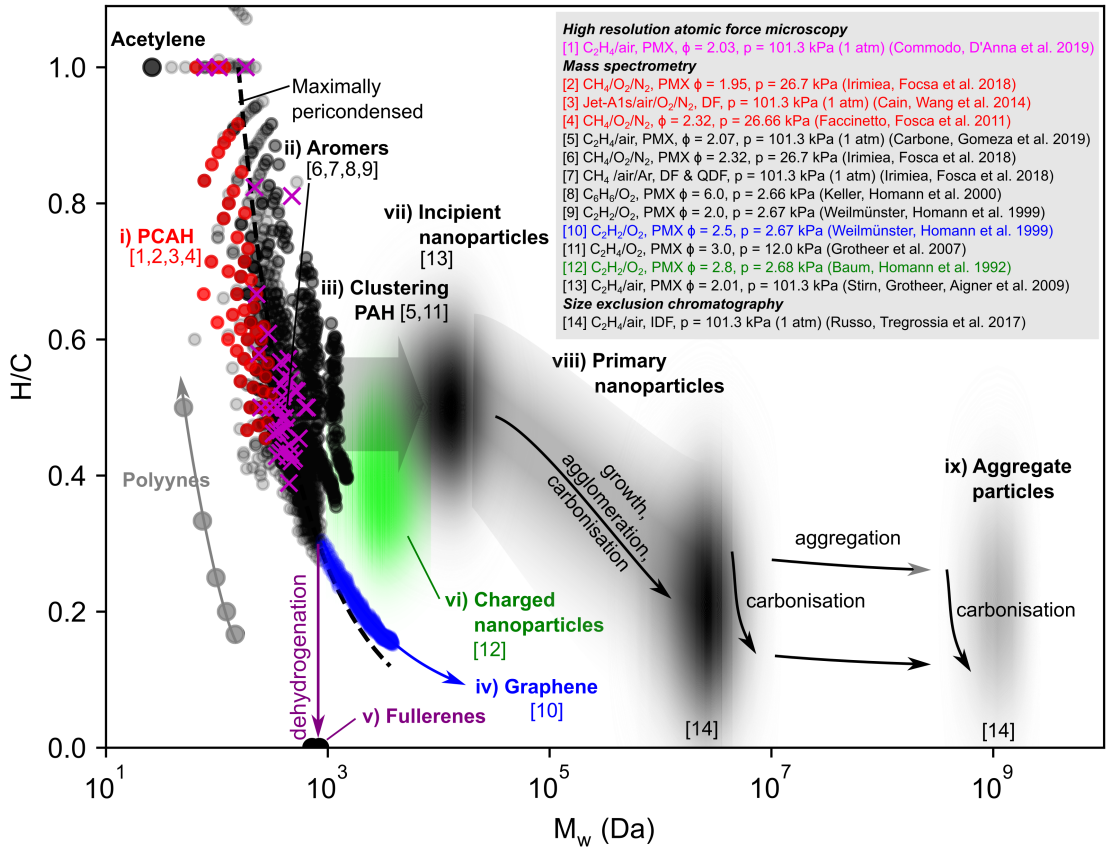


**Figure 51:** *The variety of transformation of hydrocarbons towards soot formation. The inset shows the various data sources [25, 58, 65, 88, 134, 181, 189, 220, 243, 425, 521].*

The molecular masses of the different species are determined directly from either HR-AFM [88, 444], mass spectrometry data [25, 58, 65, 134, 181, 189, 190, 220, 221, 243, 521] or size exclusion chromatography [425] from hydrocarbon flames. In modern high resolution mass spectrometers, the $H/C$ ratio can be determined directly assuming only carbon and hydrogen are present. The $H/C$ ratio of the other nanoparticles, primary particles and aggregate particles are determined from elemental analysis with the ranges chosen to cover the observed values. Arrows show the pathways from precursors to particles for which experimental data or a correlation exists, unless otherwise mentioned below. It

is helpful to make use of molecular mass data from mass spectrometry instead of mobility diameter in order to directly compare molecular growth and nanoparticle formation. However, for the primary and aggregate soot modes this requires using size exclusion chromatography results that have greater uncertainty.

Looking at Figure 51, the first and most evident trend is a decrease in hydrogen content of the carbonaceous species as the mass increases. This follows from the entropically driven nature of soot formation due to $H_2$ evolution [511]. The initial formation of polyynes from acetylene is well understood [186] and growth does not extend much beyond 10 carbon atoms due to radical induced fragmentation and cyclisation into pericondensed aromatic hydrocarbons (PCAH). **i) PCAH** primarily form via the HACA growth mechanism and recombination reactions [187]. More work is needed to understand the variety of isomers of PCAH. The generally accepted view that HACA growth proceeds through only 6-membered rings has recently been challenged computationally [255] and experimentally [88, 231, 234], with the presence of pentagonal rings being more prevalent than previously thought. These new insights require more detailed understanding of methyl additions [188, 531], ring enlargements [549], aromaticity [303], curvature [409] and fragmentation routes. Finally, synchrotron methods such as double imaging Photoelectron Photoion Coincidence Spectroscopy method ($i^2$PEPICO) promise better isomer discernment for larger PAH with pentagonal rings [347] as well as resolution improvements in PI-MS experiments.

A second large distribution of species with mass near 500 Da has also been detected in many different flame environments [11, 112, 134, 189, 221, 224, 243, 243, 428, 547] – called "**ii) aromers**" by Homann [208]. It is not entirely clear how these form but suggestions include crosslinking of $\sigma$-radicals [208] or localised $\pi$-radical recombinations that then cyclodehydrogenate to form nearly pericondensed structures. Evidence for such a crosslinking reaction recently was shown from hierarchical clustering analysis of SIMS-TOF MS providing strong evidence that the aromers arise from crosslinking of small aromatics with 4–8 hydrogen atoms lost during subsequent cyclisation [135]. Curvature integration is also not fully understood. The curvature integration seen experimentally [323] cannot be explained through HACA growth alone [152, 292] and therefore pathways such as crosslinking that allow for embedded pentagonal rings are required [420, 492].

In low-pressure flames certain pathways that do not lead to soot have been explored. HACA growth can be continued in low pressure acetylene flames to form large **iv) graphene** structures [521]. **v) Fullerenes** can form in benzene/oxygen flames [164]. The fullerenes are suggested to form due to multiple crosslinks of small aromatics, producing aromers large enough to be significantly curved to become fullerenes during dehydrogenation. It is still unclear how aromatics close to form fullerenes. Computational work suggests that hydrogen must be mostly lost from the aromatics before they can curl and close to form carbon cages [429]. Experimental work recently showed the formation of hydrogenated fullerene $C_{66}H_4$ with heptagonal rings in hydrocarbon flames [484], suggesting closure before complete dehydrogenation. It is still unclear whether subsequent dehydrogenation and $C_2$ loss could explain the formation of the symmetric fullerene $C_{60}$ – as has been proposed for plasmas in the "shrinking hot giant model" [321, 422]. The synthesis of aerosolised graphene is also of industrial significance. It is still unclear how low pressure acetylene/oxygen flames [521] and microwave reactors [105] are able to produce planar

graphene and avoid fullerene or soot formation.

**vi) Charged nanoparticles** are formed in acetylene flames (but not significantly in benzene flames). One possible explanation for this observation is an ion, cPAH electrical condensation mechanism. This could explain the correlation Homann found with the larger aromer species and these nanoparticles [210] and why their mass is low – ion-dipole interaction can only stabilise a few cPAH. However, this is simply conjecture and detailed fragmentation studies using mass spectrometry are required to understand the nanoparticles' constituents. More work is also needed to understand how electrical condensation involving cPAH can influence chemical mechanisms as briefly shown in Figure 50, but it appears that it is not the critical route for nanoparticle formation in atmospheric flames [514].

**iii) Clustering PAH** have only been observed with a periodicity of $\sim$500 Da [65, 190] suggesting that these larger aromers are the reactive structures that lead to soot formation. From HR-AFM it appears that reactive edges are in partial equilibrium with hydrogen radicals and hydrogen gas [88, 325] leading to a significant fraction of localised $\pi$-radicals and $\sigma$-radicals. More work is needed to understand which sites are in high enough concentrations to rapidly form the $<$4 nm **vii) incipient nanoparticles** in the flame [31].

Further processes lead to larger $>$ 4 nm **viii) primary nanoparticles**. The primary nanoparticle mode is found to increase in mass until it becomes the primary soot particle mode seen in aggregates around 10–20 nm in size [88]. We will not discuss the further processes involved in formation of aggregate soot particles as this is not the focus of this review, but will mention again that the liquid-like halos are thought to be due to sampling artifacts (see Figure 29). It is clear that much is still to be understood about nanoparticle formation requiring further experimental studies to fill in the gaps.

### 5.2.2 Modelling outlook

Modelling also requires significant developments going forward in order to better understand and describe soot formation. Reproducibility in modelling combustion kinetics has always been a strength within combustion science [177]. Starting with CHEMKIN—A Chemical Kinetics Software Package, developed by Sandia National Laboratories in the 1960s, standardisation of the kinetic and thermodynamic data format allowed for the widespread use of such software packages for modelling combustion. This was further facilitated by the software being open and made available on the world wide web (an informative historical description can be found by Council [91] and we have also recently reviewed the various databases available online at present [342]). These approaches have allowed experimental and increasingly powerful computational approaches to provide insights into soot formation. A recent example of the power of these techniques is the paper from Frenklach and Mebel on comparing various reactive aromatics in forming soot [152]. However, these approaches are limited by the size of the mechanisms that can be developed by hand [308]. Automation, therefore, has developed naturally as kinetic mechanisms for realistic fuels begin to contain thousands of reactions and thus require software to construct. One such example is the Reaction Mechanism Generator (RMG) [158, 176] that employs rules based on species fragmentation patterns to predict reaction pathways and thermodynamics to develop mechanisms. RMG also performs au-

tomated electronic structure calculations for specific classes of reactions [32] (another example being EStokTP: Electronic Structure to Temperature- and Pressure-Dependent Rate Constants [66]). The use of freely available software has always allowed for robust collaboration in soot modelling, starting with Frenklach's MoMIC soot library for CHEMKIN [418]. With new open data initiatives it is an imperative that software and data are made available with publications to continue the reproducibility for which this community has become known. For example, recent efforts from the Internal Sooting Flame (ISF) Workshop to standardise experimental flame configurations allowed simpler collaboration and comparisons with models.

Another challenge of modelling soot is the multiscale nature of the problem. Different scales often require different numerical approaches and this has made comparison between models challenging to date. For example, as PAH grow it becomes unfeasible to describe every possible reaction path in a kinetic mechanism; this has been tackled by switching to stochastic approaches such as kinetic Monte Carlo (KMC) simulation of aromatic growth (*e.g.* the KMC-ARS in MOpS [410] – `https://github.com/ucam-ceb-como/MOpS/`, SNAPS [286] from Violi *et al.* and implementations from Frenklach *et al.* [526, 528]). In terms of KMC this requires all of the jump processes and their associated rates to be explicitly stated and the approximations used to couple kinetic mechanisms and KMC to be disclosed in publications. Reproduction of PAH isomers that are now experimentally attainable from HR-AFM and PI-MS needs to be demonstrated with such codes. Various scales also require model reduction to allow for kinetic mechanisms to be applied to larger scale simulations, such as computational fluid dynamics (CFD) simulations. This is known as surrogate model creation, where the goal is to create a smaller kinetic mechanism that captures the main features of the combustion phenomena with a simpler model than the full mechanism or model [365, 400]. A variety of approaches for model reduction are available including support vector machines, polynomial response surface models, interpolations, radial basis functions, splines and artificial neural networks, to name a few. The importance of finding the optimal approximation for reducing a particular problem was recently highlighted [160]. Experimental approaches to model reduction are also attractive. The Hybrid Chemistry (HyChem) approach to fuel pyrolysis allows experimentally derived fragmentation patterns to be coupled to small hydrocarbon mechanisms providing a significant reduction in mechanism size [516].

This sort of multiscale modelling of soot formation, however, has led to highly customised software developed independently by various groups (see Figure 52 for our approach). This is due to challenges associated with linking of various data structures and numerical approaches. One of the early projects that sought to solve this problem was the Collaboratory for Multi-scale Chemical Science (CMCS) project started in 2001 [381] and led by members of the combustion community in the USA. This project used the recently developed semantic web tools (developed in computer science to extend the internet into a machine readable and writable platform) to link and connect models and data for combustion applications. The approach was memorably presented by Frenklach at the 2006 International Symposium on Combustion with his PrIMe database [150, 541]. While the entire framework developed in the CMCS project did not ultimately become widely used [441] the project led to critical infrastructure for modelling soot including the Active Thermochemical Tables (ATcT), the Basis Set Exchange (BSE), Group Additivity Thermodynamic Properties (GATP – now used in RMG to good effect) and the highly

successful GRI-Mech kinetic mechanism [471].

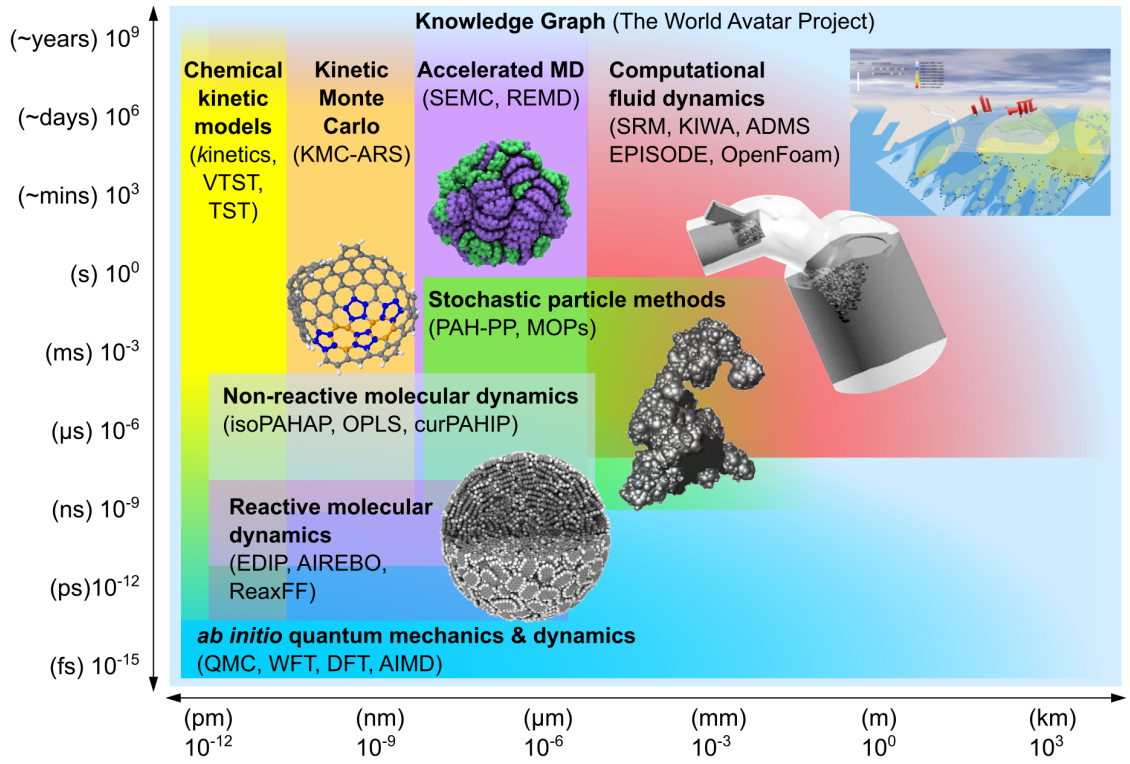


**Figure 52:** *Linking spatial and temporal scales for modelling nanoparticle formation and pollution dispersion.*

Since these initial efforts to build a web-based infrastructure for combustion science, considerable advances have been made in semantic web technologies, with current focus being on Knowledge Graph technologies. This recently led us to develop new and extended Knowledge Graph Ontologies for both the microscale; OntoKin [139] (for representing chemical kinetic reaction mechanisms including thermodynamics), OntoCompChem [272] (representing electronic structure calculations), OntoSpecies (representing molecular species), and for the macroscale; OntoCAPE [370] (representing chemical engineering plants and extended to decentralised eco-industrial parks in OntoEIP [551]), Weather Ontology [385] (representing wind, rain, temperature and humidity), OntoPowSys [113] (representing power systems) and OntoCityGML [128] (an extension of CityGML representing buildings and infrastructure [267]). While these approaches are in their infancy, they open up the possibility of rigorously and consistently linking models and data across spatial and temporal scales as demonstrated in Figure 52 as well as comparison between models and data [129]. One example was the recent virtual sensor for atmospheric pollutants emitted from ships that linked models and data from microscale kinetic mechanisms to models of engine performance and pollutant emissions, through to the atmospheric dispersion of these pollutants across Singapore [140]. Automation is captured by the OntoAgent ontology [552] which enables expansion and improvement of agents operating on the knowledge graph. We envisage that such a systematic approach will be critical for providing the infrastructure to develop the multiscale descriptions of combus-

tion to elucidate the formation of carbonaceous nanoparticles in flames.

### 5.2.3 Practical steps

The more practical aspects of reducing nanoparticle emissions from combustion devices require that these emissions are eliminated in flames or removed in aftertreatment systems. While we have shown experimental studies that are able to detect various nanoparticle modes, routine measurements of these smallest nanoparticle emissions from combustion devices are still not possible. As measurements improve, empirical models will be able to establish operating conditions to reduce nanoparticle emissions. However, fundamental understanding could provide more direct means to limit emission of these smallest combustion products. We will highlight one recent example of fuel mix design where the yield sooting index was used to provide a diesel fuel with reasonable cetane number but significantly lower sooting propensity [247]. These approaches could also be extended with particle size measurements for reducing nanoparticle emissions from engines. This is particularly important as new lean engine combustion systems are developed to eliminate soot mass but not necessarily soot nanoparticles. Similar insights into the effects of cool combustion, charge and ozone injection [235, 236], hydrogen and ammonia addition [29, 225] and biofuels [142, 432] on nanoparticle emissions are also required. Another approach is to consider aftertreatment systems. As mentioned in Section 2.2, many of the smallest nanoparticles are not filtered by aftertreatment systems [463] due to their low coagulation efficiencies [212]. Recent efforts to remove these nanoparticles with activated carbon or fibre filters need to be more extensively explored [253]. It is also unclear how nanoparticle filtration will improve as the soot cake develops [288].

Ultimately, the emission of carbonaceous nanoparticles needs to be a research and industrial priority for the future of combustion devices. We end this review with the comment from Miller, Pilling and Troe's 2005 review [355]:

> "Hopefully, whoever writes this review in 2054 will report that there is then a complete, quantitative understanding of the mechanism of soot formation in combustion."

Recent modelling and experimental advances suggest such enlightenment might occur sooner than 2054.

## Acknowledgements

Thanks to the members of the Computational Modelling Group in the Department of Chemical Engineering and Biotechnology at the University of Cambridge, who over the years have contributed to much of the work reviewed above. We would also like to thank the many collaborators that we have worked with. In particular, we thank those involved in computing the crosslinks between various reactive aromatics found in Figure 49: Angiras Menon and Laura Pascazio, with collaborators Dingyu Hou and Xiaoqing You from Tsinghua University. Thanks to Angiras Menon, Sebastian Mosbach and Jethro Akroyd

for insights into the knowledge graph technologies. Thanks to Jethro Akroyd and Louise Renwick for their careful editing of the text. This project is supported by the National Research Foundation (NRF), Prime Minister's Office, Singapore under its Campus for Research Excellence and Technological Enterprise (CREATE) programme. M. Kraft gratefully acknowledges the support of the Alexander von Humboldt foundation.

---

# References


[1] J. Abrahamson. Saturated platelets are new intermediates in hydrocarbon pyrolysis and carbon formation. *Nature*, 266(24):323–327, 1977. doi:10.1038/266323a0.

[2] B. D. Adamson, S. A. Skeen, M. Ahmed, and N. Hansen. Detection of aliphatically bridged multi-core polycyclic aromatic hydrocarbons in sooting flames with atmospheric-sampling high-resolution tandem mass spectrometry. *The Journal of Physical Chemistry A*, 122(48):9338–9349, 2018. doi:10.1021/acs.jpca.8b08947.

[3] E. M. Adkins and J. H. Miller. Extinction measurements for optical band gap determination of soot in a series of nitrogen-diluted ethylene/air non-premixed flames. *Physical Chemistry Chemical Physics*, 17(4):2686–2695, 2015. doi:10.1039/C4CP04452E.

[4] E. M. Adkins and J. H. Miller. Towards a taxonomy of topology for polynuclear aromatic hydrocarbons: linking electronic and molecular structure. *Physical Chemistry Chemical Physics*, 19(41):28458–28469, 2017. doi:10.1039/C7CP06048C.

[5] E. M. Adkins, J. A. Giaccai, and J. H. Miller. Computed electronic structure of polynuclear aromatic hydrocarbon agglomerates. *Proceedings of the Combustion Institute*, 36(1):957–964, 2017. doi:10.1016/j.proci.2016.06.186.

[6] G. Adler, A. A. Riziq, C. Erlick, and Y. Rudich. Effect of intrinsic organic carbon on the optical properties of fresh diesel soot. *Proceedings of the National Academy of Sciences*, 107(15):6699–6704, 2010. doi:10.1073/pnas.0903311106.

[7] J. Ahrens, M. Bachmann, T. Baum, J. Griesheimer, R. Kovacs, P. Weilmünster, and K.-H. Homann. Fullerenes and their ions in hydrocarbon flames. *International Journal of Mass Spectrometry and Ion Processes*, 138:133 – 148, 1994. doi:10.1016/0168-1176(94)04036-2.

[8] J. L. Allen, G. Oberdorster, K. Morris-Schaffer, C. Wong, C. Klocke, M. Sobolewski, K. Conrad, M. Mayer-Proschel, and D. Cory-Slechta. Developmental neurotoxicity of inhaled ambient ultrafine particle air pollution: Parallels with neuropathological and behavioral features of autism and other neurodevelopmental disorders. *Neurotoxicology*, 59:140–154, 2017. doi:10.1016/j.neuro.2015.12.014.

[9] A. B. Alquaity, J. Han, M. Chahine, H. Selim, M. Belhi, S. M. Sarathy, F. Bisetti, and A. Farooq. Measurements of positively charged ions in premixed methane-oxygen atmospheric flames. *Combustion Science and Technology*, 189(4):575–594, 2017. doi:10.1080/00102202.2016.1226821.

[10] H. M. Amin, A. Bennett, and W. L. Roberts. Determining fractal properties of soot aggregates and primary particle size distribution in counterflow flames up to 10atm. *Proceedings of the Combustion Institute*, 37(1):1161 – 1168, 2019. doi:10.1016/j.proci.2018.07.057.

[11] B. Apicella, M. Millan, A. Herod, A. Carpentieri, P. Pucci, and A. Ciajolo. Separation and measurement of flame-formed high molecular weight polycyclic aromatic hydrocarbons by size-exclusion chromatography and laser desorption/ionization time-of-flight mass spectrometry. *Rapid Communications in Mass Spectrometry*, 20(7):1104–1108, 2006. doi:10.1002/rcm.2419.

[12] B. Apicella, A. Ciajolo, A. Tregrossi, J. Abrahamson, R. L. Vander Wal, and C. Russo. HRTEM and EELS investigations of flame-formed soot nanostructure. *Fuel*, 225:218–224, 2018. doi:10.1016/j.fuel.2018.03.091.

[13] J. Appel, H. Bockhorn, and M. Frenklach. Kinetic modeling of soot formation with detailed chemistry and physics: laminar premixed flames of C2 hydrocarbons. *Combustion and flame*, 121(1-2):122–136, 2000. doi:10.1016/S0010-2180(99)00135-2.

[14] A. Ashton and A. Hayhurst. Kinetics of collisional ionization of alkali metal atoms and recombination of electrons with alkali metal ions in flames. *Combustion and Flame*, 21(1):69–75, 1973. doi:10.1016/0010-2180(73)90008-4.

[15] R. W. Atkinson, I. M. Carey, A. J. Kent, T. P. V. Staa, R. Anderson, and D. G. Cook. Long-Term Exposure to Outdoor Air Pollution and Incidence of Cardiovascular Diseases. *Epidemiology*, 24(1):44–53, 2013. doi:10.1097/EDE.0b013e318276ccb8.

[16] M. Bachmann, W. Wiese, and K.-H. Homann. PAH and aromers: Precursors of fullerenes and soot. *Symposium (International) on Combustion*, 26(2):2259 – 2267, 1996. doi:10.1016/S0082-0784(96)80053-1.

[17] W. M. Baird, L. A. Hooven, and B. Mahadevan. Carcinogenic polycyclic aromatic hydrocarbon-DNA adducts and mechanism of action. *Environmental and Molecular Mutagenesis*, 45(2-3):106–114, 2005. doi:10.1002/em.20095.

[18] A. Baldelli, U. Trivanovic, T. A. Sipkens, and S. N. Rogak. On determining soot maturity: A review of the role of microscopy-and spectroscopy-based techniques. *Chemosphere*, page 126532, 2020. doi:10.1016/j.chemosphere.2020.126532.

[19] M. Balthasar and M. Kraft. A stochastic approach to calculate the particle size distribution function of soot particles in laminar premixed flames. *Combustion and Flame*, 133(3):289–298, 2003. doi:10.1016/S0010-2180(03)00003-8.

[20] T. G. Baquet, H.-H. Grotheer, and M. Aigner. Simultaneous detection of two types of soot precursor particles using photoionization mass spectrometry. *Rapid Communications in Mass Spectrometry*, 21(24):4060–4064, 2007. doi:10.1002/rcm.3297.

[21] A. Barone, A. D'Alessio, and A. D'Anna. Morphological characterization of the early process of soot formation by atomic force microscopy. *Combustion and Flame*, 132(1-2):181–187, 2003. doi:10.1016/S0010-2180(02)00434-0.

[22] E. J. Barrientos, M. Lapuerta, and A. L. Boehman. Group additivity in soot formation for the example of C-5 oxygenated hydrocarbon fuels. *Combustion and Flame*, 160(8):1484–1498, 2013. doi:10.1016/j.combustflame.2013.02.024.

[23] F. Battin-Leclerc. Detailed chemical kinetic models for the low-temperature combustion of hydrocarbons with application to gasoline and diesel fuel surrogates. *Progress in Energy and Combustion Science 34*, 34:440–498, 2008. doi:10.1016/j.pecs.2007.10.002.

[24] D. L. Baulch, C. J. Cobos, R. A. Cox, C. Esser, P. Frank, T. Just, J. A. Kerr, J. Pilling, M. J .and Troe, R. W. Walker, and J. Warnatz. Evaluated kinetic data for combustion modelling. *Journal of Physical and Chemical Reference Data*, 21 (3):411–734, 1992. doi:10.1063/1.555908.

[25] T. Baum, S. Löffler, P. Löffler, P. Weilmünster, and K.-H. Homann. Fullerene ions and their relation to PAH and soot in low-pressure hydrocarbon flames. *Berichte der Bunsengesellschaft für physikalische Chemie*, 96(7):841–857, 1992. doi:10.1002/bbpc.19920960702.

[26] H. Behrens. Flame instabilities and combustion mechanism. *Symposium (International) on Combustion*, 4(1):538–545, 1953. doi:10.1016/S0082-0784(53)80075-5.

[27] M. Bendikov, H. M. Duong, K. Starkey, K. Houk, E. A. Carter, and F. Wudl. Oligoacenes: theoretical prediction of open-shell singlet diradical ground states. *Journal of the American Chemical Society*, 126(24):7416–7417, 2004. doi:10.1021/ja048919w.

[28] P. Benigni, J. D. DeBord, C. J. Thompson, P. Gardinali, and F. Fernandez-Lima. Increasing polyaromatic hydrocarbon (PAH) molecular coverage during fossil oil analysis by combining gas chromatography and atmospheric-pressure laser ionization fourier transform ion cyclotron resonance mass spectrometry (FT-ICR MS). *Energy & Fuels*, 30(1):196–203, 2016. doi:10.1021/acs.energyfuels.5b02292.

[29] A. M. Bennett, P. Liu, Z. Li, N. M. Kharbatia, W. Boyette, A. R. Masri, and W. L. Roberts. Soot formation in laminar flames of ethylene/ammonia. *Combustion and Flame*, 220:210–218, 2020. doi:10.1016/j.combustflame.2020.06.042.

[30] M. Berthelot. Sur une nouvelle série de composés organiques, le quadricarbure d'hydrogène et ses dérivés (translation: Note on a new series of organic compounds, tetra-carbon hydride and its derivatives). *Comptes rendus de l'Académie des Sciences*, 50:805–808, 1860.

[31] C. Betrancourt, F. Liu, P. Desgroux, X. Mercier, A. Faccinetto, M. Salamanca, L. Ruwe, K. Kohse-Höinghaus, D. Emmrich, A. Beyer, A. Gölzhäuser, and T. Tritscher. Investigation of the size of the incandescent incipient soot particles in premixed sooting and nucleation flames of n-butane using LII, HIM, and 1 nm-SMPS. *Aerosol Science and Technology*, 51(8):916–935, 2017. doi:10.1080/02786826.2017.1325440.

[32] P. L. Bhoorasingh, B. L. Slakman, F. Seyedzadeh Khanshan, J. Y. Cain, and R. H. West. Automated transition state theory calculations for high-throughput kinetics. *The Journal of Physical Chemistry A*, 121(37):6896–6904, 2017. doi:10.1021/acs.jpca.7b07361.

[33] H. Bhowmick and S. K. Biswas. Relationship between physical structure and tribology of single soot particles generated by burning ethylene. *Tribology Letters*, 44(2):139–149, 2011. doi:10.1007/s11249-011-9831-5.

[34] J. Birks, D. Dyson, and I. Munro. 'excimer' fluorescence II. lifetime studies of pyrene solutions. *Proceedings of the Royal Society of London. Series A. Mathematical and Physical Sciences*, 275(1363):575–588, 1963. doi:10.1098/rspa.1963.0187.

[35] J. D. Bittner and J. B. Howard. Composition profiles and reaction mechanisms in a near-sooting premixed benzene/oxygen/argon flame. *Symposium (International) on Combustion*, 18(1):1105–1116, 1981. doi:10.1016/S0082-0784(81)80115-4.

[36] H. Bladh, N.-E. Olofsson, T. Mouton, J. Simonsson, X. Mercier, A. Faccinetto, P.-E. Bengtsson, and P. Desgroux. Probing the smallest soot particles in low-sooting premixed flames using laser-induced incandescence. *Proceedings of the Combustion Institute*, 35(2):1843–1850, 2015. doi:10.1016/j.proci.2014.06.001.

[37] H. Bockhorn. *Soot Formation in Combustion: Mechanisms and Models*. Springer Science & Business Media, 1994.

[38] H. Bockhorn, F. Fetting, and H. Wenz. Investigation of the formation of high molecular hydrocarbons and soot in premixed hydrocarbon-oxygen flames. *Berichte der Bunsengesellschaft für physikalische Chemie*, 87(11):1067–1073, 1983. doi:10.1002/bbpc.19830871121.

[39] H. Bockhorn, A. D'Anna, A. Sarofim, and H. Wang, editors. *Combustion Generated Fine Carbonaceous Particles*. KIT Scientific Publishing, 2009. doi:10.5445/KSP/1000013744.

[40] J. M. Bofill, N. Bru, J. Farras, S. Olivella, A. Sole, and J. Vilarrasa. Molecular and electronic structure of the low-lying electronic states of cycloalkenylidenes. cyclopentadienylidene. *Journal of the American Chemical Society*, 110(12):3740–3746, 1988. doi:10.1021/ja00214a006.

[41] A. Bogdanov, D. Deininger, and G. Dyuzhev. Development prospects of the commercial production of fullerenes. *Technical Physics*, 45(5):521–527, 2000. doi:10.1134/1.1259670.

[42] H. Böhm, D. Hesse, H. Jander, B. Lüers, J. Pietscher, H. Wagner, and M. Weiss. The influence of pressure and temperature on soot formation in premixed flames. *Symposium (International) on combustion*, 22(1):403–411, 1989. doi:10.1016/S0082-0784(89)80047-5.

[43] P. Bonczyk. Effects of metal additives on soot precursors and particulates in a $C_2H_4/O_2/N_2$/Ar premixed flame. *Fuel*, 70(12):1403–1411, 1991. doi:10.1016/0016-2361(91)90006-V.

[44] T. C. Bond, S. J. Doherty, D. W. Fahey, P. M. Forster, T. Berntsen, B. J. Deangelo, M. G. Flanner, S. Ghan, B. Kärcher, D. Koch, S. Kinne, Y. Kondo, P. K. Quinn, M. C. Sarofim, M. G. Schultz, M. Schulz, C. Venkataraman, H. Zhang, S. Zhang, N. Bellouin, S. K. Guttikunda, P. K. Hopke, M. Z. Jacobson, J. W. Kaiser, Z. Klimont, U. Lohmann, J. P. Schwarz, D. Shindell, T. Storelvmo, S. G. Warren, and C. S. Zender. Bounding the role of black carbon in the climate system: A scientific assessment. *Journal of Geophysical Research Atmospheres*, 118(11): 5380–5552, 2013. doi:10.1002/jgrd.50171.

[45] U. Bonne, K. Homann, and H. G. Wagner. Carbon formation in premixed flames. *Symposium (International) on Combustion*, 503, 1965. doi:10.1016/S0082-0784(65)80197-7.

[46] P. J. Borm, D. Robbins, S. Haubold, T. Kuhlbusch, H. Fissan, K. Donaldson, R. Schins, V. Stone, W. Kreyling, J. Lademann, J. Krutmann, D. B. Warheit, and E. Oberdorster. The potential risks of nanomaterials: A review carried out for ECETOC. *Particle and Fibre Toxicology*, 3(11):1–35, 2006. doi:10.1186/1743-8977-3-11.

[47] C. E. Boström, P. Gerde, A. Hanberg, B. Jernström, C. Johansson, T. Kyrklund, A. Rannug, M. Törnqvist, K. Victorin, and R. Westerholm. Cancer risk assessment, indicators, and guidelines for polycyclic aromatic hydrocarbons in the ambient air. *Environmental Health Perspectives*, 110:451–488, 2002. doi:10.1289/ehp.110-1241197.

[48] M. L. Botero, E. M. Adkins, S. González-Calera, H. Miller, and M. Kraft. PAH structure analysis of soot in a non-premixed flame using high-resolution transmission electron microscopy and optical band gap analysis. *Combustion and Flame*, 164:250–258, 2016. doi:10.1016/j.combustflame.2015.11.022.

[49] M. L. Botero, D. Chen, S. González-Calera, D. Jefferson, and M. Kraft. HRTEM evaluation of soot particles produced by the non-premixed combustion of liquid fuels. *Carbon*, 96:459–473, 2016. doi:10.1016/j.carbon.2015.09.077.

[50] M. L. Botero, S. Mosbach, and M. Kraft. Sooting tendency and particle size distributions of n-heptane/toluene mixtures burned in a wick-fed diffusion flame. *Fuel*, 169:111–119, 2016. doi:10.1016/j.fuel.2015.12.014.

[51] M. L. Botero, N. Eaves, J. A. Dreyer, Y. Sheng, J. Akroyd, W. Yang, and M. Kraft. Experimental and numerical study of the evolution of soot primary particles in a diffusion flame. *Proceedings of the Combustion Institute*, 37(2):2047–2055, 2019. doi:10.1016/j.proci.2018.06.185.

[52] M. L. Botero, Y. Sheng, J. Akroyd, J. Martin, J. A. Dreyer, W. Yang, and M. Kraft. Internal structure of soot particles in a diffusion flame. *Carbon*, 141:635–642, 2019. doi:10.1016/j.carbon.2018.09.063.

[53] M. L. Botero, J. Akroyd, D. Chen, M. Kraft, and J. R. Agudelo. On the thermophoretic sampling and tem-based characterisation of soot particles in flames. *Carbon*, 2020. doi:10.1016/j.carbon.2020.09.074.

[54] D. Bourissou, O. Guerret, F. P. Gabbai, and G. Bertrand. Stable carbenes. *Chemical Reviews*, 100(1):39–92, 2000. doi:10.1021/cr940472u.

[55] K. Bowal, J. W. Martin, A. J. Misquitta, and M. Kraft. Ion-induced soot nucleation using a new potential for curved aromatics. *Combustion Science and Technology*, 191(5):1–19, 2019. doi:10.1080/00102202.2019.1565496.

[56] K. Bowal, J. Martin, and M. Kraft. Self-assembly of curved aromatic molecules in nanoparticles. submitted.

[57] W. T. Brande. XXII. On some new electro-chemical phenomena. *The Philosophical Magazine*, 44(196):124–130, 1814. doi:10.1080/14786441408637425.

[58] J. Cain, A. Laskin, R. Kholghy, and J. Thomson. Molecular characterization of organic content of soot along the centerline of a coflow diffusion flame. *Physical Chemistry Chemical Physics*, 16:25862–25875, 2014. doi:10.1039/C4CP03330B.

[59] J. P. Cain, P. L. Gassman, A. Laskin, and H. Wang. Micro-FTIR study of soot chemical composition—evidence of aliphatic hydrocarbons on nascent soot surfaces. *Physical Chemistry Chemical Physics*, 12(20):5206 – 5210, 2010. doi:10.1039/B924344E.

[60] H. Calcote and D. Manos. Effect of molecular structure on incipient soot formation. *Combustion and Flame*, 49(1-3):289–304, 1983. doi:10.1016/0010-2180(83)90172-4.

[61] H. F. Calcote. Electrical properties of flames: Burner flames in transverse electric fields. *Symposium on Combustion and Flame, and Explosion Phenomena*, 3(1): 245 – 253, 1948. doi:10.1016/S1062-2896(49)80033-X.

[62] H. F. Calcote. Mechanisms of soot nucleation in flames-A critical review. *Combustion and Flame*, 42(C):215–242, 1981. doi:10.1016/0010-2180(81)90159-0.

[63] H. F. Calcote, D. B. Olson, and D. G. Keil. Are ions important in soot formation? *Energy & Fuels*, 2(4):494–504, 1988. doi:10.1021/ef00010a016.

[64] F. Carbone, S. Moslih, and A. Gomez. Probing gas-to-particle transition in a moderately sooting atmospheric pressure ethylene/air laminar premixed flame. Part II: Molecular clusters and nascent soot particle size distributions. *Combustion and Flame*, 181:329–341, 2017. doi:10.1016/j.combustflame.2017.02.021.

[65] F. Carbone, M. R. Canagaratna, A. T. Lambe, J. T. Jayne, D. R. Worsnop, and A. Gomez. Exploratory analysis of a sooting premixed flame via on-line high resolution (APi-TOF) mass spectrometry. *Proceedings of the Combustion Institute*, 37:919–926, 2019. doi:10.1016/j.proci.2018.08.020.

[66] C. Cavallotti, M. Pelucchi, Y. Georgievskii, and S. Klippenstein. Estoktp: Electronic structure to temperature-and pressure-dependent rate constants—a code for automatically predicting the thermal kinetics of reactions. *Journal of chemical theory and computation*, 15(2):1122–1145, 2018. doi:10.1021/acs.jctc.8b00701.

[67] D. Cecere, L. Sgro, G. Basile, A. D'Alessio, A. D'Anna, and P. Minutolo. Evidence and characterization of nanoparticles produced in nonsooting premixed flames. *Combustion science and technology*, 174(11-12):377–398, 2002. doi:10.1080/00102200215079.

[68] R. K. Chakrabarty, N. D. Beres, H. Moosmüller, S. China, C. Mazzoleni, M. K. Dubey, L. Liu, and M. I. Mishchenko. Soot superaggregates from flaming wildfires and their direct radiative forcing. *Scientific reports*, 4:5508, 2014. doi:10.1038/srep05508.

[69] D. Chen and H. Wang. Cation-$\pi$ Interactions between Flame Chemiions and Aromatic Compounds. *Energy & Fuels*, 31(3):2345–2352, 2017. doi:10.1021/acs.energyfuels.6b02354.

[70] D. Chen and H. Wang. Homo–lumo gaps of homogeneous polycyclic aromatic hydrocarbon clusters. *The Journal of Physical Chemistry C*, 123(45):27785–27793, 2019. doi:10.1021/acs.jpcc.9b08300.

[71] D. Chen and H. Wang. Homo-lumo energy splitting in polycyclic aromatic hydrocarbons and their derivatives. *Proceedings of the Combustion Institute*, 37(1): 953–959, 2019. doi:10.1016/j.proci.2018.06.120.

[72] P. Chen, J. N. Metz, A. S. Mennito, S. Merchant, S. E. Smith, M. Siskin, S. P. Rucker, D. C. Dankworth, J. D. Kushnerick, N. Yao, and Y. Zhang. Petroleum pitch: Exploring a 50-year structure puzzle with real-space molecular imaging. *Carbon*, 161:456–465, 2020. doi:10.1016/j.carbon.2020.01.062.

[73] T. Chen. Formation of covalently bonded polycyclic aromatic hydrocarbons in the interstellar medium. *The Astrophysical Journal*, 866(2):113, 2018. doi:10.3847/1538-4357/aae38f.

[74] C. Chu, T. Zhang, and M. J. Thomson. The chemical structure effects of alkylbenzenes on soot formation in a laminar co-flow flame. *Combustion and Flame*, 204: 237–249, 2019. doi:10.1016/j.combustflame.2019.03.010.

[75] S.-H. Chung and A. Violi. Peri-condensed aromatics with aliphatic chains as key intermediates for the nucleation of aromatic hydrocarbons. *Proceedings of the Combustion Institute*, 33(1):693–700, 2011. doi:10.1016/j.proci.2010.06.038.

[76] S. L. Chung and N. L. Lai. Suppression of soot by metal additives during the combustion of polystyrene. *Journal of the Air and Waste Management Association*, 42(8):1082–1088, 1992. doi:10.1080/10473289.1992.10467056.

[77] T. T. Coburn and W. Jones. Carbene-carbene rearrangements in the acenaphthylcarbene-phenalenylidene system. *Tetrahedron Letters*, 14(40):3903–3906, 1973. doi:10.1016/S0040-4039(01)87068-4.

[78] D. Coe and J. Steinfeld. Fluorescence excitation and emission spectra of polycyclic aromatic hydrocarbons at flame temperatures. *Chemical Physics Letters*, 76(3): 485–489, 1980. doi:10.1016/0009-2614(80)80652-X.

[79] M. B. Colket and D. J. Seery. Reaction mechanisms for toluene pyrolysis. *Symposium (International) on Combustion*, 25(1):883–891, 1994. doi:10.1016/S0082-0784(06)80723-X.

[80] A. Comandini and K. Brezinsky. Theoretical study of the formation of naphthalene from the radical/$\pi$-bond addition between single-ring aromatic hydrocarbons. *The Journal of Physical Chemistry A*, 115(22):5547–5559, 2011. doi:10.1021/jp200201c.

[81] A. Comandini, T. Malewicki, and K. Brezinsky. Chemistry of polycyclic aromatic hydrocarbons formation from phenyl radical pyrolysis and reaction of phenyl and acetylene. *The Journal of Physical Chemistry A*, 116(10):2409–2434, 2012. doi:10.1021/jp207461a.

[82] A. Comandini, S. Abid, and N. Chaumeix. Polycyclic aromatic hydrocarbon growth by diradical cycloaddition/fragmentation. *The Journal of Physical Chemistry A*, 121(31):5921–5931, 2017. doi:10.1021/acs.jpca.7b05562.

[83] M. Commodo, L. A. Sgro, P. Minutolo, and A. D'Anna. Characterization of combustion-generated carbonaceous nanoparticles by size-dependent ultraviolet laser photoionization. *Journal of Physical Chemistry A*, 117(19):3980–3989, 2013. doi:10.1021/jp401061d.

[84] M. Commodo, G. De Falco, A. Bruno, C. Borriello, P. Minutolo, and A. D'Anna. Physicochemical evolution of nascent soot particles in a laminar premixed flame: from nucleation to early growth. *Combustion and Flame*, 162(10):3854–3863, 2015. doi:10.1016/j.combustflame.2015.07.022.

[85] M. Commodo, G. De Falco, R. Larciprete, A. D'Anna, and P. Minutolo. On the hydrophilic/hydrophobic character of carbonaceous nanoparticles formed in laminar premixed flames. *Experimental Thermal and Fluid Science*, 73:56–63, 2016. doi:10.1016/j.expthermflusci.2015.09.005.

[86] M. Commodo, A. D'Anna, G. De Falco, R. Larciprete, and P. Minutolo. Illuminating the earliest stages of the soot formation by photoemission and Raman spectroscopy. *Combustion and Flame*, 181:1339–1351, 2017. doi:10.1016/j.combustflame.2017.03.020.

[87] M. Commodo, P. H. Joo, G. De Falco, P. Minutolo, A. D'Anna, and O. L. Gülder. Raman spectroscopy of soot sampled in high-pressure diffusion flames. *Energy & Fuels*, 31(9):10158–10164, 2017. doi:10.1021/acs.energyfuels.7b01674.

[88] M. Commodo, K. Kaiser, G. De Falco, P. Minutolo, F. Schulz, A. D'Anna, and L. Gross. On the early stages of soot formation: Molecular structure elucidation by high-resolution atomic force microscopy. *Combustion and Flame*, 205:154–164, 2019. doi:10.1016/j.combustflame.2019.03.042.

[89] M. Commodo, A. E. Karataş, G. De Falco, P. Minutolo, A. D'Anna, and Ö. L. Gülder. On the effect of pressure on soot nanostructure: A raman spectroscopy investigation. *Combustion and Flame*, 219:13–19, 2020. doi:10.1016/j.combustflame.2020.04.008.

[90] P. Costa and W. Sander. Hydrogen bonding switches the spin state of diphenylcarbene from triplet to singlet. *Angewandte Chemie International Edition*, 53(20): 5122–5125, 2014. doi:10.1002/anie.201400176.

[91] N. R. Council. *Transforming Combustion Research through Cyberinfrastructure*. The National Academies Press, Washington, DC, 2011. ISBN 978-0-309-16387-3. doi:10.17226/13049.

[92] S. P. Crossley, W. E. Alvarez, and D. E. Resasco. Novel micropyrolyis index (MPI) to estimate the sooting tendency of fuels. *Energy & fuels*, 22(4):2455–2464, 2008. doi:10.1021/ef800058y.

[93] Z.-H. Cui, H. Lischka, H. Z. Beneberu, and M. Kertesz. Rotational barrier in phenalenyl neutral radical dimer: Separating pancake and van der Waals interactions. *Journal of the American Chemical Society*, 136(15):5539–5542, 2014. doi:10.1021/ja412862n.

[94] A. D'Alessio, A. Di Lorenzo, A. Sarofim, F. Beretta, S. Masi, and C. Venitozzi. Soot formation in methane-oxygen flames. *Symposium (International) on Combustion*, 15(1):1427–1438, 1975. doi:10.1016/S0082-0784(75)80401-2.

[95] A. D'Alessio, A. D'Anna, A. D'orsi, P. Minutolo, R. Barbella, and A. Ciajolo. Precursor formation and soot inception in premixed ethylene flames. *Symposium (International) on Combustion*, 24(1):973–980, 1992. doi:10.1016/S0082-0784(06)80115-3.

[96] A. D'alessio, G. Gambi, P. Minutolo, S. Russo, and A. D'Anna. Optical characterization of rich premixed $CH_4/O_2$ flamesacross the soot formation threshold. *Symposium (International) on Combustion*, 25(1):645–651, 1994. doi:10.1016/S0082-0784(06)80696-X.

[97] E. Dames, B. Sirjean, and H. Wang. Weakly bound carbon- carbon bonds in acenaphthene derivatives and hexaphenylethane. *The Journal of Physical Chemistry A*, 114(2):1161–1168, 2009. doi:10.1021/jp909662m.

[98] A. D'Anna. Combustion–formed nanoparticles. *Proceedings of the Combustion Institute*, 32:593–613, 2009. doi:10.1016/j.proci.2008.09.005.

[99] A. D'Anna and J. Kent. Aromatic formation pathways in non-premixed methane flames. *Combustion and Flame*, 132(4):715–722, 2003. doi:10.1016/S0010-2180(02)00522-9.

[100] A. D'Anna, A. Violi, A. D'Alessio, and A. F. Sarofim. A reaction pathway for nanoparticle formation in rich premixed flames. *Combustion and Flame*, 127(1): 1995–2003, 2001. doi:10.1016/S0010-2180(01)00303-0.

[101] A. D'Anna, M. Commodo, and P. Minutolo. Particle inception in a laminar premixed flame of benzene. *Combustion science and technology*, 180(5):758–766, 2008. doi:10.1080/00102200801893754.

[102] A. Das, K. Mahato, and T. Chakraborty. Excimer formation in the mixed dimers of naphthalene and 1-methoxynaphthalene in a supersonic jet. *Physical Chemistry Chemical Physics*, 3(10):1813–1818, 2001. doi:10.1039/B010098F.

[103] D. D. Das, P. C. S. John, C. S. McEnally, S. Kim, and L. D. Pfefferle. Measuring and predicting sooting tendencies of oxygenates, alkanes, alkenes, cycloalkanes, and aromatics on a unified scale. *Combustion and Flame*, 190:349–364, 2018. doi:10.1016/j.combustflame.2017.12.005.

[104] A. Dato. Graphene synthesized in atmospheric plasmas—a review. *Journal of Materials Research*, 34(1):214–230, 2019. doi:10.1557/jmr.2018.470.

[105] A. Dato, V. Radmilovic, Z. Lee, J. Phillips, and M. Frenklach. Substrate-free gas-phase synthesis of graphene sheets. *Nano letters*, 8(7):2012–2016, 2008. doi:10.1021/nl8011566.

[106] C. J. Davies, A. Mayer, J. Gabb, J. M. Walls, V. Degirmenci, P. B. Thompson, G. Cibin, S. Golunski, and S. A. Kondrat. Operando potassium K-edge X-ray absorption spectroscopy: investigating potassium catalysts during soot oxidation. *Physical Chemistry Chemical Physics*, 2020. doi:10.1039/D0CP01227K.

[107] E. Davy. Notice of a new gaseous bicarburet of hydrogen. *Report of the Sixth Meeting of the British Association for the Advancement of Science*, 5:62–63, 1836.

[108] G. De Falco, G. Mattiello, M. Commodo, P. Minutolo, X. Shi, A. D'Anna, and H. Wang. Electronic band gap of flame-formed carbon nanoparticles by scanning tunneling spectroscopy. *Proceedings of the Combustion Institute*, 2020.

[109] G. De Falco, F. Picca, M. Commodo, and P. Minutolo. Probing soot structure and electronic properties by optical spectroscopy. *Fuel*, 259:116244, 2020. doi:10.1016/j.fuel.2019.116244.

[110] S. Denifl, S. Ptasińska, B. Sonnweber, P. Scheier, D. Liu, F. Hagelberg, J. Mack, L. T. Scott, and T. D. Märk. Free-electron attachment to coronene and corannulene in the gas phase. *The Journal of Chemical Physics*, 123(10):104308, 2005. doi:10.1063/1.2008947.

[111] P. Desgroux, X. Mercier, and K. A. Thomson. Study of the formation of soot and its precursors in flames using optical diagnostics. *Proceedings of the Combustion Institute*, 34(1):1713–1738, 2013. doi:10.1016/j.proci.2012.09.004.

[112] P. Desgroux, A. Faccinetto, X. Mercier, T. Mouton, D. Aubagnac Karkar, and A. El Bakali. Comparative study of the soot formation process in a "nucleation" and a "sooting" low pressure premixed methane flame. *Combustion and Flame*, 184: 153–166, 2017. doi:10.1016/j.combustflame.2017.05.034.

[113] A. Devanand, G. Karmakar, N. Krdzavac, R. Rigo-Mariani, Y. F. Eddy, I. A. Karimi, and M. Kraft. Ontopowsys: A power system ontology for cross domain interactions in an eco industrial park. *Energy and AI*, page 100008, 2020. doi:10.1016/j.egyai.2020.100008.

[114] R. B. Devlin, C. B. Smith, M. T. Schmitt, A. G. Rappold, A. Hinderliter, D. Graff, and M. S. Carraway. Controlled exposure of humans with metabolic syndrome to concentrated ultrafine ambient particulate matter causes cardiovascular effects. *Toxicological Sciences*, 140(1):61–72, 2014. doi:10.1093/toxsci/kfu063.

[115] A. Di Lorenzo, A. D'alessio, V. Cincotti, S. Masi, P. Menna, and C. Venitozzi. UV absorption, laser excited fluorescence and direct sampling in the study of the formation of polycyclic aromatic hydrocarbons in rich CH4/O2 flames. *Symposium (International) on Combustion*, 18(1):485–491, 1981. doi:10.1016/S0082-0784(81)80054-9.

[116] S. Di Stasio, J. L. Legarrec, and J. B. Mitchell. Synchrotron radiation studies of additives in combustion, II: Soot agglomerate microstructure change by alkali and alkaline-earth metal addition to a partially premixed flame. *Energy and Fuels*, 25 (3):916–925, 2011. doi:10.1021/ef1012209.

[117] R. A. Dobbins and H. Subramaniasivam. Soot precursor particles in flames. In *Soot Formation in Combustion*, pages 290–301. Springer, 1994.

[118] R. A. Dobbins, R. A. Fletcher, and H.-C. Chang. The evolution of soot precursor particles in a diffusion flame. *Combustion and Flame*, 115(3):285–298, 1998. doi:10.1016/S0010-2180(98)00010-8.

[119] J.-B. Donnet. *Carbon black: science and technology*. CRC Press, 1993.

[120] L. Dontot, F. Spiegelman, and M. Rapacioli. Structures and energetics of neutral and cationic pyrene clusters. *The Journal of Physical Chemistry A*, 123(44):9531–9543, 2019. doi:10.1021/acs.jpca.9b07007.

[121] J. A. Dreyer, R. I. Slavchov, E. J. Rees, J. Akroyd, M. Salamanca, S. Mosbach, and M. Kraft. Improved methodology for performing the inverse abel transform of flame images for color ratio pyrometry. *Applied Optics*, 58(10):2662–2670, 2019. doi:10.1364/AO.58.002662.

[122] F. L. Dryer. Chemical kinetic and combustion characteristics of transportation fuels. *Proceedings of the Combustion Institute*, 35(1):117–144, 2015. doi:10.1016/j.proci.2014.09.008.

[123] T. Dumitrică, C. M. Landis, and B. I. Yakobson. Curvature-induced polarization in carbon nanoshells. *Chemical Physics Letters*, 360(1-2):182–188, 2002. doi:10.1016/S0009-2614(02)00820-5.

[124] R. C. Dunbar. Binding of transition-metal ions to curved $\pi$ surfaces: corannulene and coronene. *The Journal of Physical Chemistry A*, 106(42):9809–9819, 2002. doi:10.1021/jp020313b.

[125] A. D'Anna, A. D'Alessio, and P. Minutolo. Spectroscopic and chemical characterization of soot inception processes in premixed laminar flames at atmospheric pressure. In *Soot Formation in Combustion*, pages 83–103. Springer, 1994.

[126] A. D'Anna, M. Commodo, S. Violi, C. Allouis, and J. Kent. Nano organic carbon and soot in turbulent non-premixed ethylene flames. *Proceedings of the Combustion Institute*, 31(1):621–629, 2007. doi:10.1016/j.proci.2006.07.062.

[127] N. A. Eaves, S. B. Dworkin, and M. J. Thomson. Assessing relative contributions of PAHs to soot mass by reversible heterogeneous nucleation and condensation. *Proceedings of the Combustion Institute*, 36(1):935–945, 2017. doi:10.1016/j.proci.2016.06.051.

[128] A. Eibeck, M. Q. Lim, and M. Kraft. J-park simulator: An ontology-based platform for cross-domain scenarios in process industry. *Computers & Chemical Engineering*, 131:106586, 2019. doi:10.1016/j.compchemeng.2019.106586.

[129] A. Eibeck, A. Chadzynski, M. Q. Lim, K. Aditya, L. Ong, A. Devanand, G. Karmakar, S. Mosbach, R. Lau, I. A. Karimi, E. Y. S. Foo, and M. Kraft. A parallel world framework for scenario analysis in knowledge graphs. *Data-Centric Engineering*, 1, 2020. doi:10.1017/dce.2020.6.

[130] P. Elvati and A. Violi. Thermodynamics of poly-aromatic hydrocarbon clustering and the effects of substituted aliphatic chains. *Proceedings of the Combustion Institute*, 34(1):1837 – 1843, 2013. doi:10.1016/j.proci.2012.07.030.

[131] P. Elvati, V. Dillstrom, and A. Violi. Oxygen driven soot formation. *Proceedings of the Combustion Institute*, 36(1):825–832, 2017. doi:10.1016/j.proci.2016.09.019.

[132] P. Elvati, K. Turrentine, and A. Violi. The role of molecular properties on the dimerization of aromatic compounds. *Proceedings of the Combustion Institute*, 37 (1):1099–1105, 2019. doi:10.1016/j.proci.2018.05.065.

[133] A. V. Eremin. Formation of carbon nanoparticles from the gas phase in shock wave pyrolysis processes. *Progress in energy and combustion science*, 38(1):1–40, 2012. doi:10.1016/j.pecs.2011.09.002.

[134] A. Faccinetto, P. Desgroux, M. Ziskind, E. Therssen, and C. Focsa. High-sensitivity detection of polycyclic aromatic hydrocarbons adsorbed onto soot particles using laser desorption/laser ionization/time-of-flight mass spectrometry: An approach to studying the soot inception process in low-pressure flames. *Combustion and Flame*, 158(2):227–239, 2011. doi:10.1016/j.combustflame.2010.08.012.

[135] A. Faccinetto, C. Irimiea, P. Minutolo, M. Commodo, A. D'Anna, N. Nuns, Y. Carpentier, C. Pirim, P. Desgroux, and C. Focsa. Evidence on the formation of dimers of polycyclic aromatic hydrocarbons in a laminar diffusion flame. *Communications Chemistry*, 3(1):1–8, 2020. doi:10.1038/s42004-020-00357-2.

[136] A. Fahr, W. G. Mallard, and S. E. Stein. Reactions of phenyl radicals with ethene, ethyne, and benzene. *Symposium (International) on Combustion*, 21(1):825–831, 1988. doi:10.1016/S0082-0784(88)80314-X.

[137] M. Faraday. XX. On new compounds of carbon and hydrogen, and on certain other products obtained during the decomposition of oil by heat. *Philosophical Transactions of the Royal Society of London*, 115:440–466, 1825. doi:10.1098/rstl.1825.0022.

[138] M. Faraday. *A course of six lectures on the chemical history of a candle: to which is added a lecture on platinum*. Harper & Brothers, 1861.

[139] F. Farazi, J. Akroyd, S. Mosbach, P. Buerger, D. Nurkowski, M. Salamanca, and M. Kraft. Ontokin: An ontology for chemical kinetic reaction mechanisms. *Journal of Chemical Information and Modeling*, 60(1):108–120, 2019. doi:10.1021/acs.jcim.9b00960.

[140] F. Farazi, M. Salamanca, S. Mosbach, J. Akroyd, A. Eibeck, L. K. Aditya, A. Chadzynski, K. Pan, X. Zhou, S. Zhang, M. Q. Lim, and M. Kraft. Knowledge graph approach to combustion chemistry and interoperability. *ACS omega*, 5 (29):18342–18348, 2020. doi:10.1021/acsomega.0c02055.

[141] C. G. Fernández, S. Picaud, and M. Devel. Calculations of the mass absorption cross sections for carbonaceous nanoparticles modeling soot. *Journal of Quantitative Spectroscopy and Radiative Transfer*, 164:69–81, 2015. doi:10.1016/j.jqsrt.2015.05.011.

[142] F. Ferraro, C. Russo, R. Schmitz, C. Hasse, and M. Sirignano. Experimental and numerical study on the effect of oxymethylene ether-3 (ome3) on soot particle formation. *Fuel*, 286:119353, 2020. doi:10.1016/j.fuel.2020.119353.

[143] A. Fialkov. Investigations on ions in flames. *Progress in Energy and Combustion Science*, 23:399–528, 1997. doi:10.1016/S0360-1285(97)00016-6.

[144] C. Focsa, D. Duca, J. Noble, M. Vojkovic, Y. Carpentier, C. Pirim, C. Betrancourt, P. Desgroux, T. Tritscher, J. Spielvogel, M. Rahmand, A. Boies, K. F. Lee, A. N. Bhave, S. Legendre, O. Lancry, P. Kreutziger, and M. Rieker. Multi-technique physico-chemical characterization of particles generated by a gasoline engine: Towards measuring tailpipe emissions below 23 nm. *Atmospheric Environment*, page 117642, 2020. doi:10.1016/j.atmosenv.2020.117642.

[145] P. Frank, K. Bhaskaran, and T. Just. High-temperature reactions of triplet methylene and ketene with radicals. *The Journal of Physical Chemistry*, 90(10):2226–2231, 1986. doi:10.1021/j100401a046.

[146] E. Frankland. On the influence of atmospheric pressure upon some of the phenomena of combustion. *Journal of the Chemical Society*, 15(1861):168–196, 1862. doi:10.1039/JS8621500168.

[147] E. Frankland. On the source of light in luminous flames. *Journal of the Franklin Institute*, 87(5):330 – 335, 1869. doi:10.1016/0016-0032(69)90579-1.

[148] M. Frenklach. On surface growth mechanism of soot particles. *Symposium (International) on Combustion*, 26(2):2285–2293, 1996. doi:10.1016/S0082-0784(96)80056-7.

[149] M. Frenklach. Reaction mechanism of soot formation in flames. *Physical Chemistry Chemical Physics*, 4(11):2028–2037, 2002. doi:10.1039/b110045a.

[150] M. Frenklach. Transforming data into knowledge—process informatics for combustion chemistry. *Proceedings of the combustion Institute*, 31(1):125–140, 2007. doi:10.1016/j.proci.2006.08.121.

[151] M. Frenklach and L. B. Ebert. Comment on the proposed role of spheroidal carbon clusters in soot formation. *The Journal of Physical Chemistry*, 92(2):561–563, 1988. doi:10.1021/j100313a061.

[152] M. Frenklach and A. M. Mebel. On the mechanism of soot nucleation. *Physical Chemistry Chemical Physics*, 22(9):5314–5331, 2020. doi:10.1039/D0CP00116C.

[153] M. Frenklach and H. Wang. Detailed modeling of soot particle nucleation and growth. *Symposium (International) on Combustion*, 23(1):1559–1566, 1991. doi:10.1016/S0082-0784(06)80426-1.

[154] M. Frenklach, S. Taki, M. Durgaprasad, and R. Matula. Soot formation in shock-tube pyrolysis of acetylene, allene, and 1, 3-butadiene. *Combustion and Flame*, 54 (1-3):81–101, 1983. doi:10.1016/0010-2180(83)90024-X.

[155] M. Frenklach, D. W. Clary, W. C. Gardiner Jr, and S. E. Stein. Detained kinetic modeling of soot formation in shock-tube pyrolysis of acetylene. *Symposium (International) on Combustion*, 20(1):887–901, 1985. doi:10.1016/S0082-0784(85)80578-6.

[156] M. Frenklach, C. A. Schuetz, and J. Ping. Migration mechanism of aromatic-edge growth. *Proceedings of the Combustion Institute*, 30(1):1389–1396, 2005. doi:10.1016/j.proci.2004.07.048.

[157] M. Frenklach, R. I. Singh, and A. M. Mebel. On the low-temperature limit of HACA. *Proceedings of the Combustion Institute*, 37(1):969–976, 2019. doi:10.1016/j.proci.2018.05.068.

[158] C. W. Gao, J. W. Allen, W. H. Green, and R. H. West. Reaction mechanism generator: Automatic construction of chemical kinetic mechanisms. *Computer Physics Communications*, 203:212–225, 2016. doi:10.1016/j.cpc.2016.02.013.

[159] W. C. Gardiner. The chemistry of flames. *Scientific American*, 246(2):110–125, 1982.

[160] S. S. Garud, I. A. Karimi, and M. Kraft. LEAPS2: Learning based evolutionary assistive paradigm for surrogate selection. *Computers & Chemical Engineering*, 119:352–370, 2018. doi:10.1016/j.compchemeng.2018.09.008.

[161] A. Gaydon and A. Fairbairn. Carbon formation from $C_2H_2$ and CO in discharge tubes. *Symposium (International) on Combustion*, 5(1):324 – 328, 1955. doi:10.1016/S0082-0784(55)80043-4.

[162] A. G. Gaydon. *Spectroscopy and Combustion Theory Lond.* S, 1948.

[163] P. Gerhardt and K. Homann. Ions and charged soot particles in hydrocarbon flames. 2. positive aliphatic and aromatic ions in ethyne/oxygen flames. *Journal of Physical Chemistry*, 94(13):5381–5391, 1990. doi:10.1021/j100376a039.

[164] P. Gerhardt, S. Löffler, and K. Homann. Polyhedral carbon ions in hydrocarbon flames. *Chemical Physics Letters*, 137(4):306 – 310, 1987. doi:10.1016/0009-2614(87)80889-8.

[165] R. Gill and D. Olson. Estimation of soot thresholds for fuel mixtures. *Combustion Science and Technology*, 40(5-6):307–315, 1984. doi:10.1080/00102208408923814.

[166] A. Giordana, A. Maranzana, and G. Tonachini. Carbonaceous Nanoparticle Molecular Inception from Radical Addition and van der Waals Coagulation of Polycyclic Aromatic Hydrocarbon-Based Systems. A Theoretical Study. *The Journal of Physical Chemistry C*, 115(35):17237–17251, 2011. doi:10.1021/jp2010698.

[167] I. Glassman. Soot formation in combustion processes. *Symposium (International) on Combustion*, 22(1):295–311, 1989. doi:10.1016/S0082-0784(89)80036-0.

[168] A. Goel, P. Hebgen, J. B. Vander Sande, and J. B. Howard. Combustion synthesis of fullerenes and fullerenic nanostructures. *Carbon*, 40(2):177–182, 2002. doi:10.1016/S0008-6223(01)00170-1.

[169] D. R. Gold, A. Litonjua, J. Schwartz, E. Lovett, A. Larson, B. Nearing, G. Allen, M. Verrier, R. Cherry, and R. Verrier. Ambient pollution and heart rate variability. *Circulation*, 101(11):1267–1273, 2000. doi:10.1161/01.CIR.101.11.1267.

[170] F. Goulay, L. Nemes, P. E. Schrader, and H. A. Michelsen. Spontaneous emission from $C_2$(d $^3\Pi$g) and $C_3$ (A $^1\Pi$u) during laser irradiation of soot particles. *Molecular Physics*, 108(7-9):1013–1025, 2010. doi:10.1080/00268971003627824.

[171] D. C. Graham, K. J. Cavell, and B. F. Yates. Dimerization mechanisms of heterocyclic carbenes. *Journal of physical organic chemistry*, 18(4):298–309, 2005. doi:10.1002/poc.846.

[172] S. Graham, J. Homer, and J. Rosenfeld. The formation and coagulation of soot aerosols generated by the pyrolysis of aromatic hydrocarbons. *Proceedings of the Royal Society of London. A. Mathematical and Physical Sciences*, 344(1637):259–285, 1975.

[173] S. M. Graham and J. M. Goodings. Metallic ions in hydrocarbon flames. II. Mechanism for the reduction of $C_3H_3^+$ by metals in relation to soot suppression. *International journal of mass spectrometry and ion processes*, 56(2):205–222, 1984. doi:10.1016/0168-1176(84)85044-2.

[174] T. J. Grahame, R. Klemm, and R. B. Schlesinger. Public health and components of particulate matter: the changing assessment of black carbon. *Journal of the Air & Waste Management Association*, 64(6):620–660, 2014. doi:10.1080/10962247.2014.912692.

[175] B. Graziano, T. Ottenwälder, D. Manderfeld, S. Pischinger, and G. Grüefeld. Advanced methodology for the detection of smoke point heights in hydrocarbon flames. *Energy & Fuels*, 32(3):3908–3919, 2018. doi:10.1021/acs.energyfuels.7b03584.

[176] W. H. Green. Automatic generation of reaction mechanisms. In *Computer Aided Chemical Engineering*, volume 45, pages 259–294. Elsevier, 2019.

[177] W. H. Green Jr. Predictive kinetics: a new approach for the 21st century. *Advances in Chemical Engineering*, 32:1–313, 2007. doi:10.1016/S0065-2377(07)32001-2.

[178] W. J. Grieco, A. L. Lafleur, K. C. Swallow, H. Richter, K. Taghizadeh, and J. B. Howard. Fullerenes and PAH in low-pressure premixed benzene/oxygen flames. *Symposium (International) on Combustion*, 27(2):1669–1675, 1998. doi:10.1016/S0082-0784(98)80006-4.

[179] W. J. Grieco, J. B. Howard, L. C. Rainey, and J. B. V. Sande. Fullerenic carbon in combustion-generated soot. *Carbon*, 38(4):597 – 614, 2000. doi:10.1016/S0008-6223(99)00149-9.

[180] H.-H. Grotheer, H. Pokorny, K.-L. Barth, M. Thierley, and M. Aigner. Mass spectrometry up to 1 million mass units for the simultaneous detection of primary soot and of soot precursors (nanoparticles) in flames. *Chemosphere*, 57(10):1335–1342, 2004. doi:10.1016/j.chemosphere.2004.08.054.

[181] H.-H. Grotheer, K. Wolf, and K. Hoffmann. Photoionization mass spectrometry for the investigation of combustion generated nascent nanoparticles and their relation to laser induced incandescence. *Applied Physics B*, 104(2):367–383, 2011. doi:10.1007/s00340-011-4403-9.

[182] K. Guthier, P. Hebgen, K.-H. Homann, J. Hofmann, and G. Zimmermann. Addition and cyclization reactions in the thermal conversion of hydrocarbons with enyne structure, ii. analysis of radicals and carbenes from ethynylbenzene. *Liebigs Annalen*, 1995(4):637–644, 1995. doi:10.1002/jlac.199719971217.

[183] R. C. Haddon. Hybridization and the orientation and alignment of $\pi$-orbitals in nonplanar conjugated organic molecules: $\pi$-orbital axis vector analysis (POAV2). *Journal of the American Chemical Society*, 108(11):2837–2842, 1986. doi:10.1021/ja00271a009.

[184] D. K. Hahn, S. J. Klippenstein, and J. A. Miller. A theoretical analysis of the reaction between propargyl and molecular oxygen. *Faraday discussions*, 119:79–100, 2002. doi:10.1039/B102240G.

[185] S. Han, X. Li, F. Nie, M. Zheng, X. Liu, and L. Guo. Revealing the Initial Chemistry of Soot Nanoparticle Formation by ReaxFF Molecular Dynamics Simulations. *Energy & Fuels*, 31(8):8434–8444, 2017. doi:10.1021/acs.energyfuels.7b01194.

[186] N. Hansen, S. J. Klippenstein, P. Westmoreland, T. Kasper, K. Kohse-Höinghaus, J. Wang, and T. Cool. A combined ab initio and photoionization mass spectrometric study of polyynes in fuel-rich flames. *Physical Chemistry Chemical Physics*, 10(3): 366–374, 2008. doi:10.1039/B711578D.

[187] N. Hansen, T. A. Cool, P. R. Westmoreland, and K. Kohse-Höinghaus. Recent contributions of flame-sampling molecular-beam mass spectrometry to a fundamental understanding of combustion chemistry. *Progress in Energy and Combustion Science*, 35(2):168–191, 2009. doi:10.1016/j.pecs.2008.10.001.

[188] N. Hansen, M. Schenk, K. Moshammer, and K. Kohse-Höinghaus. Investigating repetitive reaction pathways for the formation of polycyclic aromatic hydrocarbons in combustion processes. *Combustion and Flame*, 180:250–261, 2017. doi:10.1016/j.combustflame.2016.09.013.

[189] J. Happold, H.-H. Grotheer, and M. Aigner. Distinction of gaseous soot precursor molecules and soot precursor particles through photoionization mass spectrometry. *Rapid Communications in Mass Spectrometry*, 21(7):1247–1254, 2007. doi:10.1002/rcm.2955.

[190] J. Happold, H.-H. Grotheer, and M. Aigner. Soot precursors consisting of stacked pericondensed PAHs. In H. Bockhorn, A. D'Anna, A. Sarofim, and H. Wang, editors, *Combustion Generated Fine Carbonaceous Particles*, chapter 18, pages 277 – 288. KIT Scientific Publishing, Karlsruhe, Germany, 2009.

[191] S. J. Harris and A. M. Weiner. A picture of soot particle inception. *Symposium (International) on Combustion*, 22(1):333 – 342, 1989. doi:10.1016/S0082-0784(89)80039-6.

[192] A. N. Hayhurst and H. R. N. Jones. Ions and soot in flames. *Journal of the Chemical Society, Faraday Transactions 2*, 83(1):1, 1987. doi:10.1039/f29878300001.

[193] B. Haynes, H. Jander, and H. G. Wagner. Optical studies of soot-formation processes in premixed flames. *Berichte der Bunsengesellschaft für physikalische Chemie*, 84(6):585–592, 1980. doi:10.1080/00102208308923666.

[194] B. S. Haynes. Combustion research for chemical processing. *Proceedings of the Combustion Institute*, 37(1):1–32, 2019. doi:10.1016/j.proci.2018.06.183.

[195] B. S. Haynes and H. G. Wagner. Soot Formation. *Progress in Energy and Combustion Science*, 7(4):229–273, 1981. doi:10.1016/0360-1285(81)90001-0.

[196] C. He, A. M. Thomas, G. R. Galimova, A. N. Morozov, A. M. Mebel, and R. I. Kaiser. Gas-Phase Formation of Fulvenallene ($C_7H_6$) via the Jahn–Teller Distorted Tropyl ($C_7H_7$) Radical Intermediate under Single-Collision Conditions. *Journal of the American Chemical Society*, 142(6):3205–3213, 2020. doi:10.1021/jacs.9b13269.

[197] D. Heymann, L. P. Chibante, R. R. Brooks, W. S. Wolbach, and R. E. Smalley. Fullerenes in the Cretaceous-Tertiary boundary layer. *Science*, 265(5172):645–647, 1994. doi:10.1126/science.265.5172.645.

[198] E. J. Highwood and R. P. Kinnersley. When smoke gets in our eyes: The multiple impacts of atmospheric black carbon on climate, air quality and health. *Environment international*, 32(4):560–566, 2006. doi:10.1016/j.envint.2005.12.003.

[199] C. I. Hiley, G. F. Whitehead, M. Zanella, C. Delacotte, T. D. Manning, and M. J. Rosseinsky. Detection and crystal structure of hydrogenated bipentacene as an intermediate in thermally induced pentacene oligomerization. *The Journal of organic chemistry*, 84(13):8481–8486, 2019. doi:10.1021/acs.joc.9b00671.

[200] W. C. Hinds. *Aerosol technology: properties, behavior, and measurement of airborne particles*. John Wiley & Sons, 1999.

[201] F. Hirsch, P. Constantinidis, I. Fischer, S. Bakels, and A. M. Rijs. Dimerization of the benzyl radical in a high-temperature pyrolysis reactor investigated by IR/UV ion dip spectroscopy. *Chemistry–A European Journal*, 24(30):7647–7652, 2018. doi:10.1002/chem.201800852.

[202] F. Hirsch, E. Reusch, P. Constantinidis, I. Fischer, S. Bakels, A. M. Rijs, and P. Hemberger. Self-reaction of ortho-benzyne at high temperatures investigated by infrared and photoelectron spectroscopy. *The Journal of Physical Chemistry A*, 122(49):9563–9571, 2018. doi:10.1021/acs.jpca.8b09640.

[203] M. M. Hirschler. Soot from fires: II. mechanisms of soot formation. *Journal of fire sciences*, 3(6):380–414, 1985. doi:10.1177/073490418500300602.

[204] J. Hoche, H.-C. Schmitt, A. Humeniuk, I. Fischer, R. Mitrić, and M. I. Röhr. The mechanism of excimer formation: an experimental and theoretical study on the pyrene dimer. *Physical Chemistry Chemical Physics*, 19(36):25002–25015, 2017. doi:10.1039/C7CP03990E.

[205] B. Hoffmann, S. Moebus, S. Möhlenkamp, A. Stang, N. Lehmann, N. Dragano, A. Schmermund, M. Memmesheimer, K. Mann, R. Erbel, and K.-H. Jöckel. Residential exposure to traffic is associated with coronary atherosclerosis. *Circulation*, 116(5):489–496, 2007. doi:10.1161/CIRCULATIONAHA.107.693622.

[206] K. Homann. Formation of large molecules, particulates and ions in premixed hydrocarbon flames; progress and unresolved questions. *Symposium (International) on Combustion*, 20:857–870, 1985. doi:10.1016/S0082-0784(85)80575-0.

[207] K. Homann and H. Wagner. Some new aspects of the mechanism of carbon formation in premixed flames. *Symposium (International) on Combustion*, 11(1):371–379, 1967. doi:10.1016/S0082-0784(67)80161-9.

[208] K. H. Homann. Fullerenes and soot formation - New pathways to large particles in flames. *Angewandte Chemie, International Edition in English*, 37(18):2435–2451, 1998. doi:10.1002/(SICI)1521-3773(19981002)37:18%3C2434::AID-ANIE2434%3E3.0.CO;2-L.

[209] K. H. Homann and E. Ströfer. Charged Soot Particles in Unseeded and Seeded Flames. In J. Lahaye and G. Prado, editors, *Soot in Combustion Systems and its Toxic Properties*, page 217. Plenum Press, New York and London, 1983.

[210] K.-H. Homann and H. G. Wagner. Some aspects of soot formation. In *Dynamics of Exothermicity (Combust. Sc. Techol. Book Series, Vol. 2)*, pages 151–184. Carbon and Breach Publishers, 1996.

[211] D. Hou and X. You. Reaction kinetics of hydrogen abstraction from polycyclic aromatic hydrocarbons by H atoms. *Physical Chemistry Chemical Physics*, 19 (45):30772–30780, 2017. doi:10.1039/c7cp04964a.

[212] D. Hou, D. Zong, C. S. Lindberg, M. Kraft, and X. You. On the coagulation efficiency of carbonaceous nanoparticles. *Journal of Aerosol Science*, 140:105478, 2020. doi:10.1016/j.jaerosci.2019.105478.

[213] J. B. Howard. Carbon addition and oxidation reactions in heterogeneous combustion and soot formation. *Symposium (International) on Combustion*, 23(1):1107–1127, 1991. doi:10.1016/S0082-0784(06)80371-1.

[214] J. B. Howard and W. J. Kausch. Soot control by fuel additives. *Progress in Energy and Combustion Science*, 6(3):263–276, 1980. doi:10.1016/0360-1285(80)90018-0.

[215] J. B. Howard, D. F. Kronholm, A. J. Modestino, and H. Richter. Method for combustion synthesis of fullerenes, July 8 2008. US Patent 7,396,520.

[216] C.-H. Huang and R. L. Vander Wal. Partial premixing effects upon soot nanostructure. *Combustion and Flame*, 168:403–408, 2016. doi:10.1016/j.combustflame.2016.01.006.

[217] S. Iavarone, L. Pascazio, M. Sirignano, A. De Candia, A. Fierro, L. De Arcangelis, and A. D'Anna. Molecular dynamics simulations of incipient carbonaceous nanoparticle formation at flame conditions. *Combustion Theory and Modelling*, 21 (1):49–61, 2017. doi:10.1080/13647830.2016.1242156.

[218] S. Iijima. Direct observation of the tetrahedral bonding in graphitized carbon black by high resolution electron microscopy. *Journal of Crystal Growth*, 50(3):675–683, 1980. doi:10.1016/0022-0248(80)90013-5.

[219] A. Indarto, A. Giordana, G. Ghigo, A. Maranzana, and G. Tonachini. Polycyclic aromatic hydrocarbon formation mechanism in the "particle phase". a theoretical study. *Physical Chemistry Chemical Physics*, 12(32):9429–9440, 2010. doi:10.1039/C000491J.

[220] C. Irimiea, A. Faccinetto, Y. Carpentier, I.-K. Ortega, N. Nuns, E. Therssen, P. Desgroux, and C. Focsa. A comprehensive protocol for chemical analysis of flame combustion emissions by secondary ion mass spectrometry. *Rapid Communications in Mass Spectrometry*, 32(13):1015–1025, 2018. doi:10.1002/rcm.8133.

[221] C. Irimiea, A. Faccinetto, X. Mercier, I.-K. Ortega, N. Nuns, E. Therssen, P. Desgroux, and C. Focsa. Unveiling trends in soot nucleation and growth: When secondary ion mass spectrometry meets statistical analysis. *Carbon*, 144:815 – 830, 2019. doi:10.1016/j.carbon.2018.12.015.

[222] S. Irle, G. Zheng, Z. Wang, and K. Morokuma. The $C_{60}$ formation puzzle "solved": QM/MD simulations reveal the shrinking hot giant road of the dynamic fullerene self-assembly mechanism. *Journal of Physical Chemistry B*, 110:14531–14545, 2006. doi:10.1021/jp061173z.

[223] T. Ishiguro, Y. Takatori, and K. Akihama. Microstructure of diesel soot particles probed by electron microscopy: First observation of inner core and outer shell. *Combustion and Flame*, 108(1-2):231–234, 1997. doi:10.1016/S0010-2180(96)00206-4.

[224] R. S. Jacobson, A. R. Korte, A. Vertes, and J. H. Miller. The molecular composition of soot. *Angewandte Chemie International Edition*, 59(11):4484–4490, 2020. doi:10.1002/anie.201914115.

[225] A. Jamrozik, K. Grab-Rogaliński, and W. Tutak. Hydrogen effects on combustion stability, performance and emission of diesel engine. *International Journal of Hydrogen Energy*, 2020. doi:10.1016/j.ijhydene.2020.05.049.

[226] H. Jander and H. G. Wagner. *"Soot Formation in Combustion": An International Round Table Discussion*. Vandenhoeck & Ruprecht, 1990.

[227] N. A. Janssen, G. Hoek, M. Simic-Lawson, P. Fischer, L. Van Bree, H. Ten Brink, M. Keuken, R. W. Atkinson, H. R. Anderson, B. Brunekreef, and F. R. Cassee1. Black carbon as an additional indicator of the adverse health effects of airborne particles compared with PM10 and PM2.5. *Environmental health perspectives*, 119(12):1691–1699, 2011. doi:10.1289/ehp.1003369.

[228] D. Jensen. Prediction of soot formation rates: a new approach. *Proceedings of the Royal Society of London. A. Mathematical and Physical Sciences*, 338(1614): 375–396, 1974. doi:10.1098/rspa.1974.0092.

[229] P. Jensen and P. Bunker. The potential surface and stretching frequencies of $\tilde{X}^3B_1$ methylene ($CH_2$) determined from experiment using the Morse oscillator-rigid bender internal dynamics Hamiltonian. *The Journal of chemical physics*, 89(3):1327–1332, 1988. doi:10.1063/1.455184.

[230] H. Jin, J. Yang, L. Xing, J. Hao, Y. Zhang, C. Cao, Y. Pan, and A. Farooq. An experimental study of indene pyrolysis with synchrotron vacuum ultraviolet photoionization mass spectrometry. *Physical Chemistry Chemical Physics*, 21(10): 5510–5520, 2019. doi:10.1039/C8CP07285J.

[231] K. Johansson, J. Lai, S. Skeen, D. Popolan-Vaida, K. Wilson, N. Hansen, A. Violi, and H. Michelsen. Soot precursor formation and limitations of the stabilomer grid. *Proceedings of the Combustion Institute*, 35(2):1819–1826, 2015. doi:10.1016/j.proci.2014.05.033.

[232] K. O. Johansson, T. Dillstrom, M. Monti, F. El Gabaly, M. F. Campbell, P. E. Schrader, D. M. Popolan-Vaida, N. K. Richards-Henderson, K. R. Wilson, A. Violi, and H. A. Michelsen. Formation and emission of large furans and oxygenated

hydrocarbons from flames. *Proceedings of the National Academy of Sciences*, 113 (30):8374–8379, 2016. doi:10.1073/pnas.1604772113.

[233] K. O. Johansson, T. Dillstrom, P. Elvati, M. F. Campbell, P. E. Schrader, D. M. Popolan-Vaida, N. K. Richards-Henderson, K. R. Wilson, A. Violi, and H. A. Michelsen. Radical-radical reactions, pyrene nucleation, and incipient soot formation in combustion. *Proceedings of the Combustion Institute*, 36(1):799–806, 2017. doi:10.1016/j.proci.2016.07.130.

[234] K. O. Johansson, M. P. Head-Gordon, P. E. Schrader, K. R. Wilson, and H. A. Michelsen. Resonance-stabilized hydrocarbon-radical chain reactions may explain soot inception and growth. *Science*, 361(6406):997–1000, 2018. doi:10.1126/science.aat3417.

[235] Y. Ju and W. Sun. Plasma assisted combustion: Dynamics and chemistry. *Progress in Energy and Combustion Science*, 48:21–83, 2015. doi:10.1016/j.pecs.2014.12.002.

[236] Y. Ju, C. B. Reuter, O. R. Yehia, T. I. Farouk, and S. H. Won. Dynamics of cool flames. *Progress in Energy and Combustion Science*, 75:100787, 2019. doi:10.1016/j.pecs.2019.100787.

[237] S. V. Kalinin and V. Meunier. Electronic flexoelectricity in low-dimensional systems. *Physical Review B*, 77(3):1–4, 2008. doi:10.1103/PhysRevB.77.033403.

[238] H. K. Kammler, L. Mädler, and S. E. Pratsinis. Flame synthesis of nanoparticles. *Chemical Engineering & Technology: Industrial Chemistry-Plant Equipment-Process Engineering-Biotechnology*, 24(6):583–596, 2001. doi:10.1002/1521-4125(200106)24:6<583::AID-CEAT583>3.0.CO;2-H.

[239] J. H. Kang, J. Cho, and Y. T. Ko. Investigation on the effect of nanoparticle size on the blood–brain tumour barrier permeability by in situ perfusion via internal carotid artery in mice. *Journal of drug targeting*, 27(1):103–110, 2019. doi:10.1080/1061186X.2018.1497037.

[240] A. E. Karataş and Ö. L. Gülder. Soot formation in high pressure laminar diffusion flames. *Progress in Energy and Combustion Science*, 38(6):818–845, 2012. doi:10.1016/j.pecs.2012.04.003.

[241] D. Kashchiev. *Nucleation*. Butterworth-Heinemann, 2000.

[242] G. A. Kelesidis, E. Goudeli, and S. E. Pratsinis. Flame synthesis of functional nanostructured materials and devices: Surface growth and aggregation. *Proceedings of the Combustion Institute*, 36(1):29–50, 2017. doi:10.1016/j.proci.2016.08.078.

[243] A. Keller, R. Kovacs, and K.-H. Homann. Large molecules, ions, radicals and small soot particles in fuel-rich hydrocarbon flames. part iv. large polycyclic aromatic hydrocarbons and their radicals in a fuel-rich benzene–oxygen flame. *Physical Chemistry Chemical Physics*, 2(8):1667–1675, 2000. doi:10.1039/A908190I.

[244] M. Keller, T. de Bruin, M. Matrat, A. Nicolle, and L. Catoire. A theoretical multiscale approach to study the initial steps involved in the chemical reactivity of soot precursors. *Energy & Fuels*, 33(10):10255–10266, 2019. doi:10.1021/acs.energyfuels.9b02284.

[245] I. M. Kennedy. Models of soot formation and oxidation. *Progress in Energy and Combustion Science*, 23(2):95–132, 1997. doi:10.1016/S0360-1285(97)00007-5.

[246] M. Kertesz. Pancake bonding: An unusual pi-stacking interaction. *Chemistry–A European Journal*, 25(2):400–416, 2019. doi:10.1002/chem.201802385.

[247] T. Kessler, P. C. S. John, J. Zhu, C. S. McEnally, L. D. Pfefferle, and J. H. Mack. A comparison of computational models for predicting yield sooting index. *Proceedings of the Combustion Institute*, 2020. doi:10.1016/j.proci.2020.07.009.

[248] J. Kewley and J. S. Jackson. The burning of mineral oils in wick-fed lamps. *Journal of the Institute of Petroleum*, 13:364–394, 1927.

[249] M. Kholghy, M. Saffaripour, C. Yip, and M. J. Thomson. The evolution of soot morphology in a laminar coflow diffusion flame of a surrogate for Jet A-1. *Combustion and Flame*, 160(10):2119–2130, 2013. doi:10.1016/j.combustflame.2013.04.008.

[250] M. R. Kholghy, A. Veshkini, and M. J. Thomson. The core-shell internal nanostructure of soot - A criterion to model soot maturity. *Carbon*, 100(January):508–536, 2016. doi:10.1016/j.carbon.2016.01.022.

[251] M. R. Kholghy, G. A. Kelesidis, and S. E. Pratsinis. Reactive polycyclic aromatic hydrocarbon dimerization drives soot nucleation. *Physical Chemistry Chemical Physics*, 20:10926–10938, 2018. doi:10.1039/C7CP07803J.

[252] M. R. Kholghy, N. A. Eaves, A. Veshkini, and M. J. Thomson. The role of reactive PAH dimerization in reducing soot nucleation reversibility. *Proceedings of the Combustion Institute*, 37(1):1003–1011, 2019. doi:10.1016/j.proci.2018.07.110.

[253] C. Kim, S. Kang, and D. Y. Pui. Removal of airborne sub-3 nm particles using fibrous filters and granular activated carbons. *Carbon*, 104:125–132, 2016. doi:10.1016/j.carbon.2016.03.060.

[254] W. Kirmse. Persistent triplet carbenes. *Angewandte Chemie International Edition*, 42(19):2117–2119, 2003. doi:10.1021/cr800518t.

[255] V. Kislov, A. Sadovnikov, and A. Mebel. Formation mechanism of polycyclic aromatic hydrocarbons beyond the second aromatic ring. *The Journal of Physical Chemistry A*, 117(23):4794–4816, 2013. doi:10.1021/jp402481y.

[256] D. Kittelson and M. Kraft. Particle formation and models. *Encyclopedia of Automotive Engineering*, pages 1–23, 2014.

[257] D. B. Kittelson, W. F. Watts, and J. P. Johnson. Nanoparticle emissions on Minnesota highways. *Atmospheric Environment*, 38(1):9–19, 2004. doi:10.1016/j.atmosenv.2003.09.037.

[258] D. B. Kittelson, W. F. Watts, and J. P. Johnson. On-road and laboratory evaluation of combustion aerosols-Part1: Summary of diesel engine results. *Journal of Aerosol Science*, 37(8):913–930, 2006. doi:10.1016/j.jaerosci.2005.08.005.

[259] D. B. Kittelson, W. F. Watts, J. P. Johnson, J. J. Schauer, and D. R. Lawson. On-road and laboratory evaluation of combustion aerosols-Part 2: Summary of spark ignition engine results. *Journal of Aerosol Science*, 37(8):931–949, 2006. doi:10.1016/j.jaerosci.2005.08.008.

[260] D. Klein. Graphitic polymer strips with edge states. *Chemical Physics Letters*, 217 (3):261–265, 1994. doi:10.1016/0009-2614(93)E1378-T.

[261] A. Klemenc, R. Wechsberg, and G. Wagner. Über das Verhalten von Kohlensuboxyd und die in homogener Gasphase verlaufende Reaktion $C_3O_2 \rightleftharpoons CO_2 + C_2$. *Zeitschrift für Physikalische Chemie*, 170(1):97–111, 1934. doi:10.1515/zpch-1934-17009.

[262] K. Kobayashi. Electronic structure of a stepped graphite surface. *Physical Review B*, 48(3):1757, 1993. doi:10.1103/PhysRevB.48.1757.

[263] Y. Kobayashi, T. Furuhata, K. Amagai, and M. Arai. Soot precursor measurements in benzene and hexane diffusion flames. *Combustion and Flame*, 154(3):346–355, 2008. doi:10.1016/j.combustflame.2008.03.022.

[264] K. Kohse-Höinghaus. Combustion in the future: The importance of chemistry. *Proceedings of the Combustion Institute*, 2020. doi:10.1016/j.proci.2020.06.375.

[265] K. Kohse-Höinghaus, P. Oßwald, T. A. Cool, T. Kasper, N. Hansen, F. Qi, C. K. Westbrook, and P. R. Westmoreland. Biofuel combustion chemistry: From ethanol to biodiesel. *Angewandte Chemie - International Edition*, 49(21):3572–3597, 2010. doi:10.1002/anie.200905335.

[266] S. Kolakkandy, S. Pratihar, A. J. A. Aquino, H. Wang, and W. L. Hase. Properties of Complexes Formed by $Na^+$ , $Mg^{2+}$ , and $Fe^{2+}$ Binding with Benzene Molecules. *The Journal of Physical Chemistry A*, 118(40):9500–9511, 2014. doi:10.1021/jp5029257.

[267] T. H. Kolbe, G. Gröger, and L. Plümer. CityGML: Interoperable access to 3D city models. In *Geo-information for disaster management*, pages 883–899. Springer, 2005.

[268] J. Kolc and J. Michl. $\pi$, $\pi$-biradicaloid hydrocarbons. pleiadene family. i. photochemical preparation from cyclobutene precursors. *Journal of the American Chemical Society*, 95(22):7391–7401, 1973. doi:10.1021/ja00803a030.

[269] D. Koley, E. Arunan, and S. Ramakrishnan. Computational investigations on covalent dimerization/oligomerization of polyacenes: Is it relevant to soot formation? *Journal of Computational Chemistry*, 33(21):1762–1772, 2012. doi:10.1002/jcc.23014.

[270] A. Konishi and T. Kubo. Benzenoid quinodimethanes. In *Physical Organic Chemistry of Quinodimethanes*, pages 69–105. Springer, 2017.

[271] M. Kono, K. Iinuma, and S. Kumagai. The effect of DC to 10 mhz electric field on flame luminosity and carbon formation. *Symposium (International) on Combustion*, 18(1):1167–1174, 1981. doi:10.1016/S0082-0784(81)80121-X.

[272] N. Krdzavac, S. Mosbach, D. Nurkowski, P. Buerger, J. Akroyd, J. Martin, A. Menon, and M. Kraft. An ontology and semantic web service for quantum chemistry calculations. *Journal of chemical information and modeling*, 59(7): 3154–3165, 2019. doi:10.1021/acs.jcim.9b00227.

[273] A. Krestinin. Polyyne model of soot formation process. *Symposium (International) on Combustion*, 27(1):1557–1563, 1998. doi:10.1016/S0082-0784(98)80564-X.

[274] H. Kroto. $C_{60}^{B}$ buckminsterfullerene, other fullerenes and the icospiral shell. *Computers & Mathematics with Applications*, 17(1):417—423, 1989. doi:10.1016/0898-1221(89)90171-5.

[275] H. W. Kroto. New light on 'the case of imperfect combustion'. *Journal of the Chemical Society, Faraday Transactions*, 87(18):2871–2875, 1991. doi:10.1039/FT9918702871.

[276] H. W. Kroto and K. McKay. The formation of quasi-icosahedral spiral shell carbon particles. *Nature*, 331(6154):328–331, 1988. doi:10.1038/331328a0.

[277] H. W. Kroto, J. R. Heath, S. C. O'Brien, R. F. Curl, and R. E. Smalley. C60: Buckminsterfullerene. *Nature*, 318(6042):162–163, 1985. doi:10.1038/318162a0.

[278] R. A. Krueger and G. Blanquart. Predicting aromatic exciplex fluorescence emission energies. *Phys. Chem. Chem. Phys.*, 21(20):10325–10335, 2019. doi:10.1039/C9CP02027F.

[279] R. A. Krueger and G. Blanquart. Predicting the photoresponse of soot nuclei: Spectroscopic characteristics of aromatic aggregates containing five-membered rings. *Combustion and Flame*, 217:85–92, 2020. doi:10.1016/j.combustflame.2019.10.028.

[280] P. Kumar, P. Fennell, and R. Britter. Effect of wind direction and speed on the dispersion of nucleation and accumulation mode particles in an urban street canyon. *Science of the total environment*, 402(1):82–94, 2008. doi:10.1016/j.scitotenv.2008.04.032.

[281] A. G. Kvashnin, P. B. Sorokin, and B. I. Yakobson. Flexoelectricity in Carbon Nanostructures: Nanotubes, Fullerenes, and Nanocones. *The Journal of Physical Chemistry Letters*, 6(14):2740–2744, 2015. doi:10.1021/acs.jpclett.5b01041.

[282] D. Kvaskoff, H. Lüerssen, P. Bednarek, and C. Wentrup. Phenylnitrene, phenylcarbene, and pyridylcarbenes. rearrangements to cyanocyclopentadiene and fulvenallene. *Journal of the American Chemical Society*, 136(43):15203–15214, 2014. doi:10.1021/ja506151p.

[283] A. L. Lafleur, J. B. Howard, J. A. Marr, and T. Yadav. Proposed fullerene precursor corannulene identified in flames both in the presence and absence of fullerene production. *The Journal of Physical Chemistry*, 97(51):13539–13543, 1993. doi:10.1021/j100153a020.

[284] A. L. Lafleur, J. B. Howard, K. Taghizadeh, E. F. Plummer, L. T. Scott, A. Necula, and K. C. Swallow. Identification of $C_{20}H_{10}$ Dicyclopentapyrenes in Flames: Correlation with Corannulene and Fullerene Formation. *The Journal of Physical Chemistry*, 100(43):17421–17428, 1996. doi:10.1021/jp9605313.

[285] J. Lahaye and G. Prado. Formation of carbon particles from a gas phase: Nucleation phenomenon. *Water, Air, and Soil Pollution*, 3(4):473–481, 1974. doi:10.1007/BF00341000.

[286] J. Y. Lai, P. Elvati, and A. Violi. Stochastic atomistic simulation of polycyclic aromatic hydrocarbon growth in combustion. *Physical Chemistry Chemical Physics*, 16(17):7969–7979, 2014. doi:10.1039/C4CP00112E.

[287] P. J. Landrigan, R. Fuller, N. J. R. Acosta, O. Adeyi, R. Arnold, N. N. Basu, A. B. Baldé, R. Bertollini, S. Bose-O'Reilly, J. I. Boufford, P. N. Breysse, T. Chiles, C. Mahidol, A. M. Coll-Seck, M. L. Cropper, J. Fobil, V. Fuster, M. Greenstone, A. Haines, D. Hanrahan, D. Hunter, M. Khare, A. Krupnick, B. Lanphear, B. Lohani, K. Martin, K. V. Mathiasen, M. A. McTeer, C. J. L. Murray, J. D. Ndahimananjara, F. Perera, J. Potočnik, A. S. Preker, J. Ramesh, J. Rockström, C. Salinas, L. D. Samson, K. Sandilya, P. D. Sly, K. R. Smith, A. Steiner, R. B. Stewart, W. A. Suk, O. C. P. van Schayck, G. N. Yadama, K. Yumkella, and M. Zhong. The Lancet Commission on pollution and health. *The Lancet*, 2017. doi:10.1016/S0140-6736(17)32345-0.

[288] C. T. Lao, J. Akroyd, N. Eaves, A. Smith, N. Morgan, A. Bhave, and M. Kraft. Modelling particle mass and particle number emissions during the active regeneration of diesel particulate filters. *Proceedings of the Combustion Institute*, 37(4): 4831–4838, 2019. doi:10.1016/j.proci.2018.07.079.

[289] J. Lawton and F. Weinberg. *Electrical aspects of combustion*. Clarendon P., Oxford, 1969.

[290] K. C. Le, C. Lefumeux, P.-E. Bengtsson, and T. Pino. Direct observation of aliphatic structures in soot particles produced in low-pressure premixed ethylene flames via online raman spectroscopy. *Proceedings of the Combustion Institute*, 37 (1):869–876, 2019. doi:10.1016/j.proci.2018.08.003.

[291] G. Leon, N. Eaves, J. Akroyd, S. Mosbach, and M. Kraft. A new methodology to calculate process rates in a kinetic Monte Carlo model of PAH growth. *Combustion and Flame*, 209:133–143, 2019. doi:10.1016/j.combustflame.2019.07.032.

[292] G. Leon, A. Menon, L. Pascazio, E. J. Bringley, A. J., and M. Kraft. Kinetic Monte Carlo statistics of curvature integration by HACA growth and bay closure reactions for PAH growth in a counterflow diffusion flame. *Proceedings of the Combustion Institute*, In Press, 2020. doi:10.1016/j.proci.2020.06.352.

[293] V. B. Lewes. XXV.–the luminosity of coal-gas flames. *Journal of the Chemical Society, Transactions*, 61:322–339, 1892. doi:10.1039/CT8926100322.

[294] V. B. Lewes and J. F. Thorpe. Iii. the cause of luminosity in the flames of hydrocarbon gases. *Proceedings of the Royal Society of London*, 57(340-346):450–468, 1894. doi:10.1098/rspl.1894.0174.

[295] Y. Li and F. Qi. Recent applications of synchrotron VUV photoionization mass spectrometry: insight into combustion chemistry. *Accounts of chemical research*, 43(1):68–78, 2010. doi:10.1021/ar900130b.

[296] Y. Li, L. Zhang, T. Yuan, K. Zhang, J. Yang, B. Yang, F. Qi, and C. K. Law. Investigation on fuel-rich premixed flames of monocyclic aromatic hydrocarbons: Part I. Intermediate identification and mass spectrometric analysis. *Combustion and Flame*, 157(1):143–154, 2010. doi:10.1016/j.combustflame.2009.07.021.

[297] J. S. Lighty, J. M. Veranth, and A. F. Sarofim. Combustion aerosols: factors governing their size and composition and implications to human health. *Journal of the Air & Waste Management Association*, 50(9):1565–1618, 2000. doi:10.1080/10473289.2000.10464197.

[298] R. Lindstedt and B. Waldheim. Modeling of soot particle size distributions in premixed stagnation flow flames. *Proceedings of the Combustion Institute*, 34(1): 1861–1868, 2013. doi:10.1016/j.proci.2012.05.047.

[299] M. Lippmann. Toxicological and epidemiological studies of cardiovascular effects of ambient air fine particulate matter (PM2. 5) and its chemical components: coherence and public health implications. *Critical reviews in toxicology*, 44(4):299–347, 2014. doi:10.3109/10408444.2013.861796.

[300] C. Liu, A. V. Singh, C. Saggese, Q. Tang, D. Chen, K. Wan, M. Vinciguerra, M. Commodo, G. De Falco, P. Minutolo, A. D'Anna, and H. Wang. Flame-formed carbon nanoparticles exhibit quantum dot behaviors. *Proceedings of the National Academy of Sciences*, 116(26):12692–12697, 2019. doi:10.1073/pnas.1900205116.

[301] H. Liu, T. Ye, and C. Mao. Fluorescent carbon nanoparticles derived from candle soot. *Angewandte Chemie - International Edition*, 46(34):6473–6475, 2007. doi:10.1002/anie.200701271.

[302] J. Liu, H. Ke, K. Zhong, X. He, X. Xue, L. Wang, and C. Zhang. Higher activity leading to higher disorder: A case of four light hydrocarbons to variable morphological carbonaceous materials by pyrolysis. *The Journal of Physical Chemistry C*, 122(51):29516–29525, 2018. doi:10.1021/acs.jpcc.8b07762.

[303] M. Liu and W. H. Green. Capturing aromaticity in automatic mechanism generation software. *Proceedings of the Combustion Institute*, 37(1):575 – 581, 2019. doi:10.1016/j.proci.2018.06.006.

[304] M. Liu, V. I. Artyukhov, H. Lee, F. Xu, and B. I. Yakobson. Carbyne from first principles: chain of C atoms, a nanorod or a nanorope. *ACS nano*, 7(11):10075–10082, 2013. doi:10.1021/nn404177r.

[305] P. Liu, B. Chen, Z. Li, A. Bennett, S. Sioud, S. M. Sarathy, and W. L. Roberts. Evolution of oxygenated polycyclic aromatic hydrocarbon chemistry at flame temperatures. *Combustion and Flame*, 209:441–451, 2019. doi:10.1016/j.combustflame.2019.08.018.

[306] P. Liu, Y. Li, S. M. Sarathy, and W. L. Roberts. Gas-to-Liquid Phase Transition of PAH at Flame Temperatures. *The Journal of Physical Chemistry A*, 124(19):3896–3903, 2020. doi:10.1021/acs.jpca.0c01912.

[307] S. Liu, M. F. Jarrold, and M. T. Bowers. Ion-molecule clustering in simple systems. a study of the temperature dependence of the dimerization reactions of $CH_2CF_2^+$, $C_6H_6^+$ (benzene), and $C_6D_6^+$ (benzene-$d_6$) in their parent neutral gases: experiment and theory. *The Journal of Physical Chemistry*, 89(14):3127–3134, 1985. doi:10.1021/j100260a035.

[308] T. Lu and C. K. Law. Toward accommodating realistic fuel chemistry in large-scale computations. *Progress in Energy and Combustion Science*, 35(2):192–215, 2009. doi:10.1016/j.pecs.2008.10.002.

[309] J. Luo, Y. Zhang, Q. Zhang, J. Liu, and J. Wang. Evaluation of sooting tendency of acetone–butanol–ethanol (ABE) fuels blended with diesel fuel. *Fuel*, 209:394–401, 2017. doi:10.1016/j.fuel.2017.08.019.

[310] L. Madden, L. Moskaleva, S. Kristyan, and M. Lin. Ab initio MO study of the unimolecular decomposition of the phenyl radical. *The Journal of Physical Chemistry A*, 101(36):6790–6797, 1997. doi:10.1021/jp970723d.

[311] E. R. Magaril and R. Z. Magaril. *Engine fuels*. KDU, Moscow, 2008.

[312] T. Makonese, J. Meyer, and S. Von Solms. Characteristics of spherical organic particles emitted from fixed-bed residential coal combustion. *Atmosphere*, 10(8):441, 2019. doi:10.3390/atmos10080441.

[313] L. Malorni, V. Guida, M. Sirignano, G. Genovese, C. Petrarca, and P. Pedata. Exposure to sub-10 nm particles emitted from a biodiesel-fueled diesel engine: In vitro toxicity and inflammatory potential. *Toxicology letters*, 270:51–61, 2017. doi:10.1016/j.toxlet.2017.02.009.

[314] A. Mansouri, L. Zimmer, S. B. Dworkin, and N. A. Eaves. Impact of pressure-based haca rates on soot formation in varying-pressure coflow laminar diffusion flames. *Combustion and Flame*, 218:109–120, 2020. doi:10.1016/j.combustflame.2020.03.030.

[315] Q. Mao, A. C. T. van Duin, and K. H. Luo. Formation of incipient soot particles from polycyclic aromatic hydrocarbons: A ReaxFF molecular dynamics study. *Carbon*, 121:380–388, 2017. doi:10.1016/j.carbon.2017.06.009.

[316] Q. Mao, D. Hou, K. H. Luo, and X. You. Dimerization of polycyclic aromatic hydrocarbon molecules and radicals under flame conditions. *The Journal of Physical Chemistry A*, 122(44):8701–8708, 2018. doi:10.1021/acs.jpca.8b07102.

[317] Q. Mao, L. Cai, R. Langer, and H. Pitsch. The role of resonance-stabilized radical chain reactions in polycyclic aromatic hydrocarbon growth: Theoretical calculation and kinetic modeling. *Proceedings of the Combustion Institute*, 2020. doi:10.1016/j.proci.2020.07.117.

[318] A. Maranzana and G. Tonachini. Antagonistic functionalized nucleation and oxidative degradation in combustive formation of pyrene-based clusters mediated by triplet O and $O_2$: Theoretical study. *ChemPhysChem*, 16(12):2615–2624, 2015. doi:10.1002/cphc.201500332.

[319] N. M. Marinov, W. J. Pitz, and C. K. Westbrook. Aromatic and Polycyclic Aromatic Hydrocarbon Formation in a Laminar Premixed n -Butane Flame. *Combustion and Flame*, 213:192–213, 1998. doi:10.1016/S0010-2180(97)00275-7.

[320] H. Marsh and F. R. Reinoso. *Activated carbon*. Elsevier, 2006.

[321] J. W. Martin, G. J. McIntosh, R. Arul, R. N. Oosterbeek, M. Kraft, and T. Söhnel. Giant fullerene formation through thermal treatment of fullerene soot. *Carbon*, 125:132–138, 2017. doi:10.1016/j.carbon.2017.09.045.

[322] J. W. Martin, R. I. Slavchov, E. K. Yapp, J. Akroyd, S. Mosbach, and M. Kraft. The polarization of polycyclic aromatic hydrocarbons curved by pentagon incorporation: the role of the flexoelectric dipole. *The Journal of Physical Chemistry C*, 121(48):27154–27163, 2017. doi:10.1021/acs.jpcc.7b09044.

[323] J. W. Martin, M. Botero, R. I. Slavchov, K. Bowal, J. Akroyd, S. Mosbach, and M. Kraft. Flexoelectricity and the formation of carbon nanoparticles in flames. *The Journal of Physical Chemistry C*, 122(38):22210–22215, 2018. doi:10.1021/acs.jpcc.8b08264.

[324] J. W. Martin, K. L. Bowal, A. Menon, R. I. Slavchov, J. Akroyd, S. Mosbach, and M. Kraft. Polar curved polycyclic aromatic hydrocarbons in soot formation. *Proceedings of the Combustion Institute*, 37(1):1117–1123, 2019. doi:10.1016/j.proci.2018.05.046.

[325] J. W. Martin, D. Hou, A. Menon, L. Pascazio, J. Akroyd, X. You, and M. Kraft. Reactivity of polycyclic aromatic hydrocarbon soot precursors: Implications of localized $\pi$-radicals on rim-based pentagonal rings. *The Journal of Physical Chemistry C*, 123(43):26673–26682, 2019. doi:10.1021/acs.jpcc.9b07558.

[326] J. W. Martin, A. Menon, C. T. Lao, J. Akroyd, and M. Kraft. Dynamic polarity of curved aromatic soot precursors. *Combustion and Flame*, 206:150–157, 2019. doi:10.1016/j.combustflame.2019.04.046.

[327] D. Martin-Jimenez, S. Ahles, D. Mollenhauer, H. A. Wegner, A. Schirmeisen, and D. Ebeling. Bond-level imaging of the 3d conformation of adsorbed organic molecules using atomic force microscopy with simultaneous tunneling feedback. *Physical Review Letters*, 122:196101, 2019. doi:10.1103/PhysRevLett.122.196101.

[328] A. Matsugi. Thermal decomposition of benzyl radicals: Kinetics and spectroscopy in a shock tube. *The Journal of Physical Chemistry A*, 124(5):824–835, 2020. doi:10.1021/acs.jpca.9b10705.

[329] F. Mauß and H. Bockhorn. Soot formation in premixed hydrocarbon flames: Prediction of temperature and pressure dependence. *Zeitschrift für Physikalische Chemie*, 188(1-2):45–60, 1995. doi:10.1524/zpch.1995.188.Part_1_2.045.

[330] F. Mauss, T. Schäfer, and H. Bockhorn. Inception and growth of soot particles in dependence on the surrounding gas phase. *Combustion and Flame*, 99(3-4): 697–705, 1994. doi:10.1016/0010-2180(94)90064-7.

[331] F. Mauss, B. Trilken, H. Breitbach, and N. Peters. Soot formation in partially premixed diffusion flames at atmospheric pressure. In *Soot formation in combustion*, pages 325–349. Springer, 1994.

[332] J. McArragher and K. Tan. Soot formation at high pressures: a literature review. *Combustion Science and Technology*, 5(1):257–261, 1972. doi:10.1080/00102207208952530.

[333] M. N. McCabe, P. Hemberger, E. Reusch, A. Bodi, and J. Bouwman. Off the beaten path: Almost clean formation of indene from the ortho-benzyne + allyl reaction. *The journal of physical chemistry letters*, 11(8):2859–2863, 2020. doi:10.1021/acs.jpclett.0c00374.

[334] C. S. McEnally and L. D. Pfefferle. Improved sooting tendency measurements for aromatic hydrocarbons and their implications for naphthalene formation pathways. *Combustion and Flame*, 148(4):210–222, 2007. doi:10.1016/j.combustflame.2006.11.003.

[335] C. S. McEnally and L. D. Pfefferle. Sooting tendencies of nonvolatile aromatic hydrocarbons. *Proceedings of the Combustion Institute*, 32 I(1):673–679, 2009. doi:10.1016/j.proci.2008.06.197. URL `http://dx.doi.org/10.1016/j.proci.2008.06.197`.

[336] C. S. McEnally, L. D. Pfefferle, B. Atakan, and K. Kohse-Höinghaus. Studies of aromatic hydrocarbon formation mechanisms in flames: Progress towards closing the fuel gap. *Progress in Energy and Combustion Science*, 32(3):247–294, 2006. doi:10.1016/j.pecs.2005.11.003.

[337] M. L. McKee, H. P. Reisenauer, and P. R. Schreiner. Combined ab initio molecular dynamics and experimental studies of carbon atom addition to benzene. *The Journal of Physical Chemistry A*, 118(15):2801–2809, 2014. doi:10.1021/jp501107b.

[338] J. McKinnon and J. Howard. Application of soot formation model: effects of chlorine. *Combustion science and technology*, 74(1-6):175–197, 1990. doi:10.1080/00102209008951687.

[339] J. T. McKinnon, E. Meyer, and J. B. Howard. Infrared analysis of flame-generated PAH samples. *Combustion and Flame*, 105(1-2):161–166, 1996. doi:10.1016/0010-2180(95)00185-9.

[340] A. M. Mebel, Y. Georgievskii, A. W. Jasper, and S. J. Klippenstein. Temperature- and pressure-dependent rate coefficients for the HACA pathways from benzene to naphthalene. *Proceedings of the Combustion Institute*, 36(1):919–926, 2017. doi:10.1016/j.proci.2016.07.013.

[341] A. Menon, J. A. Dreyer, J. W. Martin, J. Akroyd, J. Robertson, and M. Kraft. Optical band gap of cross-linked, curved, and radical polyaromatic hydrocarbons. *Physical Chemistry Chemical Physics*, 21(29):16240–16251, 2019. doi:10.1039/C9CP02363A.

[342] A. Menon, N. B. Krdzavac, and M. Kraft. From database to knowledge graph—using data in chemistry. *Current Opinion in Chemical Engineering*, 26: 33–37, 2019. doi:10.1016/j.coche.2019.08.004.

[343] A. Menon, G. Leon, J. Akroyd, and M. Kraft. A density functional theory study on the kinetics of seven-member ring formation in polyaromatic hydrocarbons. *Combustion and Flame*, 217:152–174, 2020. doi:10.1016/j.combustflame.2020.03.032.

[344] A. Menon, J. W. Martin, G. Leon, D. Hou, L. Pascazio, X. You, and M. Kraft. Reactive localized $\pi$-radicals on rim-based pentagonal rings: properties and concentration in flames. *Proceedings of the Combustion Institute*, In Press, 2020. doi:10.1016/j.proci.2020.07.042.

[345] W. Merchan-Merchan, S. McCollam, and J. F. C. Pugliese. Soot formation in diffusion oxygen-enhanced biodiesel flames. *Fuel*, 156:129–141, 2015. doi:10.1016/j.fuel.2015.04.011.

[346] X. Mercier, O. Carrivain, C. Irimiea, A. Faccinetto, and E. Therssen. Dimers of polycyclic aromatic hydrocarbons: the missing pieces in the soot formation process. *Physical Chemistry Chemical Physics*, 21(16):8282–8294, 2019. doi:10.1039/C9CP00394K.

[347] X. Mercier, A. Faccinetto, S. Batut, G. Vanhove, D. Božanić, H. Hróðmarsson, G. Garcia, and L. Nahon. Selective identification of cyclopentaring-fused PAHs and side-substituted PAHs in a low pressure premixed sooting flame by photoelectron photoion coincidence spectroscopy. *Physical Chemistry Chemical Physics*, 22 (28):15926–15944, 2020. doi:10.1039/D0CP02740E.

[348] P. Michaud, J. Delfau, and A. Barassin. The positive ion chemistry in the post-combustion zone of sooting premixed acetylene low pressure flat flames. *Symposium (International) on Combustion*, 18(1):443 – 451, 1981. doi:10.1016/S0082-0784(81)80050-1.

[349] H. A. Michelsen. Probing soot formation, chemical and physical evolution, and oxidation: A review of in situ diagnostic techniques and needs. *Proceedings of the Combustion Institute*, 36(1):717–735, 2017. doi:10.1016/j.proci.2016.08.027.

[350] H. A. Michelsen, A. V. Tivanski, M. K. Gilles, L. H. Van Poppel, M. A. Dansson, and P. R. Buseck. Particle formation from pulsed laser irradiation of soot aggregates studied with a scanning mobility particle sizer, a transmission electron microscope, and a scanning transmission x-ray microscope. *Applied optics*, 46(6):959–977, 2007. doi:10.1364/AO.46.000959.

[351] H. A. Michelsen, M. Colket, P.-E. Bengtsson, A. D'Anna, P. Desgroux, B. S. Haynes, J. H. Miller, G. J. Nathan, H. Pitsch, and H. Wang. A review of terminology used to describe soot formation and evolution under combustion and pyrolytic conditions. *ACS nano*, 2020. doi:10.1021/acsnano.0c06226.

[352] G. Millar, T. Abel, J. Allen, P. Barn, M. Noullett, J. Spagnol, and P. L. Jackson. Evaluating human exposure to fine particulate matter part I: Measurements. *Geography Compass*, 4(4):281–302, 2010. doi:10.1111/j.1749-8198.2010.00325.x.

[353] G. Millar, T. Abel, J. Allen, P. Barn, M. Noullett, J. Spagnol, and P. L. Jackson. Evaluating human exposure to fine particulate matter part ii: Modeling. *Geography Compass*, 4(7):731–749, 2010. doi:10.1111/j.1749-8198.2010.00344.x.

[354] J. A. Miller and C. F. Melius. Kinetic and thermodynamic issues in the formation of aromatic compounds in flames of aliphatic fuels. *Combustion and Flame*, 91(1): 21–39, 1992. doi:10.1016/0010-2180(92)90124-8.

[355] J. A. Miller, M. J. Pilling, and J. Troe. Unravelling combustion mechanisms through a quantitative understanding of elementary reactions. *Proceedings of the Combustion Institute*, 30(1):43–88, 2005. doi:10.1016/j.proci.2004.08.281.

[356] J. H. Miller. The kinetics of polynuclear aromatic hydrocarbon agglomeration in flames. *Symposium (International) on Combustion*, 23(1):91 – 98, 1991. doi:10.1016/S0082-0784(06)80246-8.

[357] J. H. Miller. Aromatic excimers: evidence for polynuclear aromatic hydrocarbon condensation in flames. *Proceedings of the Combustion Institute*, 30(1):1381–1388, 2005. doi:10.1016/j.proci.2004.08.192.

[358] J. H. Miller, W. G. Mallard, and K. C. Smyth. The observation of laser-induced visible fluorescence in sooting diffusion flames. *Combustion and Flame*, 47:205–214, 1982. doi:10.1016/0010-2180(82)90101-8.

[359] J. H. Miller, K. C. Smyth, and W. G. Mallard. Calculations of the dimerization of aromatic hydrocarbons: Implications for soot formation. *Symposium (International) on Combustion*, 20(1):1139–1147, 1985. doi:10.1016/S0082-0784(85)80604-4.

[360] M. R. Miller, C. A. Shaw, and J. P. Langrish. From particles to patients: Oxidative stress and the cardiovascular effects of air pollution. *Future Cardiology*, 8(4):577–602, 2012. doi:10.2217/fca.12.43.

[361] M. R. Miller, J. B. Raftis, J. P. Langrish, S. G. Mclean, P. Samutrtai, S. P. Connell, S. Wilson, A. T. Vesey, P. H. B. Fokkens, A. J. F. Boere, P. Krystek, C. J. Campbell, P. W. F. Hadoke, K. Donaldson, F. R. Cassee, D. E. Newby, R. Du, N. L. Mills, R. Duffin, and N. L. Mills. Inhaled nanoparticles accumulate at sites of vascular disease. *ACS Nano*, 11(5):10623–10624, 2017. doi:10.1021/acsnano.6b08551.

[362] N. L. Mills, N. Amin, S. D. Robinson, A. Anand, J. Davies, D. Patel, J. M. De La Fuente, F. R. Cassee, N. A. Boon, W. MacNee, A. M. Millar, K. Donaldson, and D. E. Newby. Do inhaled carbon nanoparticles translocate directly into the circulation in humans? *American Journal of Respiratory and Critical Care Medicine*, 173(4):426–431, 2006. doi:10.1164/rccm.200506-865OC.

[363] P. Minutolo, G. Gambi, A. D'Alessio, and S. Carlucci. Spectroscopic characterisation of carbonaceous nanoparticles in premixed flames. *Atmospheric Environment*, 33(17):2725–2732, 1999. doi:10.1016/S1352-2310(98)00330-6.

[364] P. Minutolo, A. D'Anna, M. Commodo, R. Pagliara, G. Toniato, and C. Accordini. Emission of ultrafine particles from natural gas domestic burners. *Environmental Engineering Science*, 25(10):1357–1364, 2008. doi:10.1089/ees.2007.0188.

[365] A. Mitsos, G. M. Oxberry, P. I. Barton, and W. H. Green. Optimal automatic reaction and species elimination in kinetic mechanisms. *Combustion and Flame*, 155(1-2):118–132, 2008. doi:10.1016/j.combustflame.2008.03.004.

[366] M. Mojica, J. A. Alonso, and F. Méndez. Synthesis of fullerenes. *Journal of Physical Organic Chemistry*, 26(7):526–539, 2013. doi:10.1002/poc.3121.

[367] P. Møller, P. H. Danielsen, D. G. Karottki, K. Jantzen, M. Roursgaard, H. Klingberg, D. M. Jensen, D. V. Christophersen, J. G. Hemmingsen, Y. Cao, and S. Loft. Oxidative stress and inflammation generated DNA damage by exposure to air pollution particles. *Mutation Research - Reviews in Mutation Research*, 762:133–166, 2014. doi:10.1016/j.mrrev.2014.09.001.

[368] M. J. Montgomery, D. D. Das, C. S. McEnally, and L. D. Pfefferle. Analyzing the robustness of the yield sooting index as a measure of sooting tendency. *Proceedings of the Combustion Institute*, 37(1):911–918, 2019. doi:10.1016/j.proci.2018.06.105.

[369] P. P. Morajkar, M. K. Abdrabou, A. Raj, M. Elkadi, S. Stephen, and M. I. Ali. Transmission of trace metals from fuels to soot particles: An ICP-MS and soot nanostructural disorder study using diesel and diesel/karanja biodiesel blend. *Fuel*, 280:118631, 2020. doi:10.1016/j.fuel.2020.118631.

[370] J. Morbach, A. Yang, and W. Marquardt. Ontocape—a large-scale ontology for chemical process engineering. *Engineering applications of artificial intelligence*, 20(2):147–161, 2007. doi:10.1016/j.engappai.2006.06.010.

[371] W. A. Morgan, E. D. Feigelson, H. Wang, and M. Frenklach. A new mechanism for the formation of meteoritic kerogen-like material. *Science*, 252(5002):109–112, 1991. doi:10.1126/science.252.5002.109.

[372] Z. Mou, K. Uchida, T. Kubo, and M. Kertesz. Evidence of σ-and π-dimerization in a series of phenalenyls. *Journal of the American Chemical Society*, 136(52): 18009–18022, 2014. doi:10.1021/ja509243p.

[373] T. Mouton, X. Mercier, and M. Wartel. Laser-induced incandescence technique to identify soot nucleation and very small particles in low-pressure methane flames. *Applied Physics B*, 112:369–379, 2013. doi:10.1007/s00340-013-5446-x.

[374] R. Mueller, L. Mädler, and S. E. Pratsinis. Nanoparticle synthesis at high production rates by flame spray pyrolysis. *Chemical Engineering Science*, 58(10): 1969–1976, 2003. doi:10.1016/S0009-2509(03)00022-8.

[375] J. Mukherjee, A. F. Sarofim, and J. P. Longwell. Polycyclic aromatic hydrocarbons from the high-temperature pyrolysis of pyrene. *Combustion and Flame*, 96(3): 191–200, 1994. doi:10.1016/0010-2180(94)90008-6.

[376] M. R. Mulay, A. Chauhan, S. Patel, V. Balakrishnan, A. Halder, and R. Vaish. Candle soot: Journey from a pollutant to a functional material. *Carbon*, 144:684–712, 2019. doi:10.1016/j.carbon.2018.12.083.

[377] R. S. Mulliken and W. B. Person. *Molecular complexes: a lecture and reprint volume*. Wiley-Interscience, 1969.

[378] A. Münzer, L. Xiao, Y. H. Sehlleier, C. Schulz, and H. Wiggers. All gas-phase synthesis of graphene: Characterization and its utilization for silicon-based lithium-ion batteries. *Electrochimica Acta*, 272:52–59, 2018. doi:10.1016/j.electacta.2018.03.137.

[379] L. Murr and K. Garza. Natural and anthropogenic environmental nanoparticulates: Their microstructural characterization and respiratory health implications. *Atmospheric Environment*, 43(17):2683–2692, 2009. doi:10.1016/j.atmosenv.2009.03.002.

[380] S. Musikhin, P. Fortugno, J. C. Corbin, G. J. Smallwood, T. Dreier, K. J. Daun, and C. Schulz. Characterization of few-layer graphene aerosols by laser-induced incandescence. *Carbon*, 2020. doi:10.1016/j.carbon.2020.05.052.

[381] J. D. Myers, T. C. Allison, S. Bittner, B. Didier, M. Frenklach, W. H. Green, Y.-L. Ho, J. Hewson, W. Koegler, C. Lansing, D. Leahy, M. Lee, R. McCoy, M. Minkoff, S. Nijsure, G. von Laszewski, D. Montoya, L. Oluwole, C. Pancerella, R. Pinzon, W. Pitz, L. A. Rahn, B. Ruscic, K. Schuchardt, E. Stephan, A. Wagner, T. Windus, and C. Yang. A collaborative informatics infrastructure for multi-scale science. *Cluster Computing*, 8(4):243–253, 2005. doi:10.1007/s10586-005-4092-4.

[382] B. Náfrádi, M. Choucair, K.-P. Dinse, and L. Forró. Room temperature manipulation of long lifetime spins in metallic-like carbon nanospheres. *Nature communications*, 7:12232, 2016. doi:10.1038/ncomms12232.

[383] H. Nagai, M. Nakano, K. Yoneda, R. Kishi, H. Takahashi, A. Shimizu, T. Kubo, K. Kamada, K. Ohta, E. Botek, and B. Champagne. Signature of multiradical character in second hyperpolarizabilities of rectangular graphene nanoflakes. *Chemical Physics Letters*, 489(4-6):212–218, 2010. doi:10.1016/j.cplett.2010.03.013.

[384] R. Niessner. The many faces of soot: Characterization of soot nanoparticles produced by engines. *Angewandte Chemie International Edition*, 53:12366–12379, 2014. doi:10.1002/anie.201402812.

[385] I. of Computer Engineering at Technical University of Vienna. Weather ontology. `http://www.auto.tuwien.ac.at/downloads/thinkhome/ontology/WeatherOntology.owl`, last accessed 2018-12-18).

[386] B. Öktem, M. P. Tolocka, B. Zhao, H. Wang, and M. V. Johnston. Chemical species associated with the early stage of soot growth in a laminar premixed ethylene–oxygen–argon flame. *Combustion and Flame*, 142(4):364–373, 2005. doi:10.1016/j.combustflame.2005.03.016.

[387] K. Ono, Y. Matsukawa, K. Dewa, A. Watanabe, K. Takahashi, Y. Saito, Y. Matsushita, H. Aoki, K. Era, T. Aoki, and T. Yamaguchi. Formation mechanisms of soot from high-molecular-weight polycyclic aromatic hydrocarbons. *Combustion and Flame*, 162(6):2670–2678, 2015. doi:10.1016/j.combustflame.2015.03.022.

[388] M. Orchin and L. Reggel. Aromatic cyclodehydrogenation. v. a synthesis of fluoranthene1. *Journal of the American Chemical Society*, 69(3):505–509, 1947. doi:10.1021/ja01195a009.

[389] A. M. Oyarzún, C. D. Latham, L. R. Radovic, P. R. Briddon, and M. J. Rayson. Spin density distributions on graphene clusters and ribbons with carbene-like active sites. *Physical Chemistry Chemical Physics*, 20(42):26968–26978, 2018. doi:10.1039/C8CP03313G.

[390] H. B. Palmer and C. F. Cullis. The formation of carbon from gases. *Chemistry and Physics of Carbon*, 1:265–325, 1965.

[391] D. G. Park, B. C. Choi, M. S. Cha, and S. H. Chung. Soot Reduction Under DC Electric Fields in Counterflow Non-Premixed Laminar Ethylene Flames. *Combustion Science and Technology*, 186(4-5):644–656, 2014. doi:10.1080/00102202.2014.883794.

[392] J. Park, S. Burova, A. Rodgers, and M. Lin. Experimental and theoretical studies of the $C_6H_5^+$ $C_6H_6$ reaction. *The Journal of Physical Chemistry A*, 103(45):9036–9041, 1999. doi:10.1021/jp9920592.

[393] W. Parker and H. Wolfhard. 418. Carbon formation in flames. *Journal of the Chemical Society (Resumed)*, pages 2038–2049, 1950. doi:10.1039/JR9500002038.

[394] L. Pascazio, M. Sirignano, and A. D. Anna. Simulating the morphology of clusters of polycyclic aromatic hydrocarbons : The influence of the intermolecular potential. *Combustion and Flame*, 185:53–62, 2017. doi:10.1016/j.combustflame.2017.07.003.

[395] L. Pascazio, J. W. Martin, M. L. Botero, M. Sirignano, A. D'Anna, and M. Kraft. Mechanical properties of soot particles: The impact of crosslinked polycyclic aromatic hydrocarbons. *Combustion Science and Technology*, 0(0):1–21, 2019. doi:10.1080/00102202.2019.1668380.

[396] L. Pascazio, J. Martin, A. Menon, D. You, J. Akroyd, and M. Kraft. Penta-linked planar aromatics in nascent soot formation. *In press*, 2020. doi:10.1016/j.proci.2020.09.029.

[397] L. Pascazio, J. W. Martin, K. Bowal, J. Akroyd, and M. Kraft. Exploring the internal structure of soot particles using nanoindentation: A reactive molecular dynamics study. *Combustion and Flame*, 219:45–56, 2020. doi:10.1016/j.combustflame.2020.04.029.

[398] M. B. Pastor, A. J. Kuhn, P. T. Nguyen, M. V. Santander, C. Castro, and W. L. Karney. Hydrogen shifts and benzene ring contractions in phenylenes. *Journal of Physical Organic Chemistry*, 26(9):750–754, 2013. doi:10.1002/poc.3126.

[399] P. Pedata, T. Stoeger, R. Zimmermann, A. Peters, G. Oberdörster, and A. D'Anna. Are we forgetting the smallest, sub 10 nm combustion generated particles? *Particle and fibre toxicology*, 12(1):34, 2015. doi:10.1186/s12989-015-0107-3.

[400] P. Pepiot, L. Cai, and H. Pitsch. Model reduction and lumping procedures. In *Computer Aided Chemical Engineering*, volume 45, pages 799–827. Elsevier, 2019.

[401] M. R. Philpott and Y. Kawazoe. Triplet states of zigzag edged hexagonal graphene molecules $c_{6m**2}h_{6m}$ (m= 1, 2, 3,. . . , 10) and carbon based magnetism. *The Journal of Chemical Physics*, 134(12):124706, 2011. doi:10.1063/1.3569135.

[402] E. R. Place and F. J. Weinberg. Electrical control of flame carbon. *Proceedings of the Royal Society A: Mathematical, Physical and Engineering Sciences*, 289 (1417):192–205, 1966. doi:10.1098/rspa.1966.0006.

[403] S. Pogodin and I. Agranat. Theoretical notions of aromaticity and antiaromaticity: phenalenyl ions versus fluorenyl ions. *The Journal of organic chemistry*, 72(26): 10096–10107, 2007. doi:10.1021/jo701939c.

[404] D. Polino, A. Famulari, and C. Cavallotti. Analysis of the reactivity on the $C_7H_6$ potential energy surface. *The Journal of Physical Chemistry A*, 115(27):7928–7936, 2011. doi:10.1021/jp2019236.

[405] C. Pope, J. Marr, and J. Howard. Chemistry of fullerenes $C_{60}$ and $C_{70}$ formation in flames. *The Journal of Physical Chemistry*, 97:11001–11013, 1993. doi:10.1021/j100144a018.

[406] G. Porter. Carbon formation in the combustion wave. *Symposium (International) on Combustion*, 4(1):248–252, 1953. doi:10.1016/S0082-0784(53)80031-7.

[407] F. Qi. Combustion chemistry probed by synchrotron VUV photoionization mass spectrometry. *Proceedings of the Combustion Institute*, 34(1):33–63, 2013. doi:10.1016/j.proci.2012.09.002.

[408] H.-J. Qian, A. C. T. van Duin, K. Morokuma, and S. Irle. Reactive Molecular Dynamics Simulation of Fullerene Combustion Synthesis: ReaxFF vs DFTB Potentials. *Journal of Chemical Theory and Computation*, 7(7):2040–2048, 2011. doi:10.1021/ct200197v.

[409] A. Raj. Structural effects on the growth of large polycyclic aromatic hydrocarbons by $C_2H_2$. *Combustion and Flame*, 204:331 – 340, 2019. doi:10.1016/j.combustflame.2019.03.027.

[410] A. Raj, M. Celnik, R. Shirley, M. Sander, R. Patterson, R. West, and M. Kraft. A statistical approach to develop a detailed soot growth model using PAH characteristics. *Combustion and Flame*, 156(4):896–913, 2009. doi:10.1016/j.combustflame.2009.01.005.

[411] A. Raj, P. L. W. Man, T. S. Totton, M. Sander, R. A. Shirley, and M. Kraft. New polycyclic aromatic hydrocarbon (PAH) surface processes to improve the model prediction of the composition of combustion-generated PAHs and soot. *Carbon*, 48(2):319–332, 2010. doi:10.1016/j.carbon.2009.09.030.

[412] A. Raj, I. D. C. Prada, A. A. Amer, and S. H. Chung. A reaction mechanism for gasoline surrogate fuels for large polycyclic aromatic hydrocarbons. *Combustion and Flame*, 159(2):500–515, 2012. doi:10.1016/j.combustflame.2011.08.011.

[413] A. Raj, S. Y. Yang, D. Cha, R. Tayouo, and S. H. Chung. Structural effects on the oxidation of soot particles by $O_2$: Experimental and theoretical study. *Combustion and Flame*, 160(9):1812 – 1826, 2013. doi:10.1016/j.combustflame.2013.03.010.

[414] A. Ratkiewicz and T. N. Truong. Kinetics of the C–C bond beta scission reactions in alkyl radical reaction class. *The Journal of Physical Chemistry A*, 116(25):6643–6654, 2012. doi:10.1021/jp3018265.

[415] P. Reilly, R. Gieray, W. Whitten, and J. Ramsey. Direct observation of the evolution of the soot carbonization process in an acetylene diffusion flame via real-time aerosol mass spectrometry. *Combustion and Flame*, 122(1-2):90–104, 2000. doi:10.1016/S0010-2180(00)00105-X.

[416] A. Reis. Beiträge zur Kenntnis der Flammen. *Zeitschrift für Physikalische Chemie*, 88(1):513–568, 1914. doi:10.1515/zpch-1914-8836.

[417] T. Rengarajan, P. Rajendran, N. Nandakumar, B. Lokeshkumar, P. Rajendran, and I. Nishigaki. Exposure to polycyclic aromatic hydrocarbons with special focus on cancer. *Asian Pacific Journal of Tropical Biomedicine*, 5:182–189, 2015. doi:10.1016/S2221-1691(15)30003-4.

[418] K. Revzan, N. Brown, and M. Frenklach. Soot formation codes. *URL: http://www. me. berkeley. edu/soot S*, 1999.

[419] Y. M. Rhee, T. J. Lee, M. S. Gudipati, L. J. Allamandola, and M. Head-Gordon. Charged polycyclic aromatic hydrocarbon clusters and the galactic extended red emission. *Proceedings of the National Academy of Sciences of the United States of America*, 104(13):5274–5278, 2007. doi:10.1073/pnas.0609396104.

[420] H. Richter and J. Howard. Formation of polycyclic aromatic hydrocarbons and their growth to soot: a review of chemical reaction pathways. *Progress in Energy and Combustion Science*, 26(4-6):565–608, 2000. doi:10.1016/S0360-1285(00)00009-5.

[421] A. Rinkenburger, T. Toriyama, K. Yasuda, and R. Niessner. Catalytic Effect of Potassium Compounds in Soot Oxidation. *ChemCatChem*, 9(18):3513–3525, 2017. doi:10.1002/cctc.201700338.

[422] A. Rodríguez-Fortea, S. Irle, and J. M. Poblet. Fullerenes: formation, stability, and reactivity. *Wiley Interdisciplinary Reviews: Computational Molecular Science*, 1 (3):350–367, 2011. doi:10.1002/wcms.21.

[423] T. Rönkkö, A. Virtanen, J. Kannosto, J. Keskinen, M. Lappi, and L. Pirjola. Nucleation mode particles with a nonvolatile core in the exhaust of a heavy duty diesel vehicle. *Environmental Science and Technology*, 41(18):6384–6389, 2007. doi:10.1021/es0705339.

[424] K. Rummel and P.-O. Veh. Die Strahlung leuchtender Flammen. Erster Teil: Schrifttumsgrundlagen, Arbeitshypothesen und Vorversuche (Translation: The radiance of glowing flames. Part 1: Foundations, working hypotheses and preliminary experiments). *Archiv für das Eisenhüttenwesen*, 14(10):489–499, 1941. doi:10.1002/srin.194101863.

[425] C. Russo, B. Apicella, J. Lighty, A. Ciajolo, and A. Tregrossi. Optical properties of organic carbon and soot produced in an inverse diffusion flame. *Carbon*, 124: 372–379, 2017. doi:10.1016/j.carbon.2017.08.073.

[426] C. Russo, B. Apicella, and A. Ciajolo. Blue and green luminescent carbon nanodots from controllable fuel-rich flame reactors. *Scientific reports*, 9(1):1–8, 2019. doi:10.1038/s41598-019-50919-1.

[427] H. Sabbah, L. Biennier, S. J. Klippenstein, I. R. Sims, and B. R. Rowe. Exploring the role of PAHs in the formation of soot: pyrene dimerization. *The Journal of Physical Chemistry Letters*, 1(19):2962–2967, 2010. doi:10.1021/jz101033t.

[428] H. Sabbah, M. Commodo, F. Picca, G. De Falco, P. Minutolo, A. D'Anna, and C. Joblin. Molecular content of nascent soot: Family characterization using two-step laser desorption laser ionization mass spectrometry. *Proceedings of the Combustion Institute*, 2020. doi:10.1016/j.proci.2020.09.022.

[429] B. Saha, S. Shindo, S. Irle, and K. Morokuma. Quantum chemical molecular dynamics simulations of dynamic fullerene self-assembly in benzene combustion. *ACS Nano*, 3(8):2241–2257, 2009. doi:10.1021/nn900494s.

[430] B. Saha, S. Irle, and K. Morokuma. Hot giant fullerenes eject and capture $C_2$ molecules: QM/MD simulations with constant density. *Journal of Physical Chemistry C*, 115(46):22707–22716, 2011. doi:10.1021/jp203614e.

[431] H. Saigusa and E. C. Lim. Excimer formation in van der waals dimers and clusters of aromatic molecules. *Accounts of chemical research*, 29(4):171–178, 1996. doi:10.1021/ar950169v.

[432] M. Salamanca, M. Sirignano, and A. D'Anna. Particulate formation in premixed and counter-flow diffusion ethylene/ethanol flames. *Energy & fuels*, 26(10):6144–6152, 2012.

[433] M. Salamanca, M. L. Botero, J. W. Martin, J. A. Dreyer, J. Akroyd, and M. Kraft. The impact of cyclic fuels on the formation and structure of soot. *Combustion and Flame*, 219:1–12, 2020. doi:10.1016/j.combustflame.2020.04.026.

[434] R. C. Santos, C. E. Bernardes, H. P. Diogo, M. F. M. Piedade, J. N. Canongia Lopes, and M. E. Minas da Piedade. Energetics of the thermal dimerization of acenaphthylene to heptacyclene. *The Journal of Physical Chemistry A*, 110(6):2299–2307, 2006. doi:10.1021/jp056275o.

[435] A. F. Sarofim, J. P. Longwell, M. J. Wornat, and J. Mukherjee. The role of biaryl reactions in PAH and soot formation. In *Soot Formation in Combustion*, pages 485–499. Springer, 1994. doi:10.1007/978-3-642-85167-4_27.

[436] R. Schalla and G. McDonald. Mechanism of soot formation in flames. *Fifth Symposium (International) on Combustion*, 1955.

[437] M. Schenk, S. Lieb, H. Vieker, A. Beyer, A. Gölzhäuser, H. Wang, and K. Kohse-Höinghaus. Imaging nanocarbon materials: soot particles in flames are not structurally homogeneous. *ChemPhysChem*, 14(14):3248–3254, 2013. doi:10.1002/cphc.201300581.

[438] M. Schenk, S. Lieb, H. Vieker, A. Beyer, A. Gölzhäuser, H. Wang, and K. Kohse-Höinghaus. Morphology of nascent soot in ethylene flames. *Proceedings of the Combustion Institute*, 35(2):1879–1886, 2015. doi:10.1016/j.proci.2014.05.009.

[439] D. E. Schraufnagel, J. Balmes, C. T. Cowl, S. De Matteis, S.-H. Jung, K. Mortimer, R. Perez-Padilla, M. B. Rice, H. Riojas-Rodroguez, A. Sood, et al. Air pollution and non-communicable diseases: a review by the forum of international respiratory societies' environmental committee. part 2: air pollution and organ systems. *Chest*, 155(2):409–416, 2019. doi:10.1016/j.chest.2018.10.041.

[440] P. R. Schreiner, W. L. Karney, P. von Ragué Schleyer, W. T. Borden, T. P. Hamilton, and H. F. Schaefer. Carbene rearrangements unsurpassed: details of the $C_7H_6$ potential energy surface revealed. *The Journal of Organic Chemistry*, 61(20):7030–7039, 1996. doi:10.1021/jo960884y.

[441] K. Schuchardt, C. Pancerella, L. A. Rahn, B. Didier, D. Kodeboyina, D. Leahy, J. D. Myers, O. O. Oluwole, W. Pitz, B. Ruscic, et al. Portal-based knowledge environment for collaborative science. *Concurrency and Computation: Practice and Experience*, 19(12):1703–1716, 2007. doi:10.1002/cpe.1201.

[442] C. A. Schuetz and M. Frenklach. Nucleation of soot: Molecular dynamics simulations of pyrene dimerization. *Proceedings of the Combustion Institute*, 29(2): 2307–2314, 2002. doi:10.1016/S1540-7489(02)80281-4.

[443] F. Schulz, M. Commodo, K. Kaiser, G. D. Falco, P. Minutolo, G. Meyer, A. D'Anna, and L. Gross. Insights into incipient soot formation by atomic force microscopy. *Proceedings of the Combustion Institute*, 37(1):885 – 892, 2019. doi:10.1016/j.proci.2018.06.100.

[444] F. Schulz, M. Commodo, K. Kaiser, G. D. Falco, P. Minutolo, G. Meyer, A. D'Anna, and L. Gross. Insights into incipient soot formation by atomic force microscopy. *Proceedings of the Combustion Institute*, 37(1):885 – 892, 2019. doi:10.1016/j.proci.2018.06.100.

[445] L. T. Scott, M. S. Bratcher, and S. Hagen. Synthesis and Characterization of a $C_{36}H_{12}$ Fullerene Subunit. *Journal of the American Chemical Society*, 118(36): 8743–8744, 1996. doi:10.1021/ja9621511.

[446] K. Sendt and B. S. Haynes. Density functional study of the chemisorption of $o_2$ on the zig-zag surface of graphite. *Combustion and Flame*, 143(4):629–643, 2005. doi:10.1016/j.combustflame.2005.08.026.

[447] L. Sgro, G. Basile, A. Barone, A. D'Anna, P. Minutolo, A. Borghese, and A. D'Alessio. Detection of combustion formed nanoparticles. *Chemosphere*, 51 (10):1079–1090, 2003. doi:10.1016/S0045-6535(02)00718-X.

[448] L. Sgro, A. De Filippo, G. Lanzuolo, and A. D'Alessio. Characterization of nanoparticles of organic carbon (noc) produced in rich premixed flames by differential mobility analysis. *Proceedings of the Combustion Institute*, 31(1):631–638, 2007. doi:10.1016/j.proci.2006.08.026.

[449] L. Sgro, A. Simonelli, L. Pascarella, P. Minutolo, D. Guarnieri, N. Sannolo, P. Netti, and A. D'Anna. Toxicological properties of nanoparticles of organic compounds (noc) from flames and vehicle exhausts. *Environmental science & technology*, 43(7):2608–2613, 2009. doi:10.1021/es8034768.

[450] L. A. Sgro, A. D'Anna, and P. Minutolo. Charge distribution of incipient flame-generated particles. *Aerosol Science and Technology*, 44(8):651–662, 2010. doi:10.1080/02786826.2010.483701.

[451] L. A. Sgro, A. D'Anna, and P. Minutolo. On the characterization of nanoparticles emitted from combustion sources related to understanding their effects on health and climate. *Journal of hazardous materials*, 211:420–426, 2012. doi:10.1016/j.jhazmat.2011.10.097.

[452] S. Shabnam, Q. Mao, A. C. van Duin, and K. Luo. Evaluation of the effect of nickel clusters on the formation of incipient soot particles from polycyclic aromatic hydrocarbons via reaxff molecular dynamics simulations. *Physical Chemistry Chemical Physics*, 21(19):9865–9875, 2019. doi:10.1039/C9CP00354A.

[453] N. Sharma, S. China, J. Bhandari, K. Gorkowski, M. Dubey, R. A. Zaveri, and C. Mazzoleni. Physical properties of aerosol internally mixed with soot particles in a biogenically dominated environment in California. *Geophysical Research Letters*, 45(20):11–473, 2018. doi:10.1029/2018GL079404.

[454] X. Shi and L. S. Bartell. Electron diffraction and monte carlo studies of liquids. 1. intermolecular interactions for benzene. *The Journal of Physical Chemistry*, 92 (20):5667–5673, 1988. doi:10.1021/j100331a024.

[455] B. Shukla and M. Koshi. A highly efficient growth mechanism of polycyclic aromatic hydrocarbons. *Physical Chemistry Chemical Physics*, 12(10):2427–2437, 2010. doi:10.1039/B919644G.

[456] B. Shukla, K. Tsuchiya, and M. Koshi. Novel products from $c_6h_5^+$ $c_6h_6/c_6h_5$ reactions. *The Journal of Physical Chemistry A*, 115(21):5284–5293, 2011. doi:10.1021/jp201817n.

[457] J. Simonsson, N. E. Olofsson, H. Bladh, M. Sanati, and P. E. Bengtsson. Influence of potassium and iron chloride on the early stages of soot formation studied using imaging LII/ELS and TEM techniques. *Proceedings of the Combustion Institute*, 36(1):853–860, 2017. doi:10.1016/j.proci.2016.07.003.

[458] J. Singh, R. I. Patterson, M. Kraft, and H. Wang. Numerical simulation and sensitivity analysis of detailed soot particle size distribution in laminar premixed ethylene flames. *Combustion and Flame*, 145(1-2):117–127, 2006. doi:10.1016/j.combustflame.2005.11.003.

[459] M. Singh, A. Sengupta, K. Zeller, G. Skoptsov, and R. L. Vander Wal. Effect of hydrogen concentration on graphene synthesis using microwave-driven plasma-mediated methane cracking. *Carbon*, 143:802–813, 2019. doi:10.1016/j.carbon.2018.11.082.

[460] R. Singh and M. Frenklach. A mechanistic study of the influence of graphene curvature on the rate of high-temperature oxidation by molecular oxygen. *Carbon*, 101:203–212, 2016. doi:10.1016/j.carbon.2016.01.090.

[461] S. Sinha and A. Raj. Polycyclic aromatic hydrocarbon (PAH) formation from benzyl radicals: a reaction kinetics study. *Physical Chemistry Chemical Physics*, 18 (11):8120–8131, 2016. doi:10.1039/C5CP06465A.

[462] S. Sinha, R. K. Rahman, and A. Raj. On the role of resonantly stabilized radicals in polycyclic aromatic hydrocarbon (PAH) formation: pyrene and fluoranthene formation from benzyl–indenyl addition. *Physical Chemistry Chemical Physics*, 19 (29):19262–19278, 2017. doi:10.1039/C7CP02539D.

[463] M. Sirignano and A. D'Anna. Filtration and coagulation efficiency of sub-10 nm combustion-generated particles. *Fuel*, 221:298–302, 2018. doi:10.1016/j.fuel.2018.02.107.

[464] M. Sirignano, A. Collina, M. Commodo, P. Minutolo, and A. D'Anna. Detection of aromatic hydrocarbons and incipient particles in an opposed-flow flame of ethylene by spectral and time-resolved laser induced emission spectroscopy. *Combustion and Flame*, 159(4):1663 – 1669, 2012. doi:10.1016/j.combustflame.2011.11.005.

[465] M. Sirignano, M. Conturso, A. Magno, S. Di Iorio, E. Mancaruso, B. M. Vaglieco, and A. D'Anna. Evidence of sub-10 nm particles emitted from a small-size diesel engine. *Experimental Thermal and Fluid Science*, 95:60–64, 2018. doi:10.1016/j.expthermflusci.2018.01.031.

[466] M. Sirignano, C. Russo, and A. Ciajolo. One-step synthesis of carbon nanoparticles and yellow to blue fluorescent nanocarbons in flame reactors. *Carbon*, 156:370–377, 2020. doi:10.1016/j.carbon.2019.09.068.

[467] N. A. Slavinskaya, U. Riedel, S. B. Dworkin, and M. J. Thomson. Detailed numerical modeling of PAH formation and growth in non-premixed ethylene and ethane flames. *Combustion and Flame*, 159(3):979–995, 2012. doi:10.1016/j.combustflame.2011.10.005.

[468] J. G. Slowik, E. S. Cross, J.-H. Han, P. Davidovits, T. B. Onasch, J. T. Jayne, L. R. Williams, M. R. Canagaratna, D. R. Worsnop, R. K. Chakrabarty, W. P. Moosmüller, Hans amd Arnott, J. P. Schwarz, R.-S. Gao, D. W. Fahey, G. L. Kok, and A. Petzold. An inter-comparison of instruments measuring black carbon content of soot particles. *Aerosol Science and Technology*, 41(3):295–314, 2007. doi:10.1080/02786820701197078.

[469] D. Small, S. V. Rosokha, J. K. Kochi, and M. Head-Gordon. Characterizing the dimerizations of phenalenyl radicals by ab initio calculations and spectroscopy: $\sigma$-bond formation versus resonance $\pi$-stabilization. *The Journal of Physical Chemistry A*, 109(49):11261–11267, 2005. doi:10.1021/jp054244n.

[470] E. C. W. Smith. The Emission Spectrum of Hydrocarbon Flames. *Proceedings of the Royal Society A: Mathematical, Physical and Engineering Sciences*, 174(956): 110–125, 1940. doi:10.1098/rspa.1940.0009.

[471] G. P. Smith, D. M. Golden, M. Frenklach, N. W. Moriarty, B. Eiteneer, M. Goldenberg, C. T. Bowman, R. K. Hanson, S. Song, W. C. Gardiner Jr, V. V. Lissianski, and Z. Qin. GRImech 3.0 reaction mechanism. *Sandia National Laboratory*, 2000.

[472] M. C. Smith, G. Liu, Z. J. Buras, T.-C. Chu, J. Yang, and W. H. Green. Direct Measurement of Radical-Catalyzed C6H6 Formation from Acetylene and Validation of Theoretical Rate Coefficients for $C_2H_3^+$ $C_2H_2$ and $C_4H_5^+$ $C_2H_2$ Reactions. *The Journal of Physical Chemistry A*, 124(14):2871–2884, 2020. doi:10.1021/acs.jpca.0c00558.

[473] K. C. Smyth, C. R. Shaddix, and D. A. Everest. Aspects of soot dynamics as revealed by measurements of broadband fluorescence and flame luminosity in flickering diffusion flames. *Combustion and Flame*, 111(3):185–207, 1997. doi:10.1016/S0010-2180(97)00017-5.

[474] P. J. Stang. Unsaturated carbenes. *Chemical Reviews*, 78(4):383–405, 1978. doi:10.1021/cr60314a003.

[475] S. E. Stein and A. Fahr. High-temperature stabilities of hydrocarbons. *The Journal of Physical Chemistry*, 89(17):3714–3725, 1985. doi:10.1021/j100263a027.

[476] R. Stirn, T. G. Baquet, S. Kanjarkar, W. Meier, K. P. Geigle, H. H. Grotheer, C. Wahl, and M. Aigner. Comparison of particle size measurements with laser-induced incandescence, mass spectroscopy, and scanning mobility particle sizing in a laminar premixed ethylene-air flame. *Combustion Science and Technology*, 181(2):329–349, 2009. doi:10.1080/00102200802483498.

[477] J. Street and A. Thomas. Carbon formation in pre-mixed flames. *Fuel*, 34(1):4–36, 1955.

[478] T. Stuyver, B. Chen, T. Zeng, P. Geerlings, F. De Proft, and R. Hoffmann. Do diradicals behave like radicals? *Chemical reviews*, 119(21):11291–11351, 2019. doi:10.1021/acs.chemrev.9b00260.

[479] Z. Sun and J. Wu. Open-shell polycyclic aromatic hydrocarbons. *Journal of Materials Chemistry*, 22(10):4151–4160, 2012. doi:10.1039/C1JM14786B.

[480] J. Swanson and D. Kittelson. Evaluation of thermal denuder and catalytic stripper methods for solid particle measurements. *Journal of Aerosol Science*, 41(12):1113–1122, 2010. doi:10.1016/j.jaerosci.2010.09.003.

[481] C. A. Taatjes, N. Hansen, D. L. Osborn, K. Kohse-Höinghaus, T. A. Cool, and P. R. Westmoreland. "Imaging" combustion chemistry via multiplexed synchrotron-photoionization mass spectrometry. *Physical Chemistry Chemical Physics*, 10(1): 20–34, 2008. doi:10.1039/b713460f.

[482] M. Thierley, H. H. Grotheer, M. Aigner, Z. Yang, A. Abid, B. Zhao, and H. Wang. On existence of nanoparticles below the sooting threshold. *Proceedings of the Combustion Institute*, 31(1):639–647, 2007. doi:10.1016/j.proci.2006.08.035.

[483] A. Thomas. Carbon formation in flames. *Combustion and Flame*, 6:46 – 62, 1962. doi:10.1016/0010-2180(62)90066-4.

[484] H.-R. Tian, M.-M. Chen, K. Wang, Z.-C. Chen, C.-Y. Fu, Q. Zhang, S.-H. Li, S.-L. Deng, Y.-R. Yao, S.-Y. Xie, R.-B. Huang, and L.-S. Zheng. An unconventional hydrofullerene $C_{66}H_4$ with symmetric heptagons retrieved in low-pressure combustion. *Journal of the American Chemical Society*, 141(16):6651–6657, 2019. doi:10.1021/jacs.9b01638.

[485] P. Toth, A. B. Palotas, E. G. Eddings, R. T. Whitaker, and J. S. Lighty. A novel framework for the quantitative analysis of high resolution transmission electron micrographs of soot ii. robust multiscale nanostructure quantification. *Combustion and Flame*, 160(5):920 – 932, 2013. doi:10.1016/j.combustflame.2013.01.003.

[486] P. Toth, D. Jacobsson, M. Ek, and H. Wiinikka. Real-time, in situ, atomic scale observation of soot oxidation. *Carbon*, 145:149–160, 2019. doi:10.1016/j.carbon.2019.01.007.

[487] T. S. Totton, A. J. Misquitta, and M. Kraft. A First Principles Development of a General Anisotropic Potential for Polycyclic Aromatic Hydrocarbons. *Journal of Chemical Theory and Computation*, 6(3):683–695, 2010. doi:10.1021/ct9004883.

[488] T. S. Totton, A. J. Misquitta, and M. Kraft. Assessing the Polycyclic Aromatic Hydrocarbon Anisotropic Potential with Application to the Exfoliation Energy of Graphite. *The Journal of Physical Chemistry A*, 115(46):13684–13693, 2011. doi:10.1021/jp208088s.

[489] T. S. Totton, A. J. Misquitta, and M. Kraft. A quantitative study of the clustering of polycyclic aromatic hydrocarbons at high temperatures. *Physical Chemistry Chemical Physics*, 14(12):4081–94, 2012. doi:10.1039/c2cp23008a.

[490] M. K. Tran, D. Dunn-Rankin, and T. K. Pham. Characterizing sooting propensity in biofuel–diesel flames. *Combustion and flame*, 159(6):2181–2191, 2012. doi:10.1016/j.combustflame.2012.01.008.

[491] D. R. Tree and K. I. Svensson. Soot processes in compression ignition engines. *Progress in Energy and Combustion Science*, 33(3):272–309, 2007. doi:10.1016/j.pecs.2006.03.002.

[492] V. M. Tsefrikas and L. T. Scott. Geodesic Polyarenes by Flash Vacuum Pyrolysis. *Chemical Reviews*, 106(12):4868–4884, 2006. doi:10.1021/cr050553y.

[493] K. Uchida, S. Ito, M. Nakano, M. Abe, and T. Kubo. Biphenalenylidene: isolation and characterization of the reactive intermediate on the decomposition pathway of phenalenyl radical. *Journal of the American Chemical Society*, 138(7):2399–2410, 2016. doi:10.1021/jacs.5b13033.

[494] D. Ugarte. Curling and closure of graphitic networks under electron-beam irradiation. *Nature*, 359(6397):707–709, 1992. doi:10.1038/359707a0.

[495] D. Ugarte. Onion-like graphitic particles. *Carbon*, 33:989–993, 1995. doi:10.1016/0008-6223(95)00027-B.

[496] B. V. Unterreiner, M. Sierka, and R. Ahlrichs. Reaction pathways for growth of polycyclic aromatic hydrocarbons under combustion conditions, a DFT study. *Physical Chemistry Chemical Physics*, 6(18):4377, 2004. doi:10.1039/b407279k.

[497] R. L. Vander Wal and A. J. Tomasek. Soot nanostructure: dependence upon synthesis conditions. *Combustion and Flame*, 136(1-2):129–140, 2004. doi:10.1016/j.combustflame.2003.09.008.

[498] R. L. Vander Wal, T. Ticich, and A. Stephens. Optical and microscopy investigations of soot structure alterations by laser-induced incandescence. *Applied Physics B*, 67(1):115–123, 1998. doi:10.1007/s003400050483.

[499] R. L. Vander Wal, V. M. Bryg, and M. D. Hays. Fingerprinting soot (towards source identification): Physical structure and chemical composition. *Journal of Aerosol Science*, 41(1):108–117, 2010. doi:10.1016/j.jaerosci.2009.08.008.

[500] A. Vasiliou, M. R. Nimlos, J. W. Daily, and G. B. Ellison. Thermal decomposition of furan generates propargyl radicals. *The Journal of Physical Chemistry A*, 113 (30):8540–8547, 2009. doi:10.1021/jp903401h.

[501] A. Violi. Cyclodehydrogenation reactions to cyclopentafused polycyclic aromatic hydrocarbons. *Journal of Physical Chemistry A*, 109(34):7781–7787, 2005. doi:10.1021/jp052384r.

[502] A. Violi and A. Venkatnathan. Combustion-generated nanoparticles produced in a benzene flame: a multiscale approach. *The Journal of Chemical Physics*, 125(5): 054302, 2006. doi:10.1063/1.2234481.

[503] A. Violi, A. Sarofim, and T. Truong. Quantum mechanical study of molecular weight growth process by combination of aromatic molecules. *Combustion and Flame*, 126(1-2):1506–1515, 2001. doi:10.1016/S0010-2180(01)00268-1.

[504] A. Violi, A. Kubota, T. Truong, W. Pitz, C. Westbrook, and A. Sarofim. A fully integrated kinetic monte carlo/molecular dynamics approach for the simulation of soot precursor growth. *Proceedings of the Combustion Institute*, 29(2):2343–2349, 2002. doi:10.1016/S1540-7489(02)80285-1.

[505] A. Violi, A. F. Sarofim, and G. A. Voth. Kinetic monte carlo-molecular dynamics approach to model soot inception. *Combustion Science and Technology*, 176(5-6): 991–1005, 2004. doi:10.1080/00102200490428594.

[506] G. Vitiello, G. De Falco, F. Picca, M. Commodo, G. D'Errico, P. Minutolo, and A. D'Anna. Role of radicals in carbon clustering and soot inception: A combined EPR and raman spectroscopic study. *Combustion and Flame*, 205:286–294, 2019. doi:10.1016/j.combustflame.2019.04.028.

[507] K. Wan, X. Shi, and H. Wang. Quantum confinement and size resolved modeling of electronic and optical properties of small soot particles. *Proceedings of the Combustion Institute*, 2020. doi:10.1016/j.proci.2020.07.145.

[508] B. Wang, M. König, C. J. Bromley, B. Yoon, M.-J. Treanor, J. A. Garrido Torres, M. Caffio, F. Grillo, H. Früchtl, N. V. Richardson, F. Esch, U. Heiz, U. Landman, and R. Schaub. Ethene to graphene: Surface catalyzed chemical pathways, intermediates, and assembly. *The Journal of Physical Chemistry C*, 121(17):9413–9423, 2017. doi:10.1021/acs.jpcc.7b01999.

[509] C. Wang, T. Huddle, E. H. Lester, and J. P. Mathews. Quantifying curvature in high-resolution transmission electron microscopy lattice fringe micrographs of coals. *Energy & Fuels*, 30(4):2694–2704, 2016.

[510] C. Wang, T. Huddle, C. H. Huang, W. Zhu, R. L. Vander Wal, E. H. Lester, and J. P. Mathews. Improved quantification of curvature in high-resolution transmission electron microscopy lattice fringe micrographs of soots. *Carbon*, 117:174–181, 2017. doi:10.1016/j.carbon.2017.02.059.

[511] H. Wang. Formation of nascent soot and other condensed-phase materials in flames. *Proceedings of the Combustion Institute*, 33(1):41–67, 2011. doi:10.1016/j.proci.2010.09.009.

[512] H. Wang and M. Frenklach. A detailed kinetic modeling study of aromatics formation in laminar premixed acetylene and ethylene flames. *Combustion and Flame*, 110(1-2):173–221, 1997. doi:10.1016/S0010-2180(97)00068-0.

[513] H. Wang, B. Weiner, and M. Frenklach. Theoretical Study of Reaction between Phenylvinyleum Ion and Acetylene. *Journal of Physical Chemistry*, 97(40):10364–10371, 1993. doi:10.1021/J100142a017.

[514] M. Wang, G. Sharma, H. Zhang, X. You, and P. Biswas. Charge characteristics of sub-10 nm soot particles in premixed ethylene flames. *Fuel*, 279:118511, 2020. doi:10.1016/j.fuel.2020.118511.

[515] Q. Wang, J. C. Saldinger, P. Elvati, and A. Violi. Molecular structures in flames: A comparison between snaps2 and recent afm results. *Proceedings of the Combustion Institute*, 2020. doi:10.1016/j.proci.2020.06.250.

[516] S. Wang, D. Wu, B. Yang, E. Ruckenstein, and H. Chen. Semimetallic carbon honeycombs: New three-dimensional graphene allotropes with Dirac cones. *Nanoscale*, 10(6):2748–2754, 2018. doi:10.1039/c7nr07824b.

[517] X. Wang, M. A. Grose, R. Caldow, B. L. Osmondson, J. J. Swanson, J. C. Chow, J. G. Watson, D. B. Kittelson, Y. Li, J. Xue, H. Jung, and S. Hu. Improvement of Engine Exhaust Particle Sizer (EEPS) size distribution measurement - II. Engine exhaust particles. *Journal of Aerosol Science*, 92:83–94, 2016. doi:10.1016/j.jaerosci.2015.11.003.

[518] Y. Wang and S. H. Chung. Soot formation in laminar counterflow flames. *Progress in Energy and Combustion Science*, 74:152–238, 2019. doi:10.1016/j.pecs.2019.05.003.

[519] Z. Wang, D. M. Popolan-Vaida, B. Chen, K. Moshammer, S. Y. Mohamed, H. Wang, S. Sioud, M. A. Raji, K. Kohse-Höinghaus, N. Hansen, P. Dagaut, S. R. Leone, and S. Mani Sarathy. Unraveling the structure and chemical mechanisms of highly oxygenated intermediates in oxidation of organic compounds. *Proceedings of the National Academy of Sciences of the United States of America*, 114(50):13102–13107, 2017. doi:10.1073/pnas.1707564114.

[520] R. J. Watson, M. L. Botero, C. J. Ness, N. M. Morgan, and M. Kraft. An improved methodology for determining threshold sooting indices from smoke point lamps. *Fuel*, 111:120–130, 2013. doi:10.1016/j.fuel.2013.04.024.

[521] P. Weilmünster, A. Keller, and K.-H. Homann. Large molecules, radicals, ions, and small soot particles in fuel-rich hydrocarbon flames: Part I: positive ions of polycyclic aromatic hydrocarbons (PAH) in low-pressure premixed flames of acetylene and oxygen. *Combustion and Flame*, 116(1-2):62–83, 1999. doi:10.1016/S0010-2180(01)00310-8.

[522] P. G. Wenthold, R. R. Squires, and W. Lineberger. Ultraviolet photoelectron spectroscopy of the o-, m-, and p-benzyne negative ions. electron affinities and singlet-triplet splittings for o-, m-, and p-benzyne. *Journal of the American Chemical Society*, 120(21):5279–5290, 1998. doi:10.1021/ja9803355.

[523] C. Wentrup and K. Wilczek. Thermal interconversion of phenylcarbene and tropylidene. preliminary communication. *Helvetica Chimica Acta*, 53(6):1459–1463, 1970. doi:10.1002/hlca.19700530628.

[524] B. L. Wersborg, J. B. Howard, and G. C. Williams. Physical mechanisms in carbon formation in flames. *Symposium (International) on Combustion*, 14(1):929–940, 1973. doi:10.1016/S0082-0784(73)80085-2.

[525] C. P. West, A. P. S. Hettiyadura, A. Darmody, G. Mahamuni, J. Davis, I. Novosselov, and A. Laskin. Molecular composition and the optical properties of brown carbon generated by the ethane flame. *ACS Earth and Space Chemistry*, 4(7):1090–1103, 2020. doi:10.1021/acsearthspacechem.0c00095.

[526] R. Whitesides and M. Frenklach. Detailed kinetic Monte Carlo simulations of graphene-edge growth. *The Journal of Physical Chemistry A*, 114(2):689–703, 2010. doi:10.1021/jp906541a.

[527] R. Whitesides and M. Frenklach. Effect of reaction kinetics on graphene-edge morphology and composition. *Zeitschrift für Physikalische Chemie*, 229(4), 2015. doi:10.1515/zpch-2014-0633.

[528] R. Whitesides, D. Domin, R. Salomón-Ferrer, W. A. Lester, and M. Frenklach. Embedded-ring migration on graphene zigzag edge. *Proceedings of the Combustion Institute*, 32 I(1):577–583, 2009. doi:10.1016/j.proci.2008.06.096.

[529] D. Wong, R. Whitesides, C. Schuertz, and M. Frenklach. Molecular dynamics simulations of PAH dimerization. In H. Bockhorn, A. D'Anna, A. Sarofim, and H. Wang, editors, *Combustion Generated Fine Carbonaceous Particles*, pages 247–257. KIT Scientific Publishing Karlsruhe, 2009.

[530] H. L. Woodcock, D. Moran, B. R. Brooks, P. v. R. Schleyer, and H. F. Schaefer. Carbene stabilization by aryl substituents. is bigger better? *Journal of the American Chemical Society*, 129(12):3763–3770, 2007. doi:10.1021/ja068899t.

[531] X. Z. Wu, Y. R. Yao, M. M. Chen, H. R. Tian, J. Xiao, Y. Y. Xu, M. S. Lin, L. Abella, C. B. Tian, C.-L. Gao, Q. Zhang, S. Y. Xie, R. B. Huang, and L. S. Zheng. Formation of Curvature Subunit of Carbon in Combustion. *Journal of the American Chemical Society*, 138(30):9629–9633, 2016. doi:10.1021/jacs.6b04898.

[532] R. E. Wyzga and A. Rohr. Long-term particulate matter exposure: Attributing health effects to individual PM components. *Journal of the Air & Waste Management Association*, 65(5):523–543, 2015. doi:10.1016/j.atmosenv.2012.07.036.

[533] S. Yan, E. G. Eddings, A. B. Palotas, R. J. Pugmire, and A. F. Sarofim. Prediction of Sooting Tendency for Hydrocarbon Liquids in Diffusion Flames. *Energy & Fuels*, 19(6):2408–2415, 2005. doi:10.1021/ef050107d.

[534] S. Yan, Y.-J. Jiang, N. D. Marsh, E. G. Eddings, A. F. Sarofim, and R. J. Pugmire. Study of the evolution of soot from various fuels. *Energy & fuels*, 19(5):1804–1811, 2005. doi:10.1021/ef049742u.

[535] H. Yang, C. Liu, D. Yang, H. Zhang, and Z. Xi. Comparative study of cytotoxicity, oxidative stress and genotoxicity induced by four typical nanomaterials: The role of particle size, shape and composition. *Journal of Applied Toxicology*, 29(1):69–78, 2009. doi:10.1002/jat.1385.

[536] W. Yang, J. Kangasluoma, M. Attoui, J. Fang, H. Junninen, M. Kulmala, T. Petäjä, and P. Biswas. The high charge fraction of flame-generated particles in the size range below 3 nm measured by enhanced particle detectors. *Combustion and Flame*, 176:72–80, 2017. doi:10.1016/j.combustflame.2016.10.003.

[537] Y. Yang, J. Mulholland, and U. Akki. Formation of furans by gas-phase reactions of chlorophenols. *Symposium (International) on Combustion*, 27(2):1761–1768, 1998. doi:10.1016/S0082-0784(98)80017-9.

[538] X. H. Yao, N. T. Lau, M. Fang, and C. K. Chan. On the time-averaging of ultrafine particle number size spectra in vehicular plumes. *Atmospheric Chemistry and Physics*, 6(12):4801–4807, 2006. doi:10.5194/acp-6-4801-2006.

[539] E. K. Yapp, C. G. Wells, J. Akroyd, S. Mosbach, R. Xu, and M. Kraft. Modelling PAH curvature in laminar premixed flames using a detailed population balance model. *Combustion and Flame*, 176:172–180, 2017. doi:10.1016/j.combustflame.2016.10.004.

[540] K. Yehliu, R. L. Vander Wal, and A. L. Boehman. Development of an hrtem image analysis method to quantify carbon nanostructure. *Combustion and Flame*, 158(9):1837–1851, 2011. doi:10.1016/j.combustflame.2011.01.009.

[541] X. You, A. Packard, and M. Frenklach. Process informatics tools for predictive modeling: Hydrogen combustion. *International Journal of Chemical Kinetics*, 44 (2):101–116, 2012. doi:10.1002/kin.20627.

[542] H. Yuan, W. Kong, F. Liu, and D. Chen. Study on soot nucleation and growth from PAHs and some reactive species at flame temperatures by reaxff molecular dynamics. *Chemical Engineering Science*, 195:748 – 757, 2019. doi:10.1016/j.ces.2018.10.020.

[543] A. V. Zabula, A. S. Filatov, S. N. Spisak, A. Y. Rogachev, and M. A. Petrukhina. A Main Group Metal Sandwich: Five Lithium Cations Jammed Between Two Corannulene Tetraanion Decks. *Science*, 333(6045):1008–1011, 2011. doi:10.1126/science.1208686.

[544] C. Zhang, C. Zhang, Y. Ma, and X. Xue. Imaging the C black formation by acetylene pyrolysis with molecular reactive force field simulations. *Physical Chemistry Chemical Physics*, 17(17):11469–11480, 2015. doi:10.1039/C5CP00926J.

[545] H. B. Zhang, X. You, H. Wang, and C. K. Law. Dimerization of polycyclic aromatic hydrocarbons in soot nucleation. *The Journal of Physical Chemistry A*, 118(8): 1287–1292, 2014. doi:10.1021/jp411806q.

[546] W. Zhang, C. Shao, and S. M. Sarathy. Analyzing the solid soot particulates formed in a fuel-rich flame by solvent-free MALDI FT ICR mass spectrometry. *Rapid Communications in Mass Spectrometry*, 2019. doi:10.1002/rcm.8596.

[547] W. Zhang, C. Shao, and S. M. Sarathy. Analyzing the solid soot particulates formed in a fuel-rich flame by solvent-free matrix-assisted laser desorption/ionization fourier transform ion cyclotron resonance mass spectrometry. *Rapid Communications in Mass Spectrometry*, 34(4):e8596, 2020. doi:10.1002/rcm.8596.

[548] B. Zhao, Z. Yang, M. V. Johnston, H. Wang, A. S. Wexler, M. Balthasar, and M. Kraft. Measurement and numerical simulation of soot particle size distribution functions in a laminar premixed ethylene-oxygen-argon flame. *Combustion and Flame*, 133(1-2):173–188, 2003. doi:10.1016/S0010-2180(02)00574-6.

[549] L. Zhao, R. I. Kaiser, W. Lu, B. Xu, M. Ahmed, A. N. Morozov, A. M. Mebel, A. H. Howlader, and S. F. Wnuk. Molecular mass growth through ring expansion in polycyclic aromatic hydrocarbons via radical–radical reactions. *Nature communications*, 10(1):1–7, 2019. doi:10.1038/s41467-019-11652-5.

[550] Z. Zheng, T. D. Durbin, G. Karavalakis, K. C. Johnson, A. Chaudhary, D. R. Cocker, J. D. Herner, W. H. Robertson, T. Huai, A. Ayala, D. B. Kittelson, and H. S. Jung. Nature of sub-23-nm particles downstream of the European particle measurement programme (PMP)-compliant system: A real-time data perspective. *Aerosol Science and Technology*, 46(8):886–896, 2012. doi:10.1080/02786826.2012.679167.

[551] L. Zhou, C. Zhang, I. A. Karimi, and M. Kraft. An ontology framework towards decentralized information management for eco-industrial parks. *Computers & Chemical Engineering*, 118:49–63, 2018. doi:10.1016/j.compchemeng.2018.07.010.

[552] X. Zhou, A. Eibeck, M. Q. Lim, N. B. Krdzavac, and M. Kraft. An agent composition framework for the J-Park Simulator-a knowledge graph for the process industry. *Computers & Chemical Engineering*, 130:106577, 2019. doi:10.1016/j.compchemeng.2019.106577.